2.0 COAL PREPARATION/UTILIZATION

Coal preparation/cleaning necessarily plays a substantial role in all aspects of coal utilization, large-scale and small-scale, including specialized applications such as coal-water mixture firing and cofiring with waste materials. Realistic applications of post-combustion treatments (e.g. flue-gas desulfurization) will continue to depend on pre-combustion processing (coal cleaning) to maintain consistent fuel quality and to minimize the load on the post-combustion system.

Research conducted under Phases I and II of this project revealed a number of specific areas where continued and/or more focused effort was required in order to develop more effective, more reliable coal processing systems. The specific objectives of the Phase III research on coal preparation were selection of specific coal-cleaning options and their associated ancillary operations and the integration of processing/cleaning operations for overall system optimization. As in the earlier phases of the project, emphasis was placed on fine-coal processing for the production of high-quality, micronized coal for dry coal and coal-water mixture applications.

2.1 Particle Size Control

2.1.1 Conventional Ball Milling

Tumbling ball mills represent an important component of fine-grinding systems used for the preparation of coal-water mixtures. The Bond Method has been used traditionally for the selection of ball mills for industrial applications. It is simple and has been quite successful for predicting required mill sizes. However, it is not suitable for optimization of mill or circuit conditions. Also, it does not predict the complete product size distribution, which is important for subsequent processes such as coal-water mixture preparation. Recently, commercial ball mill simulators have evolved based on the concepts of grinding kinetic theory using specific rates of breakage (S values) and primary breakage distributions (B values). Hence, one can examine the performance of various full-scale grinding circuits.

The method employed here follows that developed by Austin et al. (1983), which involves scale-up of the specific rates of breakage determined for the material in a laboratory test batch mill, allowing for the effects of the variables associated with milling. For ball milling, these variables typically include mill rotational speed, ball filling, powder filling, mill diameter, ball diameter, etc. Extensive work has been done to investigate the effect of these variables, and the methodology to incorporate these factors into simulations is well described by Austin et al. (1983).

The functional forms used to characterize particle breakage during grinding can be summarized as follows:

Effect of particle size (x_i)

$$S(x_i) = a\left(\frac{x_0}{x_0}\right)^{\alpha} \frac{1}{1+(x_i/\mu)^{\Lambda}} \qquad (2.1.1)$$

where $S(x_i)$ = specific rate of breakage for particle of size x_i

a = specific rate of breakage at x_o

α = an exponential constant, characteristic of the material being ground

μ, Λ = characteristic constants for describing the decrease in the specific rates of breakage as the particles become too large to be broken effectively.

Effect of ball diameter (d) and mill diameter (D)

The parameters a and μ in Equation 2.1.1 both depend on ball size and mill diameter. Specifically:

$$a \propto 1/d \text{ and } a \propto D^{0.5}$$

$$\mu \propto d^2 \text{ and } \mu \propto D^{0.2}$$

Effect of rotational speed

$$S(x_i) \propto (\phi_c\text{-}0.1)\frac{1}{1+\exp[15.7(\phi_c - 0.94)]}$$

where ϕ_c = the fraction of critical speed (defined as the rotational speed at which the balls begin to centrifuge on the mill case and cease to tumble).

Effects of ball and powder loading

$$S(x_i) \propto \left[\frac{1}{1+6.6J^{2.3}}\right]\exp(-cU)$$

where J = the fraction of the mill volume filled by the ball bed at rest

U = the fraction of the interstices of the ball bed filled with powder (at rest)

The S values determined for the material in a laboratory-scale, batch mill can be used to simulate large-scale mills via the scale-up relations given above. On the other hand, the B values are typically independent of the breaking size and milling environment so that scale-up is not usually necessary for the B values.

For a retention grinding device such as the ball mill, the length of time that material spends in the mill controls the final degree of breakage. Moreover, some fraction of the feed stays in the mill for a short time, other fractions for a longer time, etc. Therefore, estimation of the residence time distribution (RTD) is required. It has often been shown that the experimental RTD can be matched against theoretical expressions derived for a number of fully mixed reactors in series. The one-large, two-small, fully mixed reactors in series model has been found to be appropriate for ball mills.

A grinding circuit may consist of one or more mills and classifiers. Industrial grinding circuits can be categorized into the following five types.

a) open circuit
b) normal closed circuit
c) open circuit with scalped feed

d) reversed closed circuit

e) combined closed circuit

These circuits are illustrated in Figure 2.1.l. The combined closed circuit can be used to represent the other circuits by assigning the appropriate classification parameters for the pre-classifier and the post-classifiers.

Classification is the splitting of a stream of particles into two streams, with separation by size (and/or density) e.g., one stream with mainly large particles, the other with fine particles. The classifier performance is characterized by a set of numbers, one for each size interval, which describes how each size is split between the two product streams. The selectivity value, s_i for size i is defined as the fraction of size i in the feed which is sent to the coarse stream. A plot of the selectivity values vs. size is called a size selectivity curve. This curve generally has an S shape and can often be described by a log-logistic function. Using this functional form, the complete set of size selectivity values can be calculated using three characteristic parameters: the sharpness index, cut size (d_{50}) and apparent by-pass. Finally, the different streams in the complete circuit can be described by the mass balance equations, a mill model, and two classifier models.

Simulations were performed for the two most common circuits: open and normal closed circuit. Capacities were obtained for three different diameter (3, 4, 5 meter) mills, giving a circuit product passing through the one-point specification of 80% finer than 200 mesh (74 μm). All mills were operated with a slurry density of 70 wt% coal and at 70% of critical speed. Ball loading was set at 30% filling with makeup of 50.8 mm balls. The residence time distribution was assumed to fit the one-large/two-small fully mixed reactor model in the ratios 0.5, 0.25, 0.25, respectively. The performance of the classifier was assumed to be constant with the characteristic parameters of sharpness index of 0.7 and by-pass of 0.3. The d_{50} values were changed to give results over a range of circulating loads. The coal feed was assumed to fit the Rosin-Rammler distribution with size modulus k_r = 9.525 mm and m = 1. The breakage parameters (a, α, γ, ϕ and β) measured in a laboratory batch mill at 70% solids are shown in Table 2.1.1.

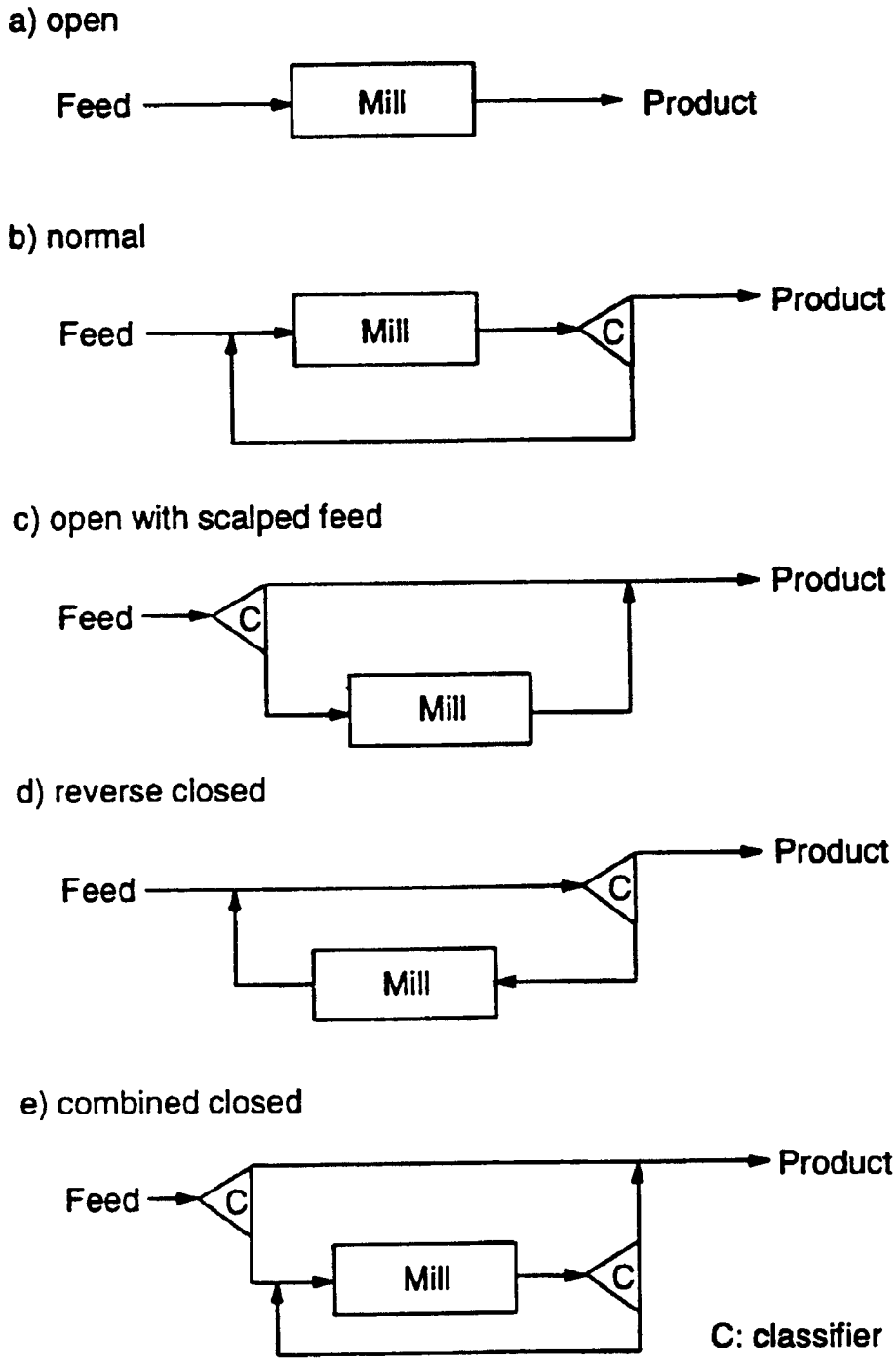

Figure 2.1.1 VARIOUS GRINDING CIRCUIT CONFIGURATIONS USED IN INDUSTRY

Table 2.1.1 Breakage Parameters for the Coals Tested at 70% Solids by Weight

Coal Seam	a	α	ϕ	γ	β
Taggart	0.85	1.37	0.52	0.44	5.0
Pittsburgh	1.90	1.33	0.45	0.58	5.0
Lower Kittanning	3.47	1.56	0.45	.36	5.0

The results of the simulations are given in Table 2.1.2. As expected, the capacity is higher for easily ground coals (high HGI). For a given coal, capacity increases with the mill diameter and is proportional to $D^{3.5}$ as shown in Figure 2.1.2. This results from the fact that for the same grinding environment, the capacity is proportional to the mill volume, which is LD^2 (for the same L/D ratio, it is D^3). Since the S values increase with the mill diameter by $D^{0.5}$ (see above), the overall effect of the mill diameter is that the capacity is proportional to $D^{3.5}$. If the circuit is closed with a classifier, the capacity increases substantially by minimizing the over-grinding of material that is already fine enough. Also, the closed circuit produces a narrower size distribution; i.e., produces less unnecessarily fine material. For a given classifier setting, increasing the feed rate coarsens the mill product, thereby causing the classifier to send more material to recycle. As a result, the circulation ratio C (ratio of the amount of recycle to that of the product) increases, and the circuit product becomes coarser. However, there is only one feed rate that can meet a particular one-point product specification. By changing the classifier setting (d_{50}), it is possible to obtain the one-point match for a range of feed rates and circulation ratios. Figure 2.1.3 shows the results. A lower value of d_{50} gives a higher circulation ratio and a steeper size distribution. Also, the production rate increases as the circulation ratio increases, as seen in Figure 2.1.4. At low circulation ratios, the product is sufficiently fine that the classifier has no effect, so the production rate is the same as that of the open circuit. On the other hand, high recycle leads

Table 2.1.2 Comparison of Circuit Capacity for Open and Closed Circuit Systems

Mill Diameter (meters)	Taggart (HGI = 47)			Pittsburgh (HGI = 56)			Lower Kittanning (HGI = 68)		
	C	TPH	d_{50} (μm)	C	TPH	d_{50} (μm)	C	TPH	d_{50} (μm)
Open Circuit									
3	-	8.45	-	-	14.82	-	-	22.58	-
4	-	21.13	-	-	39.37	-	-	61.66	-
5	-	44.02	-	-	81.12	-	-	131.25	-
Closed Circuit									
3	0.53	244	9.14	0.50	244	15.01	0.54	211	25.02
	1.03	137	13.13	0.97	133	21.47	1.03	133	32.6
	1.44	120	15.04	1.47	113	23.03	1.50	119	34.19
	2.10	112	17.09	1.97	104	23.17	1.98	108	33.23
	2.47	105	16.65	-	-	-	-	-	-
4	0.48	305	22.39	0.5	244	38.91	0.48	264	61.51
	0.98	141	35.06	0.99	133	59.16	1.00	141	92.41
	1.52	119	41.86	1.46	115	63.48	1.54	117	92.32
	1.91	112	45.23	2.06	106	64.38	1.74	111	91.02
	3.33	99	44.55	-	-	-	-	-	-
5	0.47	305	43.9	0.50	244	81.90	0.49	264	139.91
	0.97	139	71.31	0.95	132	118.42	0.96	141	191.20
	1.56	122	92.66	1.54	115	136.86	1.47	117	193.67
	2.04	112	97.73	2.07	105	135.48	1.97	111	197.62
	2.5	103	95.10	-	-	-	-	-	-

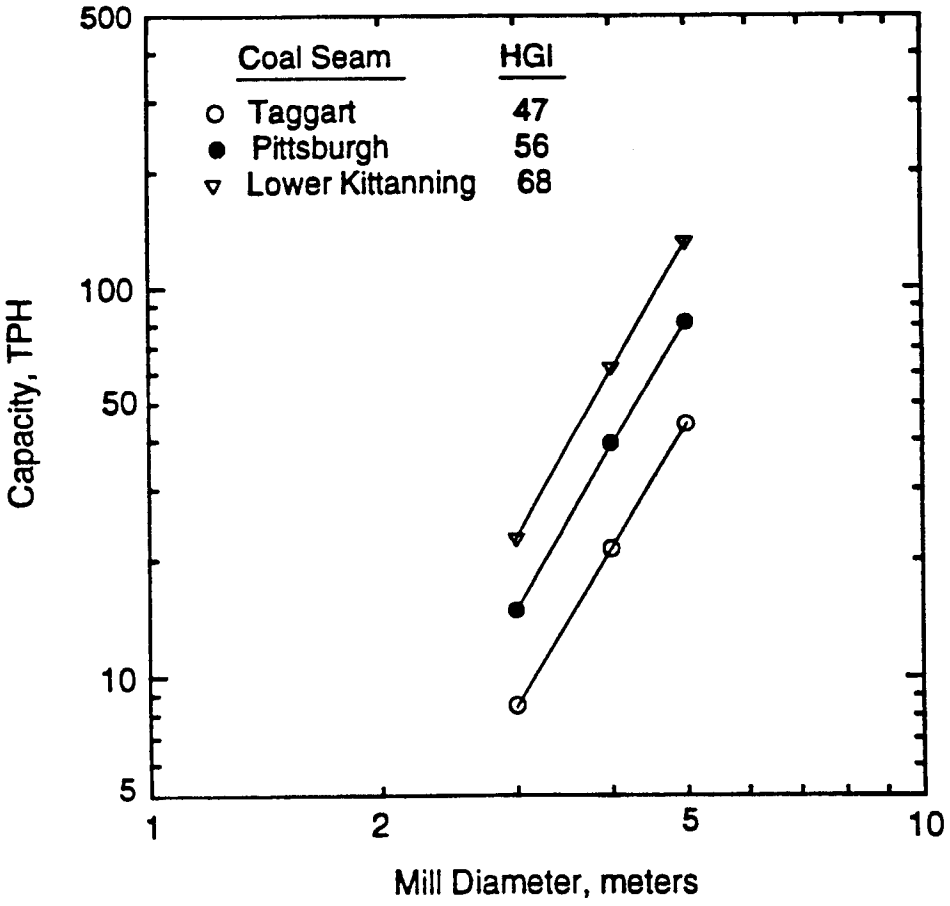

Figure 2.1.2 VARIATION OF BALL MILL CAPACITY WITH MILL DIAMETER

to increased overfilling, causing inefficient grinding. Thus, an optimum circulation ratio exists. Generally, the optimum circulation ratio is a function of the fineness of the final product. In this case, the optimum circulation ratio is found to be in the range of 1.5-2.0. At this optimum circulation ratio, the increase in capacity given by closing the circuit is also in the range of 1.5-2.0. The energy required for grinding to a one-point product specification is less for the closed circuit than for open-circuit grinding.

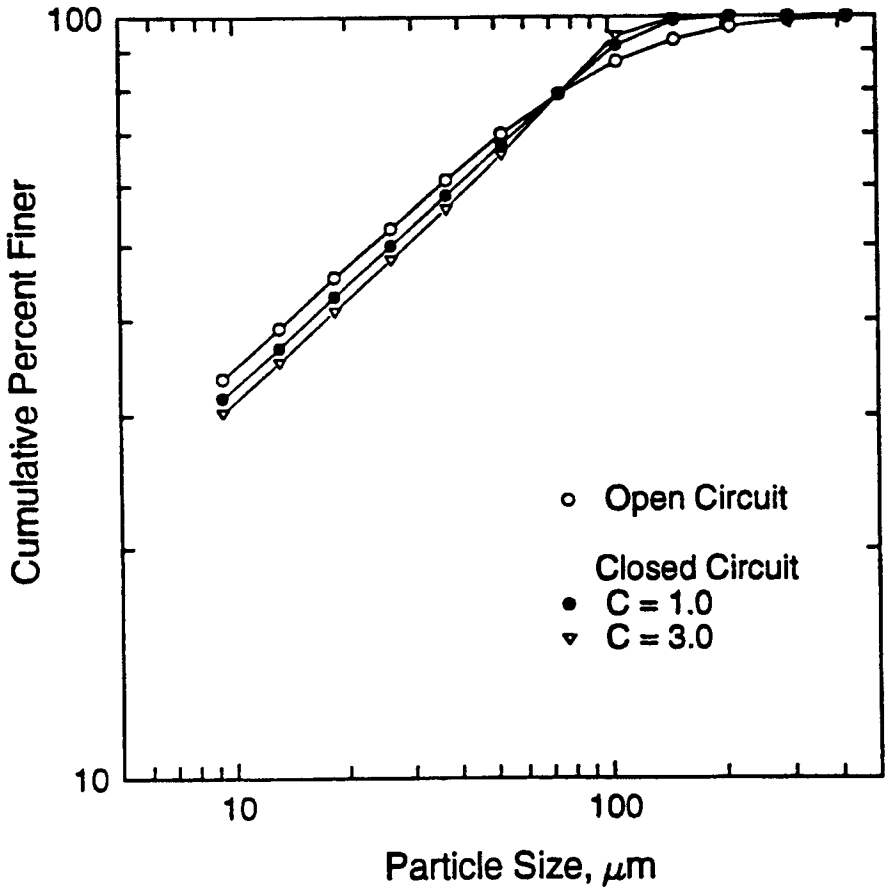

Figure 2.1.3 COMPARISON OF PRODUCT SIZE DISTRIBUTIONS RESULTING FROM OPEN AND CLOSED-CIRCUIT GRINDING

2.1.2 Stirred-Media Milling

The approach described above can also be used to predict grinding behavior in a stirred ball mill. However, the engineering and mill scale-up procedures are not as well established. It has often been suggested that the median size of the product is related to the energy input, independent of the mill size and operating conditions (Herbst and Sepulveda, 1978; Stehr and Schwedes, 1983). This suggests that the relationship of power draw to the mill dimensions and operating variables can be used to predict the product fineness. However, in recent studies (Mankosa et al., 1986, 1989; Gao and Forssberg, 1993; Zheng et al., 1995), it was reported that the energy efficiency is affected by operating conditions such as media density and size, slurry concentration, and agitation speed.

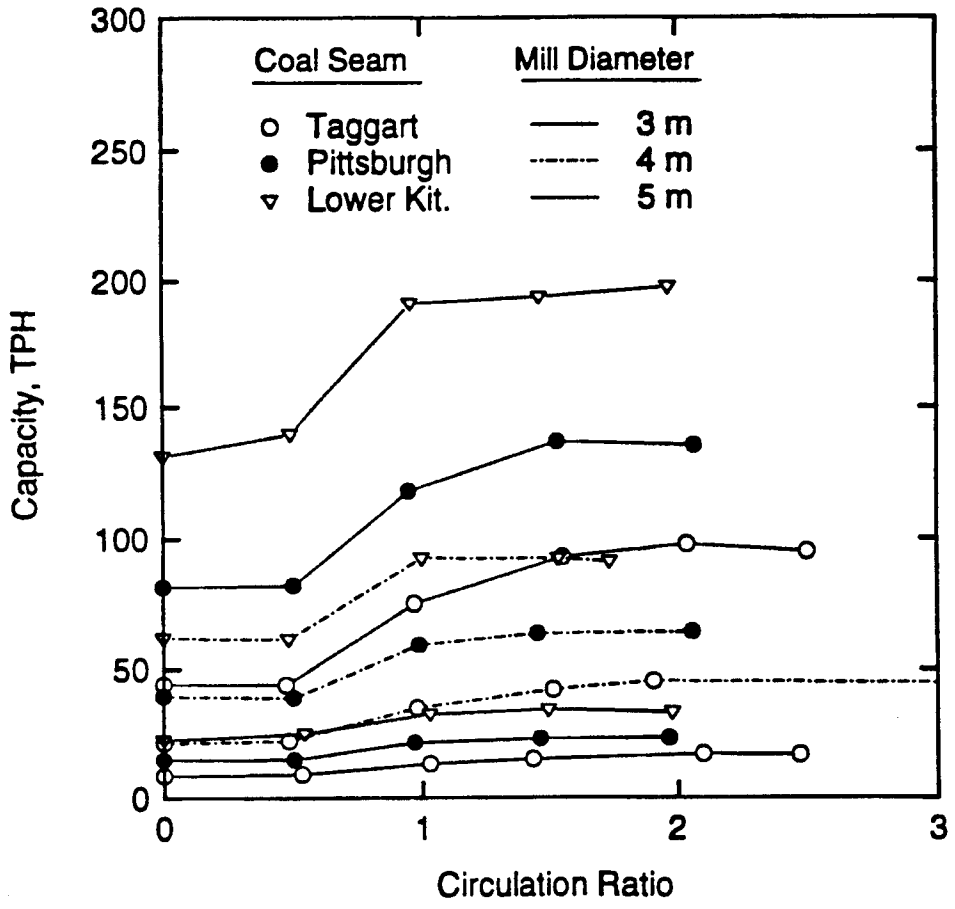

Figure 2.1.4 EFFECT OF CIRCULATION RATIO ON CAPACITY IN CLOSED-CIRCUIT GRINDING

It is clear that there are numerous apparent inconsistencies in the literature on the energy-efficiency of stirred-media milling. For the most part, these arise from interactions among many material, equipment, and operating variables. It is generally agreed, however, that there is a clear link between energy input and product fineness. Also it is known that operating conditions play an important role. Powder and media loading and the media to particle size ratio seem to be primary factors in determining energy efficiency.

Review of the literature indicates that the energy input alone can not correctly predict mill performance, i.e., size reduction. Nonetheless, the power requirement for stirred ball milling is important and has been the subject of many investigations, especially aimed at

scale-up. The standard treatment for the power, P, necessary to drive a stirrer in a Newtonian liquid operating in the turbulent regime starts with (Rushton et al., 1950):

$$P = N_p N^3 D^5 \rho \qquad (2.1.2)$$

where N is the rotational speed, D is the diameter of the stirrer, and ρ is the density of the liquid. N_p is the power number, which depends on flow conditions and system geometry. In stirred ball milling, the mill contains the solids being ground, the liquid (in wet grinding) and, more importantly, the grinding media. It is extremely unlikely, therefore, that the behavior would be Newtonian. Furthermore, the density in Equation 2.1.2 is no longer clearly defined. Since there is a considerable difference in the densities of the liquid and the media, there is a tendency for segregation of the media in the mill. At a low rotational speed, the media tend to settle, leading to an inhomogeneous distribution of the media. On the other hand, at higher rotational speeds, a vortex is formed and the media are concentrated at the wall due to centrifugal forces. Therefore, the dependency of the power draw on the rotational speed can vary significantly. Also, the movement of the media is highly dependent upon the media loading. It might be expected that the movement of the media would be more rapid at high loading, since a higher portion of media could be in direct contact with stirrers and among themselves. Therefore, it is very difficult to analyze the mill power theoretically, and it is often necessary to resort to empirical equations based on experiment (Herbst and Sepulveda, 1978; Gao et al., 1996, Zheng et al., 1995). Unfortunately, such equations may be valid only for the particular design of the system. The values of the parameters, for the range of rotational speeds of interest, may depend on media loading, size, and density and slurry concentration, density, and viscosity.

Breakage of particles occurs as a result of applied stress, which originates from energy input to the grinding device. However, as shown above, the effectiveness of the breakage action does not depend on the level of energy input alone. The nature of the energy input also plays an important role. Kwade et al. (1996) have introduced the concept of energy intensity as a critical factor in determining whether or not stress application actually leads to breakage. At low stress intensities, several stressing events may be required to cause

fracture. As the stress intensity increases, a critical value is reached above which further increase does not lead to additional breakage. In any grinding process, particles are exposed to a distribution of stress intensities. The effectiveness of the process depends on the fraction of stressing events for which the stress intensity exceeds this critical level. On the other hand, excessive stress intensities, well above the critical value, lead to reduced grinding efficiency, i.e. increased specific energy.

Breakage rates are determined by the stress frequency, modified by the stress intensity, i.e. by the frequency of *adequate* stress applications. Relationships between the stress intensity and frequency and the operating conditions in stirred-media milling have been proposed (Blecher and Schwedes, 1996; Becker et al., 1997). The stress frequency f_s clearly depends on mill geometry and agitator speed and a general relationship can be expected with the form:

$$f_s \propto N\left(\frac{d_d}{d_b}\right)^2 \tag{2.1.3}$$

where N is the rotational speed and d_d and d_b are the respective diameters of the grinding chamber and the grinding beads. The stress intensity I_s can be expected to depend on agitation speed, grinding media size and density, and on the elasticity of the media and the material being ground. The latter determines the effectiveness of energy transfer between media and particles. The following specific relationship has been proposed (Kwade 1998; Kwade et al., 1996):

$$I_s = d_b^3 \rho_b v_t^2 \left(1 + \frac{Y_s}{Y_b}\right)^{-1} \tag{2.1.4}$$

where ρ_b is the grinding bead density, v_t is the agitator tip speed, and Y_s and Y_b are the respective elastic moduli for the solid and the grinding media.

The specific grinding energy depends on the product of the stress frequency and the stress intensity, both of which vary with grinding conditions. Becker et al. (1997) showed that, for a fixed energy input, there is an optimum stress intensity that provides the most size reduction. By varying the energy input using different combinations of speed, media size,

and media density, they demonstrated that the optimum stress intensity decreased with increased energy input. The optimum intensity presumably reflects the critical intensity for fracture discussed above. Equation 2.1.4 indicates how it varies with media size. The dependence on the size of the particles being broken is not included in Equation 2.1.4. However, it has been demonstrated that breakage rates in stirred media mills follow very similar patterns to those observed in conventional ball mills (Miller et al., 2000; Cho and Hogg, 1995; Mankosa et al., 1986; Stehr et al., 1987) and relationships of the general form of Equation 2.1.1 seem to be applicable.

Based on such data as are available and on indirect evidence from the work of Kwade et al., (1996, 1998) and others (Herbst and Sepulveda, 1978; Gao and Forssberg, 1993, 1995; Mankosa et al., 1986, 1989; and Rajamani and Bourgeois, 1990), it appears that the trade-off between stress intensity and stress frequency becomes especially critical at ultrafine sizes. Changing media size can lead to enhanced breakage in one range of sizes but simultaneously to reduced rates for slightly coarser material. Staged stirred-media milling using progressively finer media may be a useful option for improving efficiency in ultrafine grinding. The use of a distribution of media sizes, as is the common practice in tumbling ball mills, should also be appropriate.

It was noted above that breakage distributions in conventional ball milling are often relatively independent of the size being broken and the milling environment. Similar behavior has been observed in stirred-media milling for relatively coarse grinding. However, it has been found that the distributions tend to become progressively narrower as the size being broken is reduced into the micron range (Strazisar and Runovc, 1996; Cho and Hogg, 1995). This effect has been attributed to the approach to a "grind limit" (Cho et al., 1996).

2.1.3 Attrition Milling

Attrition milling operates on the same basic principle as stirred-media milling, but the size reduction is accomplished by using the coal particles themselves as the media. However, there is a major difference between the stirred-media mills and attrition mills. First, the power input is substantially less for attrition milling, since the coal is lighter than

the media and hence, less energy is required to agitate the slurry. More importantly, the breakage process in attrition milling is totally different. Large coal particles act as grinding media for smaller particles, giving breakage mechanisms similar to those obtained by normal grinding media. But they also break themselves by particle-particle contact. The breakage in any grinding mill is generally achieved by three different mechanisms - fracture, chipping and abrasion. Fracture refers to complete disintegration of a particle by massive impact, chipping involves cutting off corners, while abrasion results from the wearing of surfaces by a rubbing action. The fragments produced by fracture are distributed over a broad range of sizes. On the other hand, chipping and abrasion lead to production of fine material and a residual "core" close to the original particle size. Therefore, the shape of the product size distribution is greatly influenced by the type of the breakage mechanism. In attrition milling, chipping and abrasion will play bigger roles and the resulting products are likely to be composed of two main populations - coarse (remaining cores) and fines (chipped or abraded material). This is quite appropriate for a coal-water mixture feedstock. Therefore, attrition milling potentially offers a great advantage for coal-water mixture preparation over other grinding procedures from both economic and engineering viewpoints.

Tests were conducted to explore such a potential advantage using a vertical-type, stirred-media mill. The mill was constructed with a stainless steel cylinder 3 inches wide and 4 inches high. The stirrer shaft was fitted with 3-perforated disks and was rotated by means of a 2-Hp, variable speed motor. A torque sensor, mounted on the drive shaft between the motor and the mill, was used to provide an indication of the power input to the mill. Tests were conducted to determine the breakage characteristics of large particles alone, and of small particles of various sizes when ground together with large ("media") particles. Since the rheological properties are likely to play an important role in determining the breakage mechanisms, the effect of overall solids content was examined. Some results are shown in Figures 2.1.5 and 2.1.6.

As noted above, the coarse particles serve as grinding media for the finer material but also produce fine particles by self-breakage. Consequently, in a continuous operation, the amount of "media" in the mill decreases with time and must be replenished on a regular

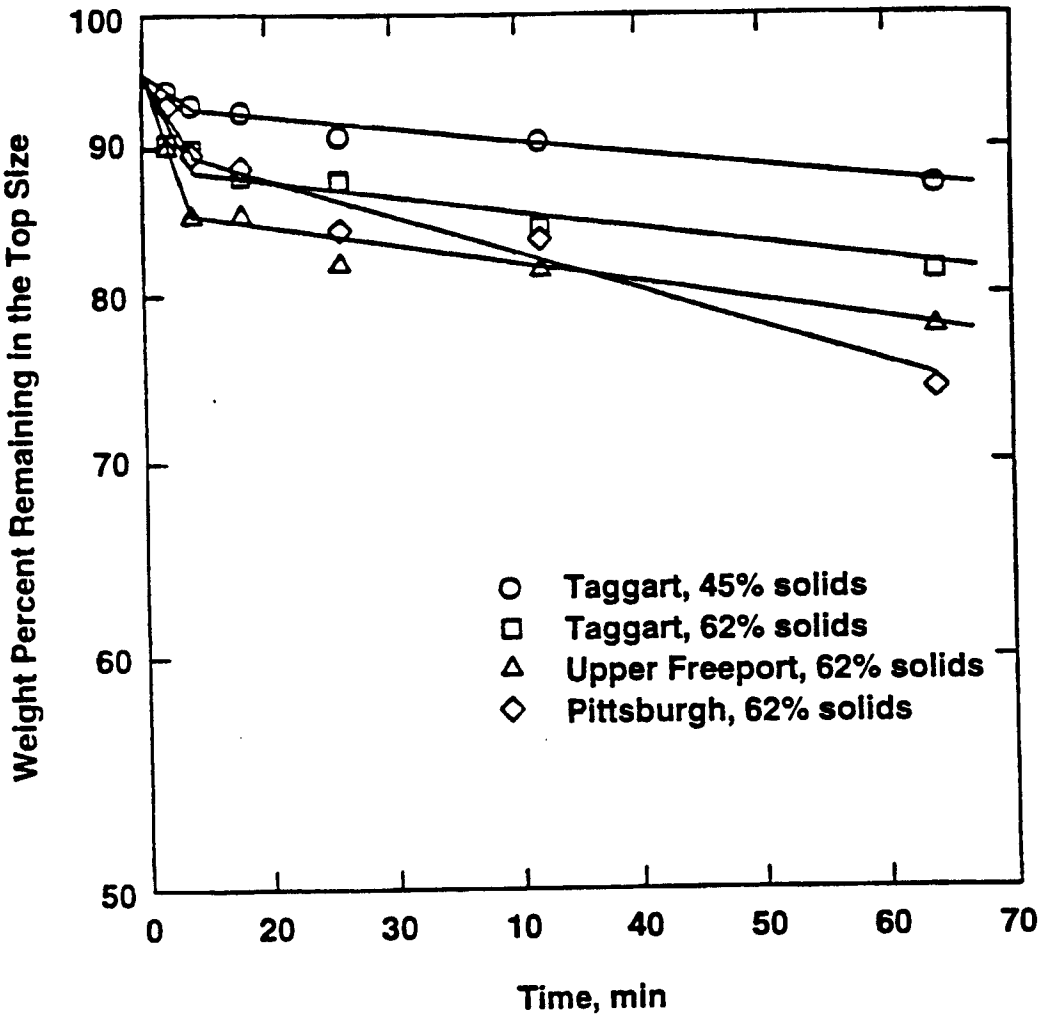

Figure 2.1.5 DISAPPEARANCE PLOTS FOR COARSE (16x20 US mesh) COAL "MEDIA" IN ATTRITION GRINDING

basis. Feed disappearance plots for 16×20 US mesh fractions from three different coals are given in Figure 2.1.5. It can be seen that disappearance rates are higher for softer coals and higher solids concentrations. The self-breakage process is clearly non-linear and is rapid initially but then slows down substantially. Around 80% of the original feed remained in its original size fraction after one hour of grinding.

The size distributions of the "media" particles after grinding for various times are shown in Figure 2.1.6. It can be seen that the curves are almost flat in the fine size ranges, and are translated upward by an increase in the amount of –400 mesh material. The initially

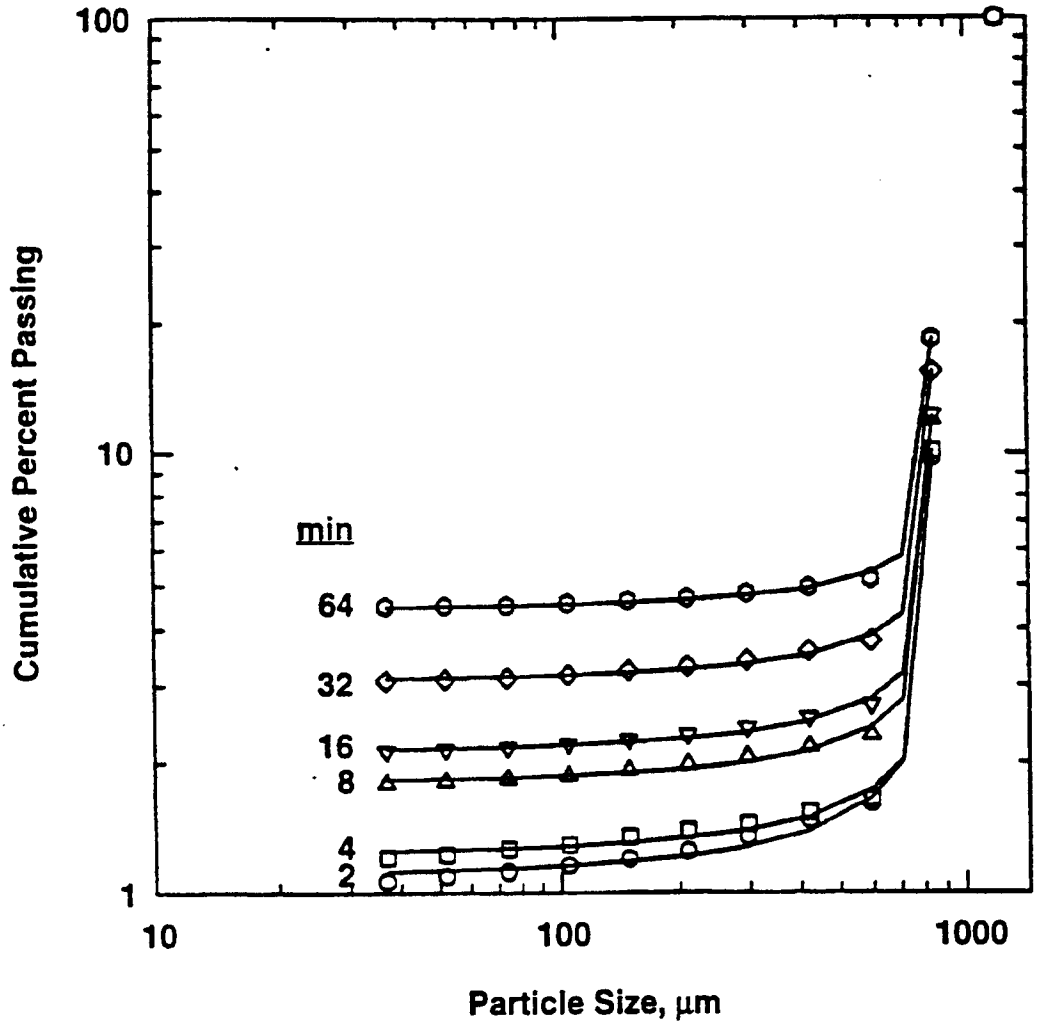

Figure 2.1.6 SIZE DISTRIBUTION OF THE PRODUCTS OF "MEDIA" ATTRITION

high disappearance rates shown in Figure 2.1.5 together with the product size distributions (Figure 2.1.6) are consistent with a chipping/abrasion model for the process. Specifically, it appears that depletion of media-size material occurs through two mechanisms:

- Large-scale chipping of a fraction f of the feed material
- Slow abrasion of the remaining portion.

The material subject to large-scale chipping or fracture presumably includes highly irregular and/or friable particles. All particles in the mill are expected to undergo abrasion.

A model for the combined chipping/abrasion process can be developed by assuming that the chipping process is approximately first-order, leading to an exponential decay in the mass of these "breakable" particles, while the abrasion process involves a slow reduction in the mass of a fixed *number* of "non-breakable" particles. Studies of the abrasion of individual rock particles in conventional autogenous grinding (Tangsripongkul 1993) have indicated that a first-order abrasion law, referred to as the Davis Wear Law (Davis 1919) may be appropriate for this process. The Davis Law can be expressed as

$$\frac{dx}{dt} = -kx \tag{2.1.5}$$

where x is the equivalent-sphere particle diameter and k is a first-order rate constant.

Formulation of the combined chipping/abrasion model leads to the following expression for the mass W(t) of material remaining in the coarse "media" size after time t:

$$W(t) = \frac{[1 - f(1 - e^{-St})][1 - R(1 + kt)]}{(1 + kt)^3 (1 - R)} \tag{2.1.6}$$

where S is the specific rate of breakage by chipping and R is the ratio of the upper and lower boundaries of the original size interval. In this formulation, it is assumed that the initial distribution of sizes within the original interval was uniform (rectangular).

The application of this model to media-size disappearance in the attrition of 16×20 US mesh Taggart seam coal is illustrated in Figure 2.1.7. It is clear that the model can describe such data well. In this case, it appears that increasing the solids loading in the mill increases the fraction susceptible to large-scale chipping, possibly by eliminating liquid films between particles which could provide a lubricating (or damping) action. The abrasion rate seems to be relatively unaffected by solids loading.

Some limited experimentation on the breakage of smaller particles by the coarse "media" has also been carried out, as part of a related but separately funded project. Some typical results, in this case for quartz particles, are shown in Figure 2.1.8. The finest feed (37-52 μm) seems to to exhibit "normal" behavior consistent with massive fracture – feed

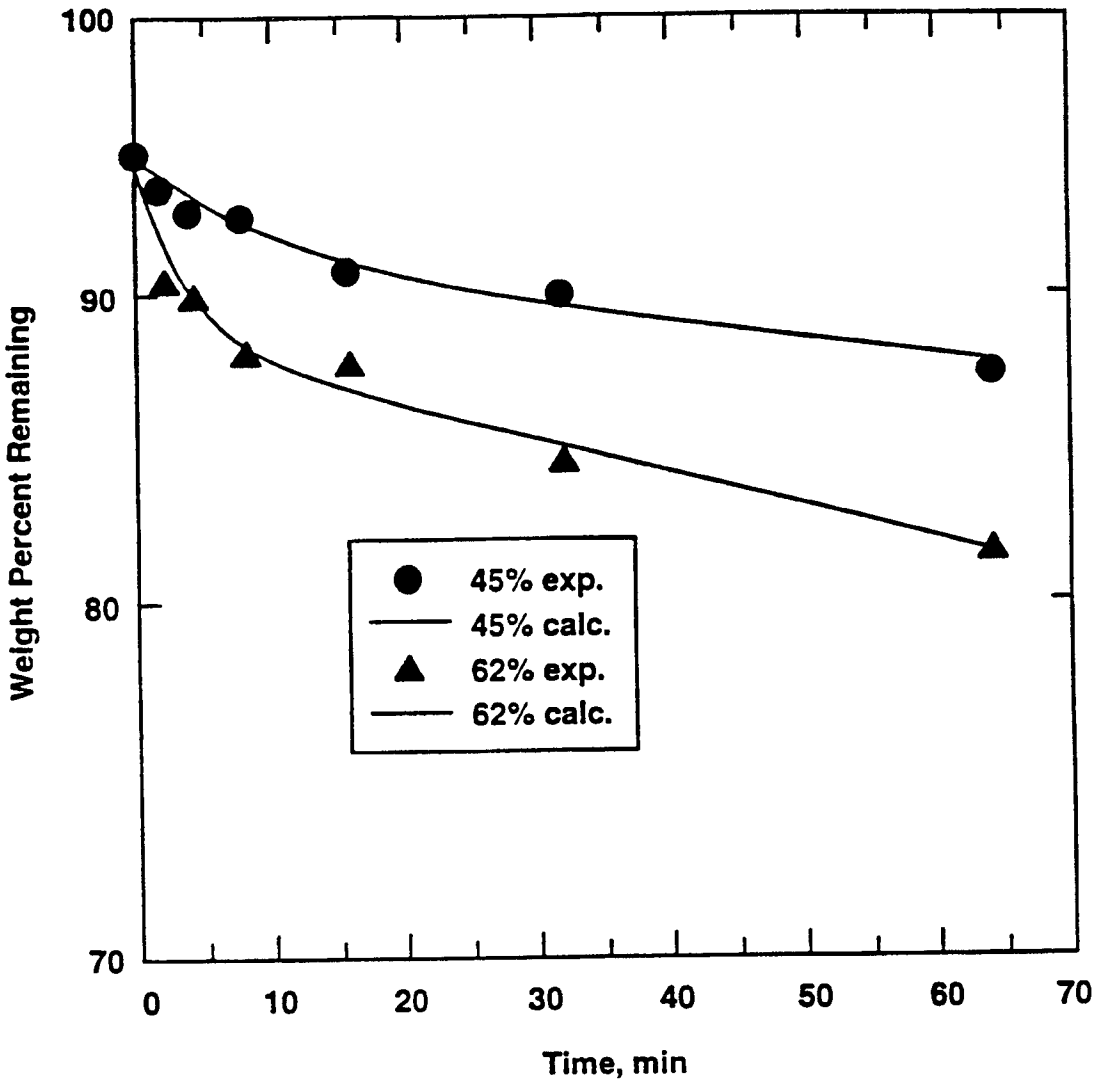

Model Parameter values used are:

Concentration	f	S(min^{-1})	k(min^{-1})	W_o
45	0.04	0.1	$1.1x10^{-4}$	0.95
62	0.07	0.3	$2.3x10^{-4}$	0.95

Figure 2.1.7 APPLICATION OF CHIPPING/ABRASION MODEL TO ATTRITION OF NOMINAL 16x20 MESH TAGGART SEAM COAL AT DIFFERENT SOLIDS CONCENTRATIONS

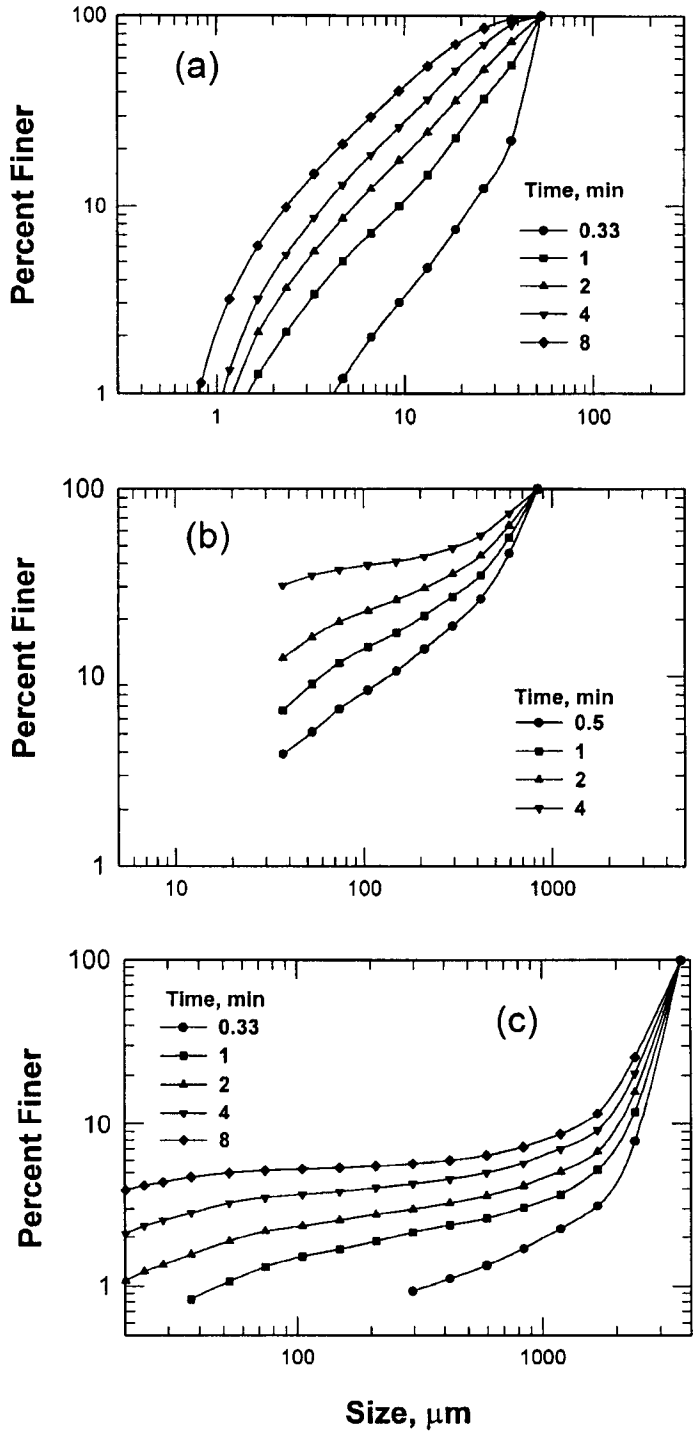

Figure 2.1.8 PRODUCT SIZE DISTRIBUTIONS IN THE ATTRITION MILLING OF QUARTZ USING QUARTZ MEDIA (6x8 mesh).
(a) 270x400 mesh feed, (b) 20x30 mesh feed, (c) 6x8 mesh media

particles are broken down progressively to finer and finer sizes (Figure 2.1.8 a). Breakdown of the coarser feeds especially the media particles themselves (Figure 2.1.8 c) shows quite different behavior. The bimodal character, indicated by the broad, flat "shelf" seen over the intermediate size ranges in the cumulative distributions, follows the same pattern as that seen for coal (Figure 2.1.6). For intermediate sizes (Figure 2.1.8 b), there appears to be a larger contribution from massive fracture as indicated by the progressive broadening of the coarse mode of the distribution.

2.1.4 Grinding Circuit Simulation

It is clear from the investigations carried out in Phases I and II of this project that single-stage grinding in a conventional ball mill does not produce size distributions with the form required for stable coal-water mixtures. Stirred ball milling was also found to be unable to produce the appropriate size distribution, although the product was much finer than that produced in the ball mill. It was concluded, therefore, that a circuit arrangement involving two-stage grinding was required to produce slurry with the proper size consist. One such circuit arrangement is shown in Figure 2.1.9.

In the first stage, crushed coal (e.g., -12 mesh), is introduced into a ball mill, along with water and dispersant where it is ground in closed circuit. The product from the first-stage grinding is then classified. The fine stream is further ground in a closed stirred ball mill circuit to produce an ultrafine fraction. This product is then combined with the coarser size fraction, producing a bimodal size distribution.

The ideal mixing ratio of coarse and fine particles for maximum packing is 60:40. Therefore, the production rates of the coarse and fine size fractions must be controlled accordingly. At the same time, the maximum size of the coarse fraction must be controlled for proper combustion, while the size ratio of the coarse and the fine fractions are kept sufficiently large (at least ten) for maximum solid loading and low viscosity.

It can be expected that the mean residence time, τ, for each mill determines the characteristics of the final circuit product. The mill residence time (and hence the extent of size reduction) is controlled by material flow rates and mill operating conditions. However,

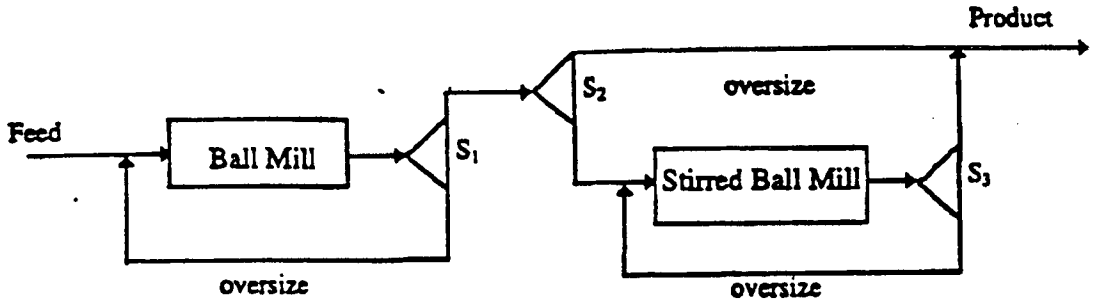

S_1 = Post-classifier for the first stage
S_2 = Pre-classifier for the second stage
S_3 = Post-classifier for the second stage

Figure 2.1.9 TWO-STAGE GRINDING CIRCUIT FOR PRODUCING COAL-WATER MIXTURES WITH A BIMODAL SIZE DISTRIBUTION

the operating variables are not completely independent of the design variables. Let Ω be the ratio of the hold-up of the first stage (W_1) to the hold-up of the second stage (W_2), that is, $\Omega=W_1/W_2$. For a simple two-stage closed circuit at steady state, the mass flow rate into the first stage (G_1) equals the mass flow rate into the second stage (G_2). Then, since the actual flow rate to the first mill is $F_1 = G_1(1+C_1)$, that to the second mill is $F_2 = G_2(1+C_2)$, $\tau_1 = W_1/F_1$ and $\tau_2 = W_2/F_2$:

$$\Omega = \frac{\tau_1(1+C_1)G_1}{\tau_2(1+C_2)G_2} \qquad (2.1.7)$$

where C_1 and C_2 are the circulation ratios of the first and the second stages, respectively.

For a fixed set of breakage parameters, mill residence time distributions, (RTD), and classifier settings, a particular value of τ_1 fixes the entire system for a given value of Ω. Therefore, the design criteria involving two mills in series are the mean residence time for the first mill, the classifier settings and the relative sizes of the two mills. Designing such a grinding circuit requires a simulator to evaluate the performance of a two mill grinding circuit under various operating conditions.

For this purpose, a general two-mill grinding circuit simulator has been developed at Penn State. The complete circuit scheme is shown in Figure 2.1.10. In its original form, the circuit consists of two ball mills in normal closed circuit, with a circuit pre-classifier and a pre-classifier before the second mill. Additionally, the circuit has three dividers so that the streams of the first and second mills can be appropriately connected. By assigning the appropriate values to the classifiers and dividers, the general two-stage circuit can be reduced to any desired circuit varying from a simple single-stage open circuit to a very complicated two-stage circuit. Evaluating the performance of a grinding circuit is achieved by combining the mill model and the classifier model via the appropriate mass balance equations. A detailed description of the computational procedure can be found elsewhere (Yildrim 1987).

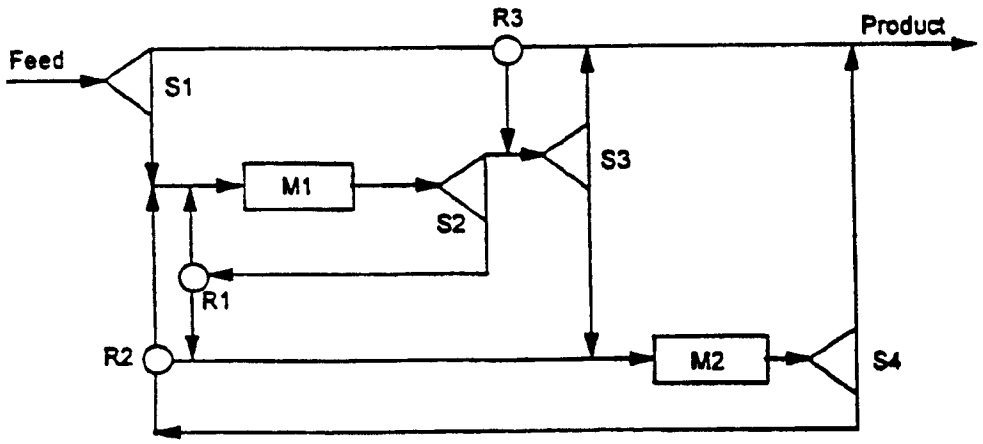

M1 = First Mill
M2 = Second Mill
S1 = Preclassifier
S2 = First Mill Classifier
S3 = Intermediate Preclassifier
S4 = Second Mill Classifier

R1 = First Mill Splitter
R2 = Second Mill Splitter
R3 = Third Splitter

Figure 2.1.10 GENERAL TWO-MILL GRINDING CIRCUIT

Before the simulator can be used to evaluate the circuit shown in Figure 2.1.9, several modifications are needed. The scale-up procedure involving the mill sizes and operating conditions for ball milling is well established as described in the previous report. However, the design procedure for stirred ball milling has not been completely established. It is often assumed that the specific energy is constant between the test and large mill for the same reduction ratios. The power draw of a stirred ball mill is a function of mill diameter and operating conditions. If operating conditions are selected for large mills to consume the same specific energy as the test mill, the simulation can be performed using the same breakage parameters as those determined by the laboratory milling tests.

Classification is done extensively throughout the coal industry. In most cases, separations are made at sizes coarser than about 40 μm using hydrocyclones. Such operations are common and existing data are available to model the size separations. However, classification of particles down to 10 μm and perhaps finer will be required for coal-water mixture production. Although separations in this size range are made in various mineral applications, they are not generally done in the coal industry. Therefore, selected tests were conducted using hydrocyclones to develop the appropriate parameters for the classification devices used in the circuit simulator.

The make-up feed size distribution (i.e., crushed product) was chosen as 80% passing 700 μm with a Gaudin-Schuhmann slope of 0.9. The parameters for the breakage rates and the breakage distribution were obtained through laboratory testing. The complete list of these parameters is given in Table 2.1.1. The ball mill was assumed to have a residence time distribution equivalent to one-large/two-small fully mixed tanks-in-series with relative hold-up ratios of 0.5, 0.25, 0.25, whereas the stirred ball mill was assumed to be fully mixed. The simulations were conducted for a 1 meter diameter by 1.5 meter long wet-overflow ball mill operating at 70 wt. % solids, a fractional ball load of 0.35, rotational speed 70% of critical, with a make-up ball size of 31.75 mm (1.25 inches). The relative size of the stirred ball mill to the ball mill was 1:10, operating at 40 wt. % solids, 0.6 fractional ball loading and a total charge volume (balls and slurry) of 0.9.

The classifiers were assumed to be hydrocyclones. The characteristic parameters for the selectivity values at various cut sizes were determined by laboratory testing and are shown in Table 2.1.3. It was assumed that an appropriate operation could be obtained to give suitable underflow and overflow slurry densities and flow rates for the desired cut sizes.

Table 2.1.3 Characteristic Parameters for the Cyclone Size Selectivity at Different Cut Sizes

Cyclone Diameter, inches	Overflow Diameter, inches	Underflow Diameter, inches	Cut Size, μm	Sharpness Index	Apparent By-pass	Flow Rate, liter/min.
1	0.28	0.06	25.2	0.56	0.04	16.2
1	0.28	0.06	17.3	0.44	0.06	16.2
1	0.28	0.13	14.2	0.43	0.06	16.5
2	0.38	0.13	39.8	0.51	0.08	37.7
2	0.38	0.19	26.7	0.36	0.12	35.6
2	0.38	0.38	14.8	0.33	0.50	35.9
10	0.38	3.00	148.0	0.53	0.20	1128.0

The predicted size distributions of the various streams for the grinding of the Taggart seam coal are shown in Figure 2.1.11, assuming the following conditions:

- residence time for the first mill $\tau_1 = 4$ minutes
- cut sizes for the first, second and third cyclones at 150 μm, 40 μm, and 17 μm, respectively.

The required mean residence time for the second mill was determined to be 3.8 minutes.

It can be seen that the final product size distribution, resulting from combining the first and second stage products, has a bimodal shape. The bimodal shape, though, is less well defined than in the batch grinding system due to the imperfect separation by the cyclones and the back-mixing occurring in the continuous mill. The median sizes for each stage product are 52 μm and 3.3 μm, respectively, and the size ratio of the coarse and finer sizes is 16. The proportion of the coarser and the finer size fraction is about 60:40, which is an ideal composition. The size ratio could be increased by reducing the cut size for the second-stage post-classifier. This would produce a more distinct bimodal shape for the final product size

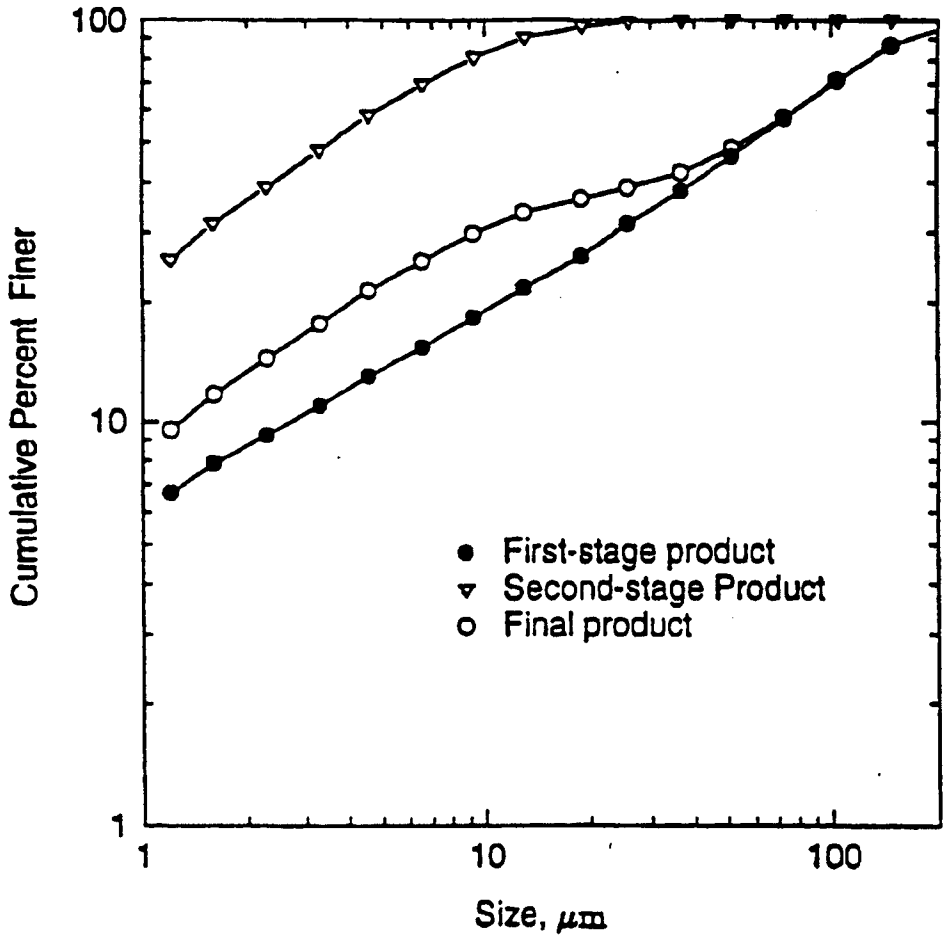

Figure 2.1.11 PRODUCT SIZE DISTRIBUTIONS IN A TWO-STAGE GRINDING CIRCUIT

distribution. However, this would also result in a decrease in the production rate for the second stage grinding, and hence, require a larger stirred ball mill.

2.1.5 Integrated Grinding/Cleaning Circuit

An important potential advantage of coal-water slurry technology over conventional coal firing lies in the opportunity for advanced coal cleaning, which is offered by the associated fine grinding but is not offset by the need for expensive product dewatering.

Integration of a multi-stage grinding operation with a physical cleaning process such as froth flotation offers several opportunities for cost-effective deep cleaning of coal. With many coals, for example, it is possible to separate a clean fraction at a relatively coarse size; grinding of the remainder of the coal can then be used to provide for sulfur and mineral matter liberation and to produce the finer fractions needed for slurry preparation. The use of an integrated grinding/cleaning process offers considerable potential for cost saving by exploiting the liberation of mineral matter obtained by fine grinding to permit extensive deep-cleaning of the coal. By integrating the grinding and cleaning steps, it should be possible to grind the raw (or pre-cleaned) feed coal only to the extent needed to achieve liberation of the sulfur and ash-forming minerals. Further, multi-stage grinding of the coal would then be carried out so as to produce the optimum size distribution for slurry formulation.

An example of an integrated grinding/cleaning process is illustrated in Figure 2.1.12. The system consists of two basic elements:

- A liberation/cleaning step in which grinding is performed only to the extent needed for liberation of the mineral matter.
- A secondary (2-stage) grinding/classification step in which additional size reduction is carried out as needed to produce the desired final product size distribution.

The first stage consists of a grinding circuit, which is closed by means of a separator (e.g., froth flotation device) rather than by the size classifier employed in conventional grinding circuits. The flotation system could be a bank of conventional cells set up to produce a low-ash, clean-coal product, a high-ash middlings product, and a refuse stream. The middlings product is recycled to the grinding to obtain further liberation. Alternatively, the same objective could be achieved using a two-stage column-flotation set-up. By maintaining a high circulation ratio, it should be possible to obtain a high degree of liberation while minimizing overgrinding of either the combustible or refuse materials.

The second, finish-grinding step consists of a closed-circuit grinding system set to maintain the desired top-size in the product slurry. A portion of the output from this circuit is further ground to form the fine component of the final, bimodal slurry.

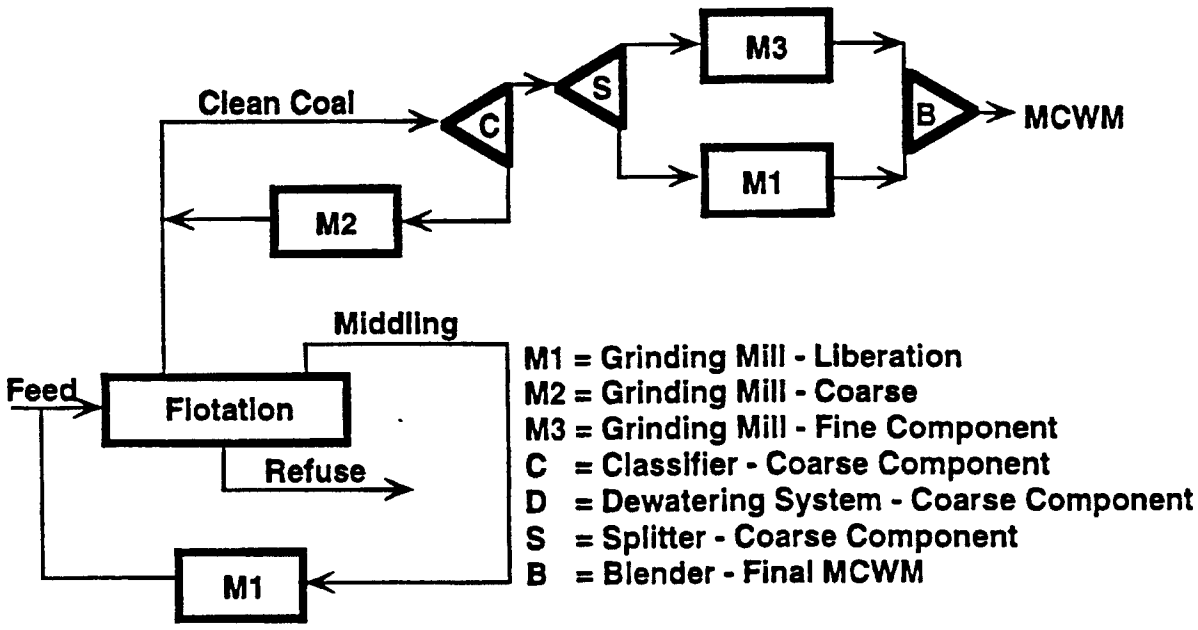

Figure 2.1.12 EXAMPLE OF AN INTEGRATED CLEANING/SIZE-REDUCTION PROCESS FOR MICRONIZED COAL-WATER MIXTURE (MCWM) PRODUCTION

Additional, intermediate stages of classification can be included in order to produce a true bimodal distribution. Alternative circuit configurations such as that shown in Figure 2.1.11 could also be used for the finish-grinding stage. A further advantage of the two-stage, finish-grinding step is that relatively simple dewatering procedures can be applied to the coarse product for control of the final slurry density.

2.2 Physical Separations

Separations of fine coal based on differences in particle size and density were performed. The size separations were carried out using a high-speed, solid-bowl centrifuge under various operating conditions. Centrifuge performance was evaluated in terms of the size selectivity curves and corresponding performance parameters -- cut size, sharpness index, and apparent bypass.

Density separations were carried out using both dense medium and magnetic fluid systems. The dense-medium separations were also made with the solid-bowl centrifuge using magnetite and water as the dense medium. The magnetic fluid separations were carried out in both batch and continuous laboratory separators using water-based magnetic fluids. These systems offer the advantage of changing the relative density of the fluid (medium) simply by varying the intensity of the magnetic field.

In order to extend the size range of fine coal cleaning further, testing was carried out using an integrated centrifugal/flotation system. In this case, fine coal was cleaned with a dense-medium cyclone followed by froth flotation. The addition of the flotation step not only increased the recovery and quality of the finer coal, but it also improved the quality of the recovered dense medium.

2.2.1 Fine Coal Classification

One of the key elements in fine coal cleaning and slurry preparation circuits is size classification, which involves the preparation of coal into the appropriate size ranges. Industrially, hydrocyclones are commonly used to classify coal down to approximately 75 μm (200 mesh). Although the size range can be extended down to about 10 μm, this requires the use of small diameter (and low capacity) cyclones. An alternative would be to use a continuous centrifuge. For this study, a continuous, solid-bowl centrifuge (Sharples Model P660) was used to classify -150 μm (-100 mesh) Upper Freeport seam coal. A schematic of the unit is given in Figure 2.2.1. The test variables included bowl and scroll speeds, and pond depth (weir setting). For all tests, the unit was operated at a constant volumetric slurry feed rate of 11.4 lpm (3 gpm) and a solids concentration of 10% coal (by weight).

For each test, simultaneous samples of the weir overflow (fine product) and scroll discharge (coarse product) were taken. Each sample was analyzed using a Microtrac X-100 particle size analyzer. From the size distribution data, the circulation ratio, which is defined as the solids mass flow rate of the coarse stream, T, divided by the solids mass flow rate of the fine stream, Q, was estimated by (Klimpel 1980):

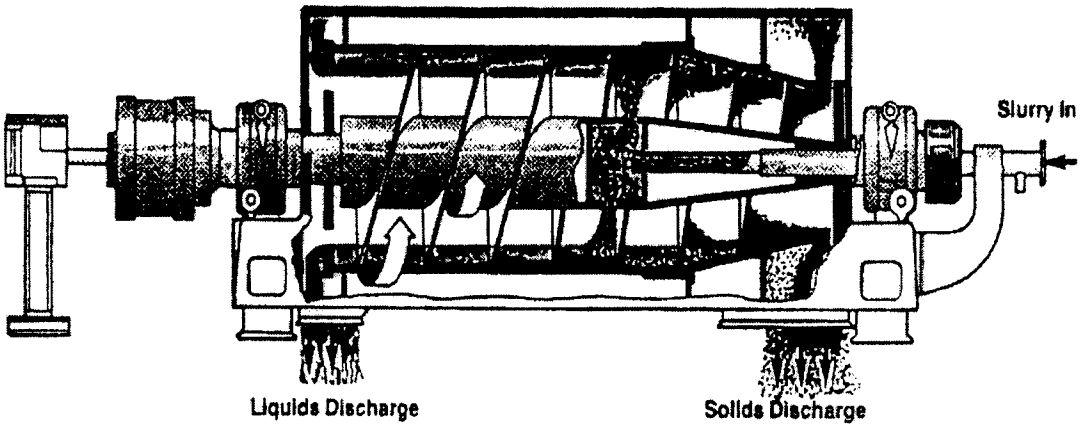

Figure 2.2.1 **SCHEMATIC OF A SOLID-BOWL CENTRIFUGE (courtesy of Alfa Centrifuges)**

$$C = \frac{\sum_{i=1}^{n-1}[p_i - q_i]}{\sum_{i=1}^{n-1}[t_i - p_i]} \qquad (2.2.1)$$

where p_i, t_i, and q_i are the fractions of material in size interval i for the feed, coarse, and fine streams, respectively, and n is the number of size intervals. The circulation ratio is related to the yield to the fine stream, Y_Q, by

$$Y_Q = \frac{1}{1+C} \qquad (2.2.2)$$

The yield to the coarse stream, Y_T, is then simply $Y_T = 1 - Y_Q$.

Knowing the product size distributions and the circulation ratio, the size selectivity values were calculated by

$$s_i = \frac{t_i C}{p'_i(1+C)} \qquad (2.2.3)$$

where p_i' is the reconstituted feed for size interval i given by

$$p'_i = \frac{q_i + t_i C}{1 + C} \tag{2.2.4}$$

The size selectivity values were corrected for apparent bypass, a, by

$$c_i = \frac{s_i - a}{1 - a} \tag{2.2.5}$$

where c_i is the corrected selectivity (classification) value for size interval i. In order to determine the characteristic performance parameters -- the cut size, d_{50}, the sharpness index, κ, and the apparent bypass, a -- the classification values were fitted to the log-logistic function given by

$$c_i = \frac{1}{1 + \left(\frac{x_i}{d_{50}}\right)^{-\lambda}} \tag{2.2.6}$$

where $\lambda = \exp[-2.1972/\kappa]$. The d_{50} value is the size that corresponds to c_i=0.5, and $\kappa = d_{25}/d_{75}$, where d_{25} and d_{75} are the sizes that correspond to c_i values of 0.25 and 0.75, respectively. The sharpness index varies from zero for no separation to one for a perfect separation. The parameters d_{50}, κ, and a were determined using a nonlinear optimization routine contained in a spreadsheet program.

The first series of tests was conducted using the minimum weir setting, which gave the shallowest pond depth (i.e., setting 1 = shallowest pool, setting 4 = deepest pool). Table 2.2.1 summarizes the operating conditions and results for this series of tests (series a). Figure 2.2.2 shows the reconstituted feed and product size distribution curves for centrifuge tests 1a and 2a. As can be seen, the product size distribution of the fine stream for test 2a was finer than that for test 1a. For example, 85.8% of the material in the fine stream was less than 11 μm for test 2a compared to 53.2% for test 1a. Figure 2.2.3 shows the size selectivity values and fitted curves obtained for tests 1a-4a, while the parameters are given in Table 2.2.1. The cut size was the coarsest at the highest scroll speed, while the cut sizes at the other conditions were comparable. At the highest scroll speed, the speed differential between the bowl and the scroll was the smallest, resulting in a slower discharge of solids.

Table 2.2.1 Summary of the Operating Conditions and Test Results for the Solid-Bowl Centrifuge (Feed Rate = 11.4 L/min, Solids Concentration = 10% by weight)

				Yield, %		Characteristic Parameters		
Test	**Bowl Speed, rpm**	**Scroll Speed, rpm**	**Weir Setting**	**Coarse Product**	**Fine Product**	**d_{50}, μm**	**κ**	**a**
1a	4600	4125	1	77.4	22.6	18.9	0.36	0.23
2a	4600	3650	1	91.0	9.0	8.1	0.47	0.28
3a	4600	2700	1	92.1	7.9	4.4	0.35	0.21
4a	4600	800	1	88.9	11.1	6.4	0.44	0.00
5a	3750	1850	1	88.9	11.1	7.7	0.56	0.14
1b	4600	4125	2	86.6	13.4	9.9	0.47	0.39
2b	4600	3650	2	91.3	8.7	7.4	0.63	0.33
3b	4600	2700	2	83.3	16.7	7.9	0.52	0.19
4b	4600	800	2	88.5	11.5	6.7	0.44	0.26
5b	3750	1850	2	88.7	11.3	7.2	0.52	0.14
1c	4600	4125	3	88.8	11.2	7.4	0.52	0.41
2c	4600	3650	3	85.4	14.6	7.0	0.59	0.22
3c	4600	2700	3	80.4	19.6	10.5	0.54	0.29
4c	4600	800	3	93.5	6.5	7.2	0.50	0.65
5c	3750	1850	3	90.0	10.0	8.6	0.53	0.48

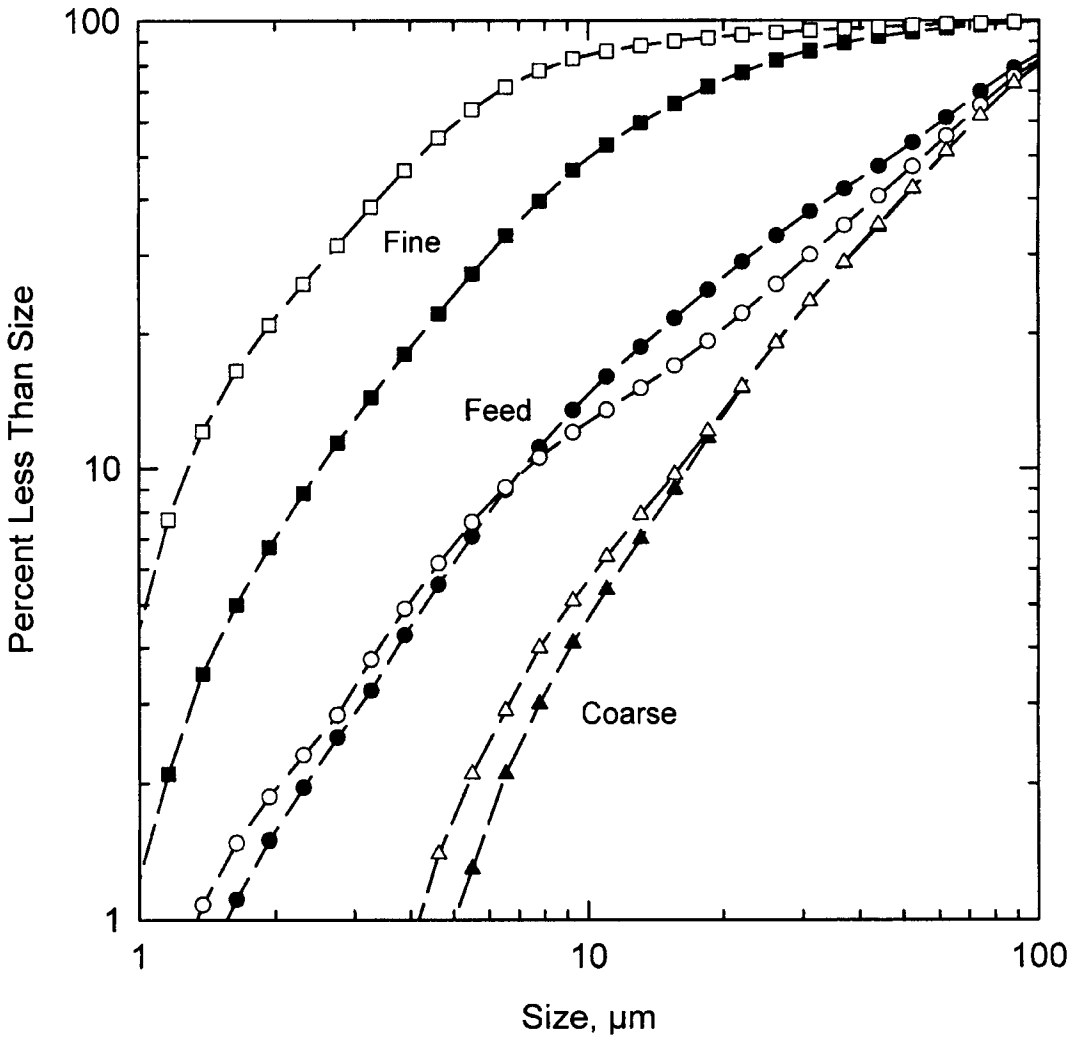

Figure 2.2.2 FEED AND PRODUCT SIZE DISTRIBUTIONS FOR CENTRIFUGE TESTS 1a AND 2a WHEN SEPARATING –100 MESH UPPER FREEPORT SEAM COAL (test 1a: filled symbols; test 2a: open symbols)

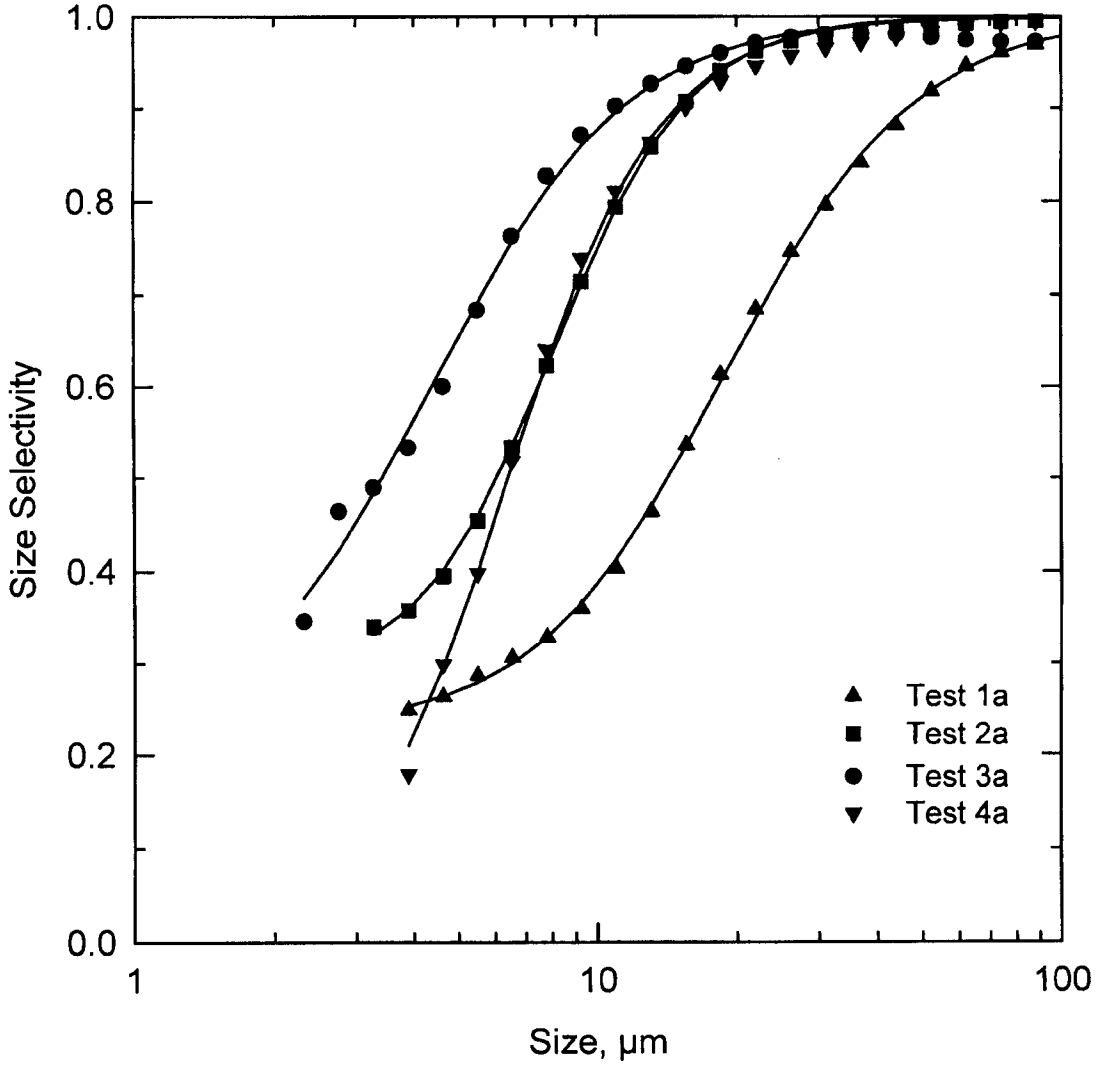

Figure 2.2.3 EFFECT OF SCROLL SPEED ON THE SIZE SELECTIVITY CURVES IN THE SOLID-BOWL CENTRIFUGE FOR WEIR SETTING 1

Hence, coarser solids reported to the weir (fines) discharge, leading to a coarser separation. This is also reflected in the lower coarse product yield for test 1a.

The next series of classification tests was carried out with a new weir setting. This resulted in the formation of a slightly deeper pool than used in the previous tests. The test variables were the same as in the previous series. Table 2.2.1 summarizes the operating conditions for these (series b) tests.

Figure 2.2.4 shows the size selectivity curves for tests 1b-4b. The corresponding parameters are given in Table 2.2.1. Overall, the cut size of the centrifuge ranged from about 7 to 10 μm, while the sharpness index ranged from 0.44 to 0.63. The primary impact of the bowl and scroll speeds at this weir setting was on the apparent bypass values, which ranged from 0.14 to 0.39 (Table 2.2.1).

The last series of tests (series c) was conducted using weir setting 3, which gave the second deepest pool setting. The operating conditions and results are also summarized Table 2.2.1. Figure 2.2.5 shows the reconstituted feed size distribution and product size distribution curves for centrifuge tests 1c and 2c. As can be seen, the product size distribution of the weir discharge stream for test 2c was slightly finer than that for test 1c, while the scroll discharge was coarser.

Figure 2.2.6 shows the corresponding size selectivity curves for tests 1c-4c. Overall, the cut sizes of the centrifuge again ranged from about 7 to 10 μm. The sharpness indexes were very similar and ranged from 0.50 to 0.59. As was seen at the other weir settings, the bowl and scroll speeds impacted the apparent bypass values, which ranged from 0.22 to 0.65 (Table 2.2.1). High bypass values indicate that a substantial fraction of the feed coal is reporting to the coarse stream, resulting in a finer size distribution of the coarse material. On the other hand, the bypass does not affect the size distribution of the fine stream.

Because the sharpness indexes were similar for these tests, it was possible to reduce the size selectivity curves to a single reduced classification curve. The reduced classification curve was generated by plotting the classification values versus the reduced size (defined as the size divided by the cut size). The reduced curve for centrifuge tests 1c-4c is shown in Figure 2.2.7.

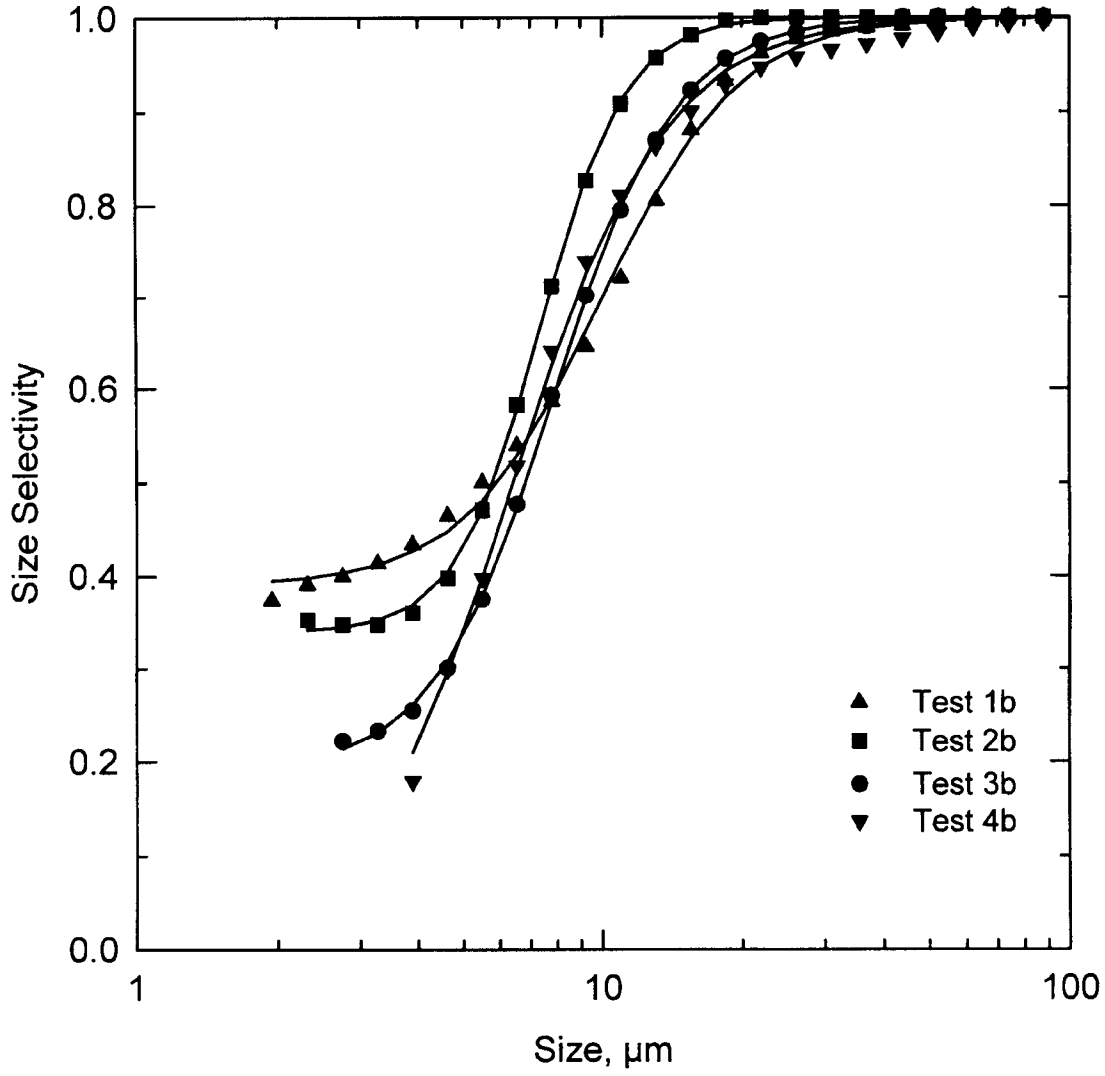

Figure 2.2.4 EFFECT OF SCROLL SPEED ON THE SIZE SELECTIVITY CURVES IN THE SOLID-BOWL CENTRIFUGE FOR WEIR SETTING 2

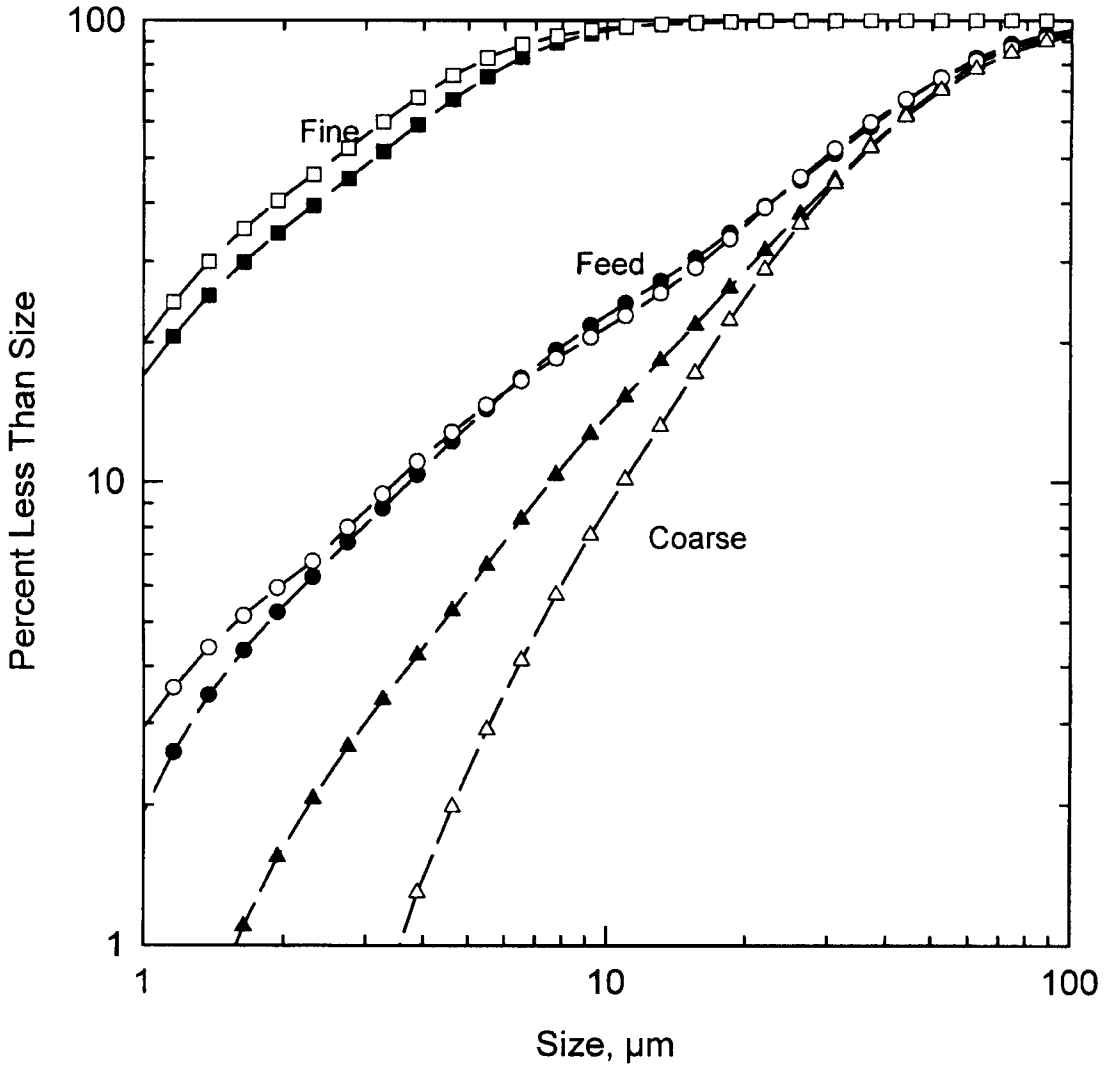

Figure 2.2.5 FEED AND PRODUCT SIZE DISTRIBUTIONS FOR CENTRIFUGE TESTS 1c AND 2c WHEN SEPARATING –100 MESH UPPER FREEPORT SEAM COAL
(test 1c: filled symbols; test 2c: open symbols)

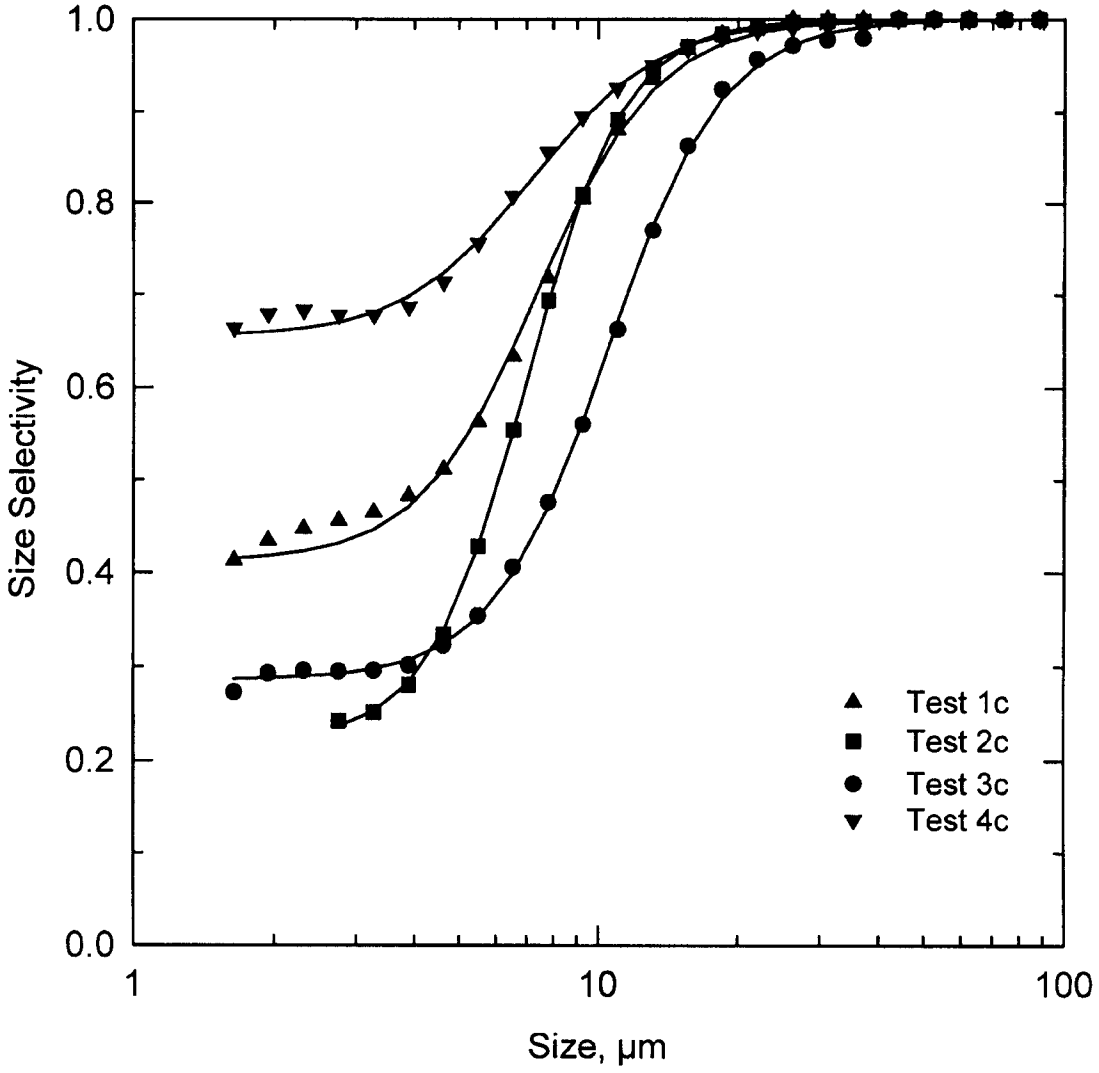

Figure 2.2.6 **EFFECT OF SCROLL SPEED ON THE SIZE SELECTIVITY CURVES IN THE SOLID-BOWL CENTRIFUGE FOR WEIR SETTING 3**

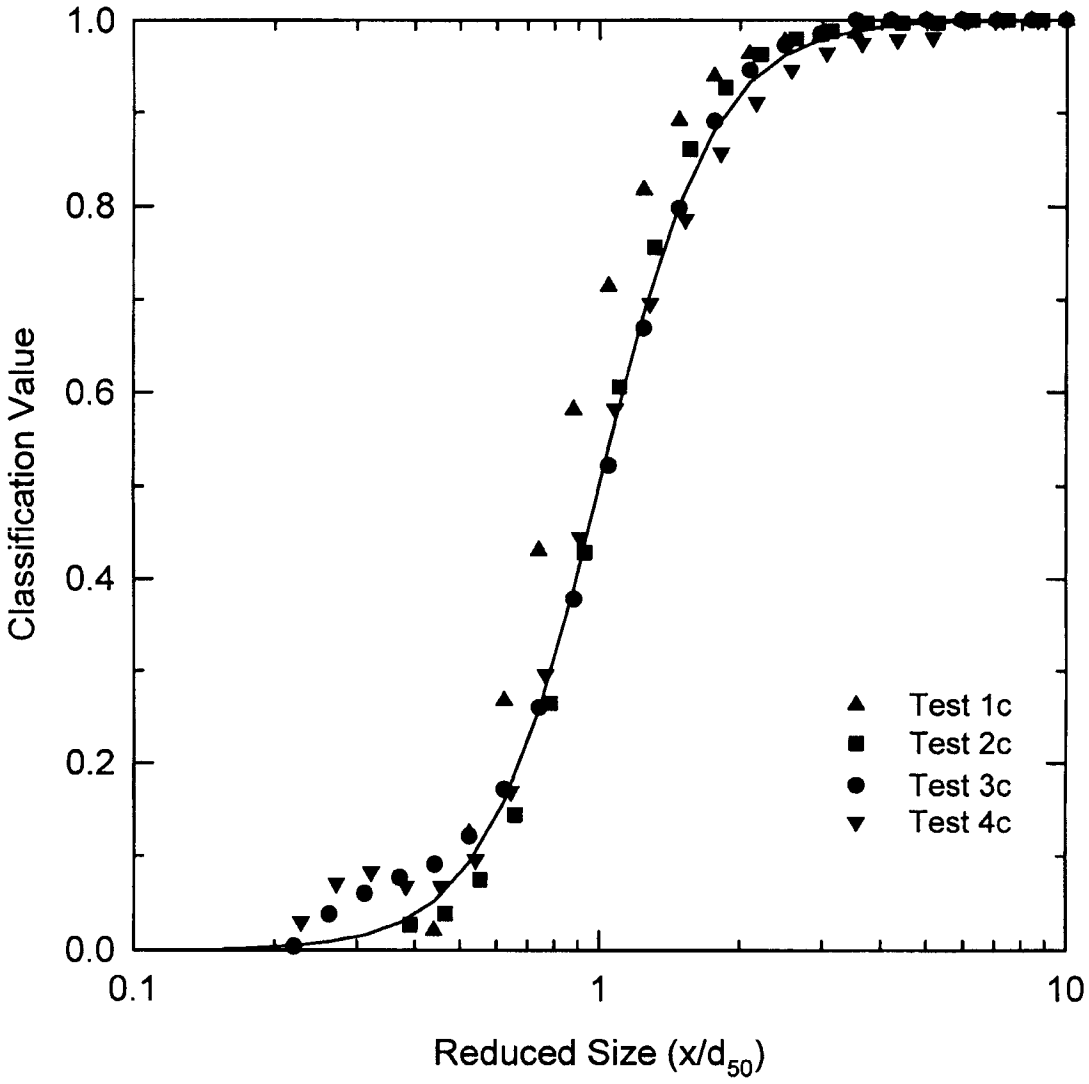

Figure 2.2.7 REDUCED CLASSIFICATION CURVE FOR CENTRIFUGE TESTS 1c –4c

Except for test 1c, the values fall on a single curve. In such cases, this curve can be used to predict separator performance. For example, by selecting an appropriate cut size and corresponding apparent bypass, it is possible to generate the size selectivity values, which in turn can be used to calculate the product size distribution for a given feed size distribution.

2.2.2 Dense-Medium Separation

Dense-medium separations were also carried out using the Sharples P660 solid-bowl centrifuge. Testing was conducted to evaluate the effect of operating conditions such as bowl and scroll speeds, weir height, relative density of the medium, medium-to-coal ratio, and feed rate on separation efficiency. All tests were run using -100 mesh Upper Freeport seam coal.

For each test, samples of the clean coal (weir overflow) and refuse (scroll discharge) streams were taken. Wet screening at 25 μm (500 mesh) was used to remove the -500 mesh material. The yield of 100x500 mesh clean coal was calculated by ash balance as

$$Y_c = \frac{A_P - A_F}{A_F - A_R} \tag{2.2.7}$$

where A_F, A_P, and A_R are the ash contents of the feed, clean coal, and refuse streams, respectively.

For selected samples, a float-sink analysis was done at several relative densities on both centrifuge products. Using these data, along with the clean coal yield, the partition values for each relative density interval were calculated by

$$K_j = \frac{p_j Y_c}{p_j Y_c + r_j (1 - Y_c)} \tag{2.2.8}$$

where p_j and r_j are the fractions of clean coal and refuse in relative density interval j, respectively. These values give the fraction of feed in a given relative density interval that reports to the clean coal. In order to determine the characteristic performance parameters -- relative density of separation, ρ_{50}, and probable error, E_p -- the partition values were fitted to the logistic function given by

$$K_j = \frac{1}{1+\exp[(1.0986/E_p)(\rho_j - \rho_{50})]} \qquad (2.2.9)$$

where ρ_j is the mean relative density of the interval. The parameters were determined using a nonlinear optimization routine.

The operating conditions and results for the first set of tests are summarized in Table 2.2.2. All tests were carried out at a relative density of the medium of 1.3. Figure 2.2.8 shows the centrifuge results for various bowl speeds at a constant scroll speed (tests 1-3), along with the washability curve for the 100x500 mesh Upper Freeport seam coal. The results approached the washability curve for the lower two bowl speeds but deviated at the higher speed. No separation was obtained at a bowl speed of 2,400 rpm (Table 1.2.2). Tests 2, 4 and 5 show the effect of changing the weir height and in turn, pond depth for constant bowl and scroll speeds. In both cases, the results indicate that the centrifuge achieved very good separations at relative densities above about 1.5, even though the relative density of the medium was 1.3. This was not unexpected because the offset (i.e., the difference between ρ_{50} and the relative density of the medium) is typically greater than 0.05 relative density units for dense-medium cyclone separations.

Table 2.2.2 Summary of the Operating Conditions and Test Results for the Solid-Bowl Centrifuge (Medium Relative Density = 1.3, Feed Rate = 11.3 L/min (3 gpm), Medium-to-Coal Ratio = 10:1, Scroll Speed = 300 rpm)

Test	Bowl Speed, rpm	Weir Setting	Overflow Ash, %	Underflow Ash, %	Overflow Yield, %
1	800	2	6.9	63.0	91.7
2	1200	2	5.4	56.1	87.9
3	1500	2	4.9	27.5	70.7
4	2400	2	-	11.5	0.0
5	800	1	5.6	46.0	85.3
6	800	3	5.8	37.2	81.7

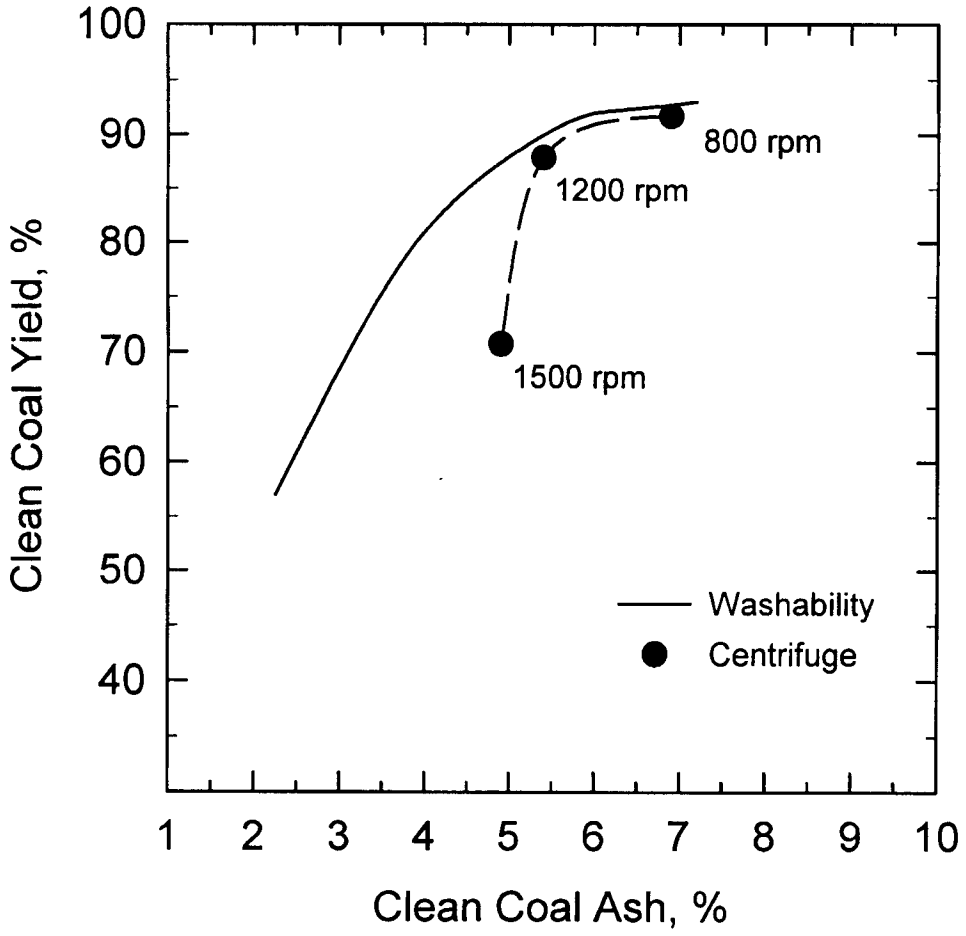

Figure 2.2.8 EFFECT OF BOWL SPEED ON THE GRADE-YIELD VALUES FOR THE SOLID-BOWL CENTRIFUGE AT A CONSTANT SCROLL SPEED OF 300 RPM AND A MEDIUM RELATIVE DENSITY OF 1.30 FOR THE 100x500 MESH UPPER FREEPORT SEAM COAL

Another set of tests was carried out with the centrifuge to evaluate the effects of bowl and scroll speeds, weir height, relative density of the medium, medium-to-coal ratio, and feed rate. Minus 100 mesh Upper Freeport seam coal was again used for all tests. Table 2.2.3 summarizes the operating conditions and results for these tests.

Figure 2.2.9 shows the partition curves obtained for several bowl speeds, with all other conditions constant. As seen, the best separation, based on the lowest probable error, was obtained for the middle bowl speed of 800 rpm (test 16). The relative density of

Table 2.2.3 Summary of the Operating Conditions and Test Results for the Solid-Bowl Centrifuge.

Test	Feed Rate,	Relative Density	Medium-to-Coal	Weir Height*	Bowl Speed,	Scroll Speed, rpm	Yield, %	Clean Coal Ash,	Refuse Ash,
1	11.4	1.3	20:1	4	500	300	56.4	8.4	15.5
2	11.4	1.3	20:1	4	700	300	69.4	6.1	23.7
3	11.4	1.3	20:1	4	800	300	66.2	6.0	22.2
4	11.4	1.3	20:1	4	900	300	62.9	6.8	19.5
5	11.4	1.3	20:1	4	1000	300	43.1	6.1	15.6
6	11.4	1.3	20:1	4	800	500	64.8	8.2	17.5
7	11.4	1.3	20:1	4	800	700	55.8	8.9	14.8
8	9.5	1.3	20:1	4	700	300	24.7	6.4	13.2
9	13.2	1.3	20:1	4	700	300	37.6	6.6	14.5
10	15.1	1.3	20:1	4	700	300	53.0	7.2	16.4
11	11.4	1.3	15:1	4	800	300	38.8	6.5	14.7
12	11.4	1.3	10:1	4	800	300	39.9	6.3	14.3
13	11.4	1.5	20:1	4	800	300	70.7	6.7	23.0
14	11.4	1.6	20:1	4	1200	300	45.9	5.8	16.4
15	11.4	1.3	20:1	1	600	300	92.3	7.7	57.7
16	11.4	1.3	20:1	1	800	300	89.4	6.0	58.1
17	11.4	1.3	20:1	1	3200	300	90.2	6.4	58.7
18	11.4	1.2	20:1	1	800	300	80.3	5.3	37.3
19	11.4	1.25	20:1	1	800	300	82.0	6.0	37.0
20	11.4	1.15	20:1	1	800	300	0.0	-	-
21	11.4	1.3	10:1	1	800	300	85.3	5.6	46.0
22	11.4	1.25	10:1	1	800	300	85.0	5.8	44.0

1 = shallowest pond depth; 4 = deepest pond depth

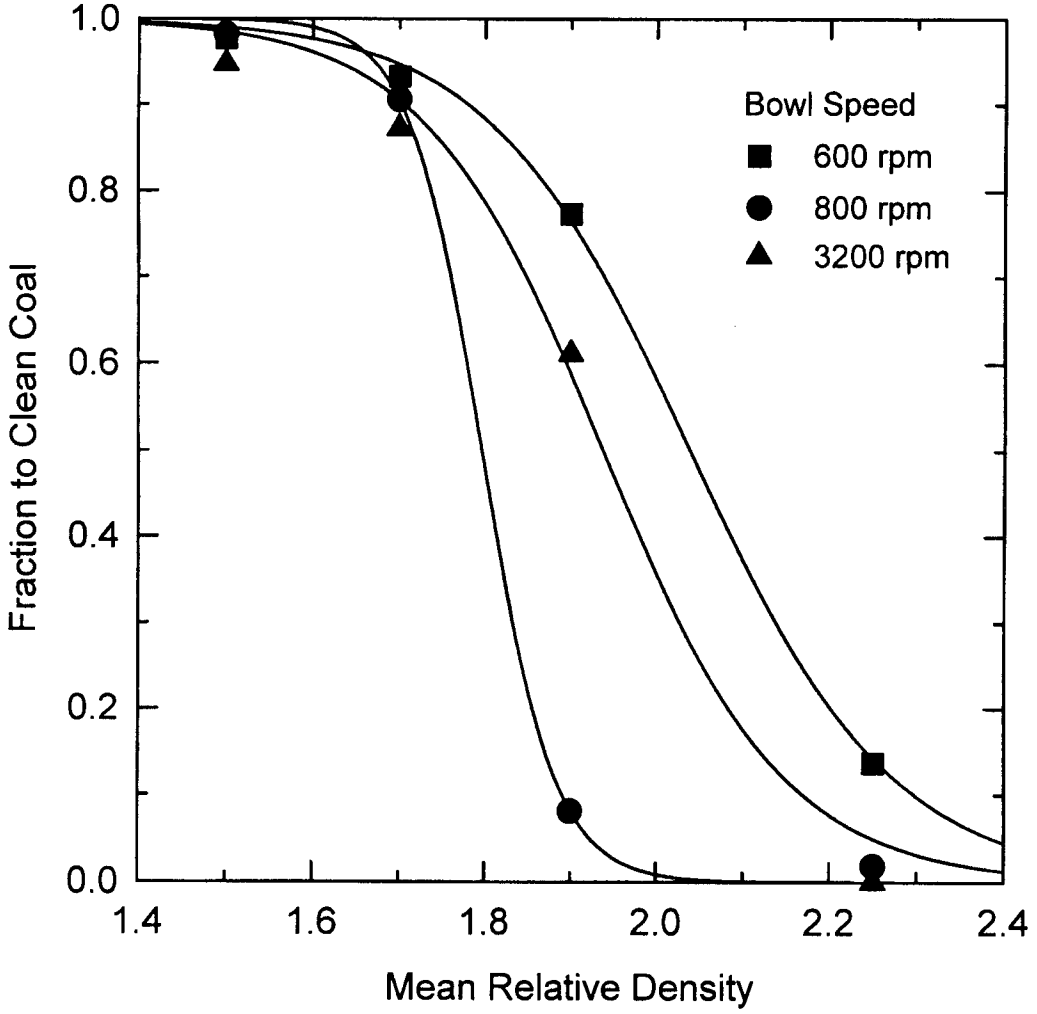

Figure 2.2.9 EFFECT OF BOWL SPEED ON THE PARTITION CURVES WHEN SEPARATING 100x150 MESH UPPER FREEPORT SEAM COAL IN THE SOLID-BOWL CENTRIFUGE
(600 rpm (test 15): E_r=0.13, r_{50}=2.04; 800 rpm (test 16): E_r=0.05, r_{50}=1.80; 3200 rpm (test 17): E_r=0.12, r_{50}=1.94)

separation was also the lowest at this condition. At the highest speed (3,200 rpm), both the E_p and ρ_{50} values were higher (test 17). Because there was a lack of coal in this relative density range, the yield and corresponding ash values were similar. However, for the bowl speed of 600 rpm (test 15), the higher relative density of separation produced a slightly higher yield (92% versus 90%) but with a much higher clean coal ash content (7.7% versus 6.4%).

Overall, the ρ_{50} values were much higher than the relative density of the medium (1.3). As noted previously, a positive offset is typical for dense-medium separations. For these tests, the higher offset can be attributed, in part, to the use of the minimum weir setting, which gave the shallowest pond depth. Hence the probability that a larger amount of material would exit to the overflow stream was higher, which was reflected in the higher ρ_{50} values.

2.2.3 Magnetic Fluid Separation

Density separations were also carried out using magnetic fluids as the dense medium. The separations were carried out using one of several laboratory separation cells constructed out of Plexiglas to fit within a Franz magnetic separator. New pole pieces were fabricated for the Franz unit to accommodate the separators, while providing the necessary magnetic field gradient (Fofana 1997).

Initially, coal separations were made using a batch unit under static conditions to calibrate the device (Figure 2.2.10). Narrow size (i.e., 6x8 mesh) and narrow relative density (e.g., 1.28x1.30) fractions of bituminous coal were prepared by heavy liquid fractionation. One of the coal fractions was placed in the magnetic fluid of a known concentration. The magnetic field intensity was increased until the material just began to float. This was repeated for ten relative density fractions to establish a calibration curve (Figure 2.2.11). Subsequent tests, which were carried out using purchased plastic tracer particles of a fixed density, confirmed the calibration curve.

After calibration, a series of separations was made using a sample of the nominal -1/4" Upper Freeport seam coal, which was screened to produce 12x14 mesh and 28x100 mesh size fractions. Separations were made at 1.3, 1.4, 1.5, 1.6, and 2.0 relative densities using the magnetic fluid separator under static conditions. A parallel approach

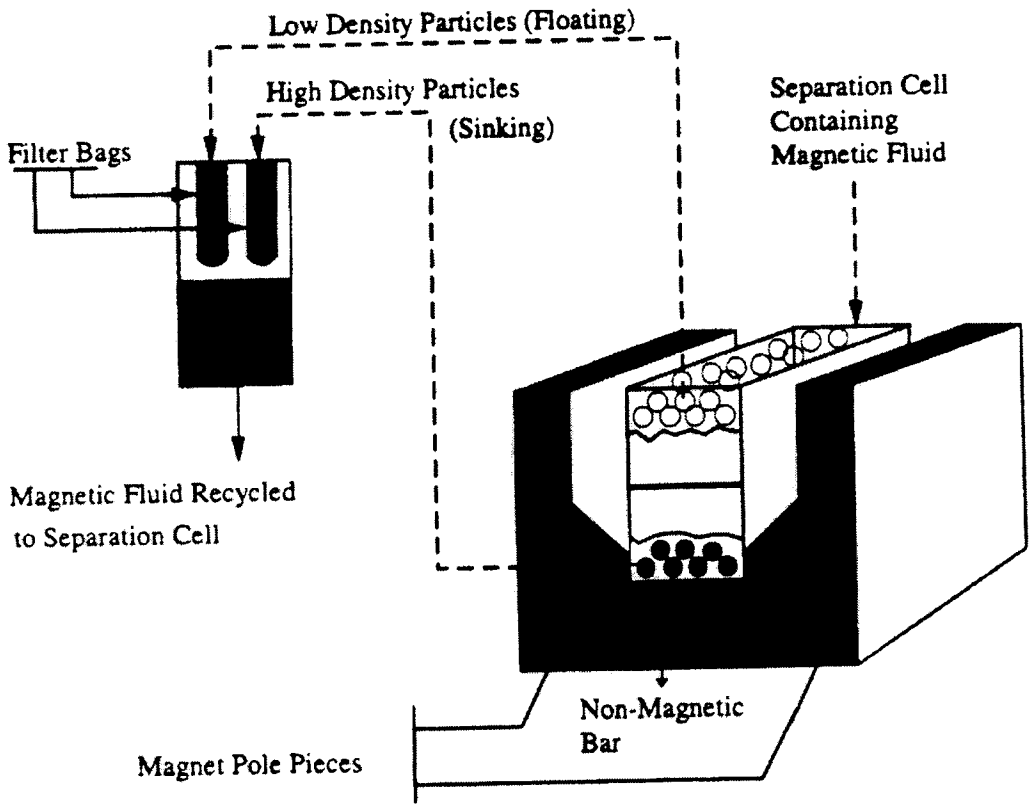

Figure 2.2.10 SCHEMATIC OF THE BATCH MAGNETIC FLUID SEPARATOR AND MAGNET POLE PIECES

was used whereby a separate sample was used for each test, thereby providing cumulative float and sink values at each relative density.

Prior to immersion in the magnetic fluid, the coal was wetted using a small amount of 0.1% Aerosol OT solution followed by rinsing with the magnetic fluid. After setting the relative density, the coal was added to the separator and allowed to stand for one hour. At that time, the products were separated by first collecting the float material followed by removal of the sink material. The samples were washed with water to remove any remaining liquid, dried, and weighed to determine the yield at each relative density. An ash analysis was done on each fractionated sample.

The resulting values, along with those obtained using heavy-liquid fractionation, are plotted in Figures 2.2.12 and 2.2.13 for the 12x14 mesh and 28x100 mesh size fractions, respectively. Ideally, both liquids should produce the theoretically best

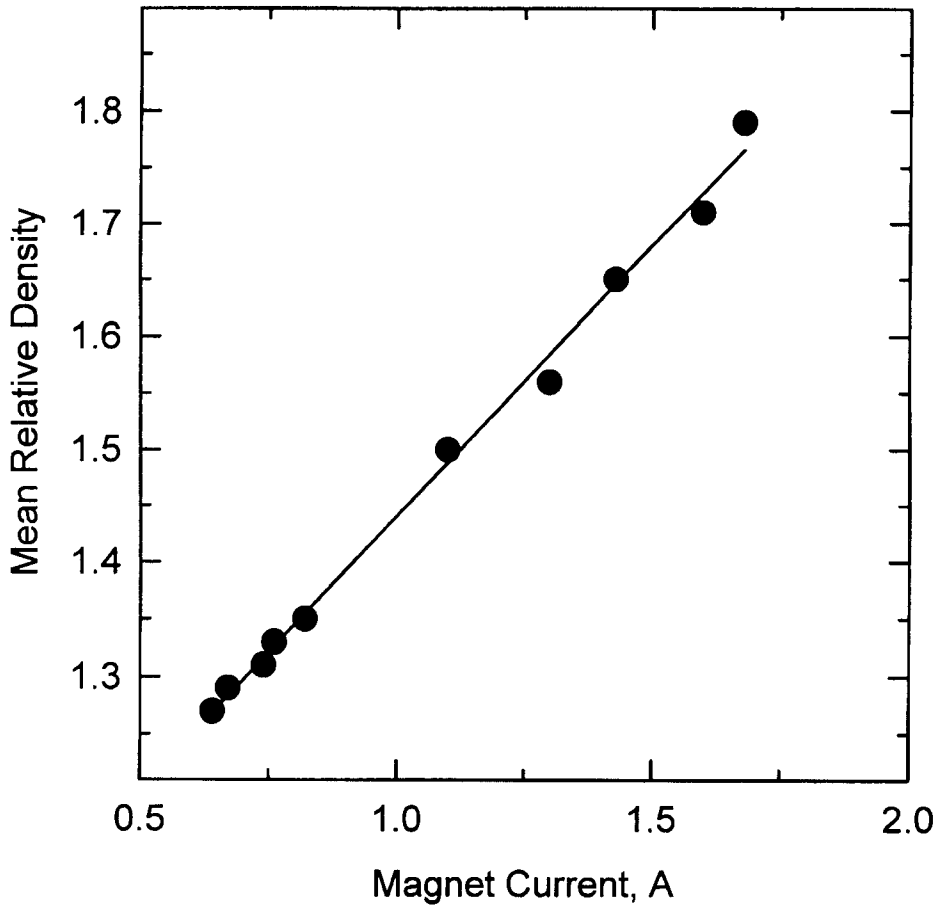

Figure 2.2.11 VARIATION OF THE RELATIVE DENSITY OF THE FLUID AS A FUNCTION OF THE APPLIED CURRENT FOR THE MAGNETIC-FLUID SEPARATOR

separation possible at a given relative density, i.e., the washability curve for the given size fraction. Therefore, the differences in the results can be attributed, in part, to the differences in the properties of the two liquids. That is, the magnetic fluid was water based, while the heavy liquids were organic. However, another explanation could be related to the slight variation in the magnetic field at different levels between the magnet poles. Because the resulting fluid density depends on the magnetic field gradient, any variation in the gradient would produce a non-uniform fluid density, leading to the differences in the float-sink results (Fofana 1997).

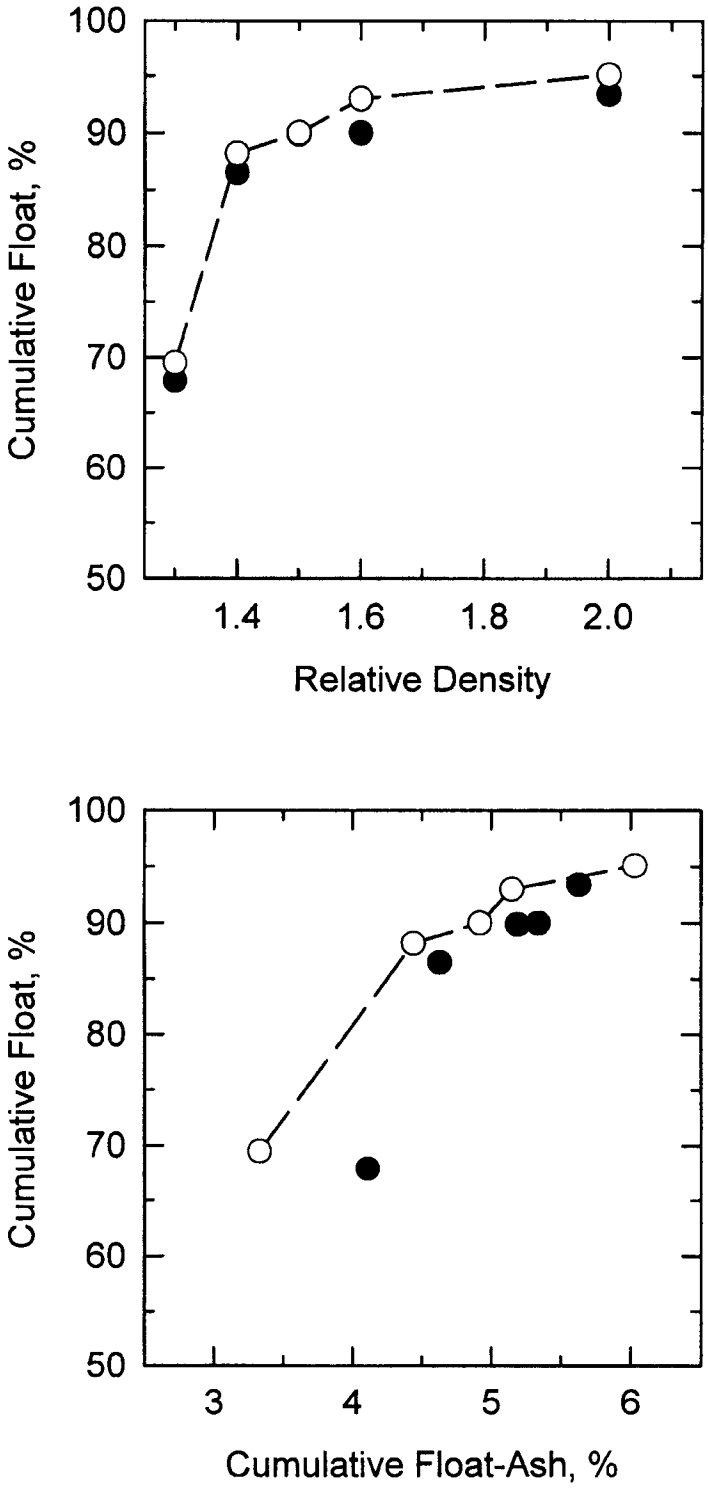

Figure 2.2.12 WASHABILITY CURVES FOR THE 12x14 MESH UPPER FREEPORT SEAM COAL
(open symbols: organic liquids; closed symbols: magnetic fluid)

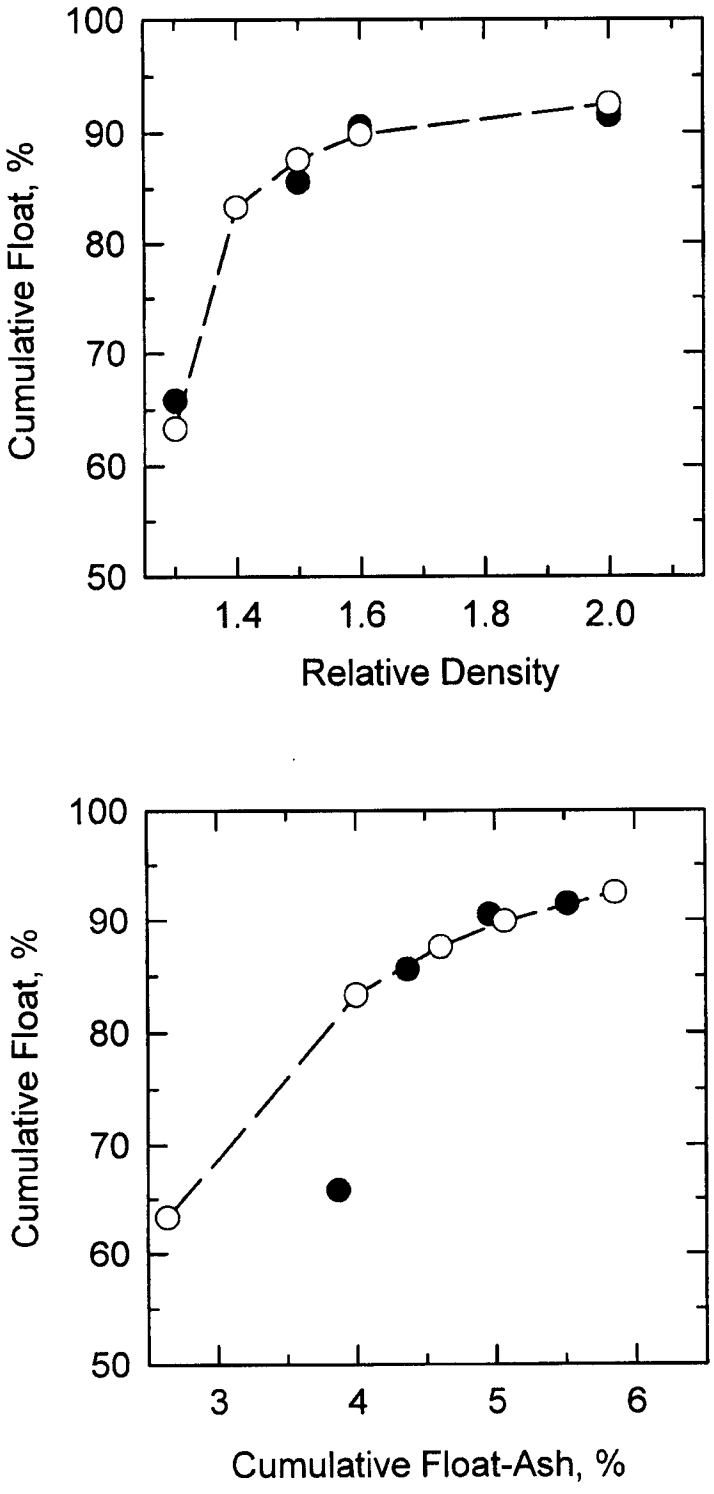

Figure 2.2.13 **WASHABILITY CURVES FOR THE 28x100 MESH UPPER FREEPORT SEAM COAL**
(open symbols: organic liquids; closed symbols: magnetic fluid)

Separations were also carried out using a continuous flow-through separator. The separator and test circuit are shown in Figure 2.2.14. The coal was added to tank 1 containing the magnetic fluid and stirred for several minutes to ensure adequate mixing. The solids concentration was fixed at 2% solids by weight. The magnet was turned on and set to the appropriate setting to produce the desired relative density. The peristaltic pump was started and set to the desired speed. The flow rate and hence, the retention time in the device, were set by adjusting the pump speed. The valve was set to tank 1 so that only the magnetic fluid was pumped through the separator. This was done to fill the unit prior to feeding the coal slurry. Care was taken to dispel any air bubbles from the separator. Once filled, the valve was set to pump the coal slurry from tank 2. The float

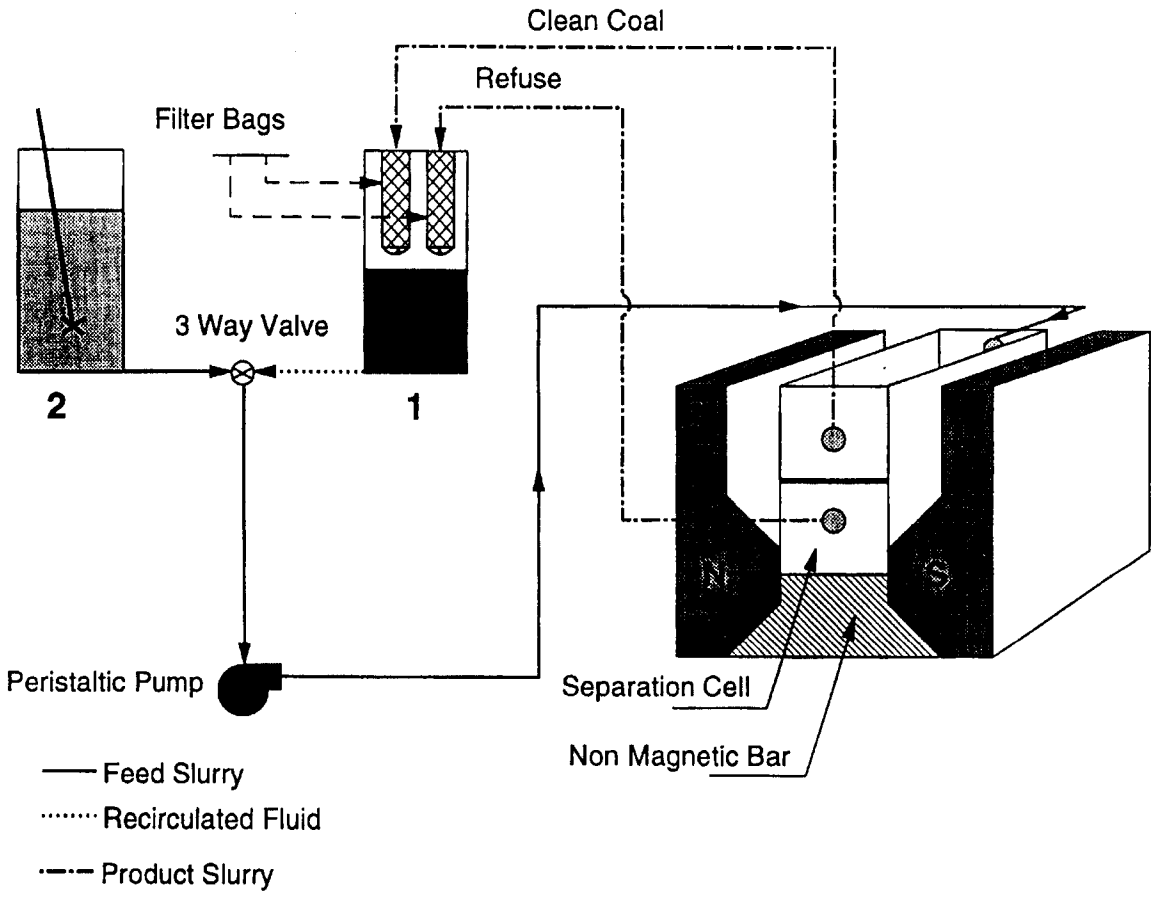

Figure 2.2.14 CONTINUOUS MAGNETIC FLUID SEPARATOR TEST CIRCUIT

and sink products were split at the discharge end and collected continuously over the test period.

Upon completion of the test, the valve was set to pump the recirculated fluid from tank 1 to flush out the remaining solids in the system. After all of the float material was removed, the pump and the magnet were shut off. Any solids remaining on the bottom of the separator were combined with the sink material. The test procedure was repeated using a new pump speed or new magnet (i.e., relative density) setting.

The products were subjected to float-sink separation at several relative densities using organic liquids. Using these data, along with the clean coal yield, the partition values were calculated for each of the test conditions. These values were then fitted to the logistic function to determine the relative density of separation and the probable error (Table 2.2.4).

Table 2.2.4 Summary of Operating Conditions and Results when Separating 28x32 mesh Upper Freeport Seam Coal in the Magnetic Fluid Separator

Flow Rate, L/min	Medium Relative Density	Mean Retention Time, s	Relative Density of Separation	Probable Error
3.3	1.3	2.7	1.35	0.30
2.4	1.3	3.6	1.37	0.22
1.7	1.3	5.2	1.39	0.11
1.7	1.4	5.2	1.47	0.12
1.7	1.6	5.2	1.78	0.17

Tests were run with 28x32 mesh Upper Freeport seam coal at a relative density of 1.3 for flow rates of 1.7, 2.4, and 3.3 Lpm. This gave retention times in the device of 5.2, 3.6, and 2.7 seconds, respectively. Figure 2.2.15 shows the partition curves obtained as a function of flow rate. As expected, the curves steepened with an increase in retention time, indicating a sharper separation. A horizontal line that corresponds to the volumetric

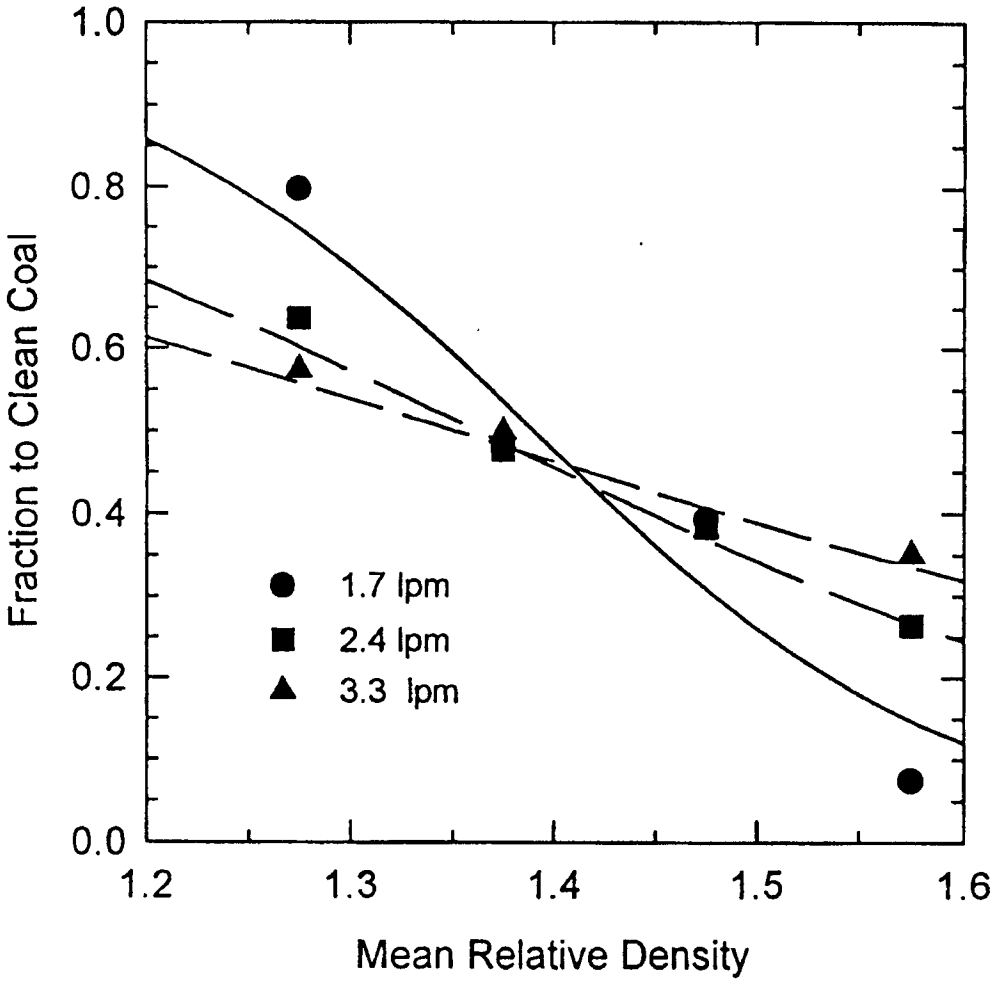

Figure 2.2.15 PARTITION CURVES FOR THE MAGNETIC FLUID SEPARATOR AS A FUNCTION OF FLOW RATE AT A MEDIUM RELATIVE DENSITY OF 1.3 FOR THE 28x32 MESH UPPER FREEPORT SEAM COAL

split of slurry to the overflow stream would be indicative of splitting rather than separation. For these tests, the volumetric split was approximately 0.5 for all flow rates.

Additional tests were run at relative densities of 1.4 and 1.6 at a flow rate of 1.7 Lpm. Figure 2.2.16 shows the variation of the partition curves as a function of the relative density of the medium. As expected, the curves shifted to the right with an increase in the medium density. For densities of 1.3 and 1.4, the probable errors were similar (Table 2.2.4) but increased at 1.6. Figure 2.2.17 compares the grade-yield curves

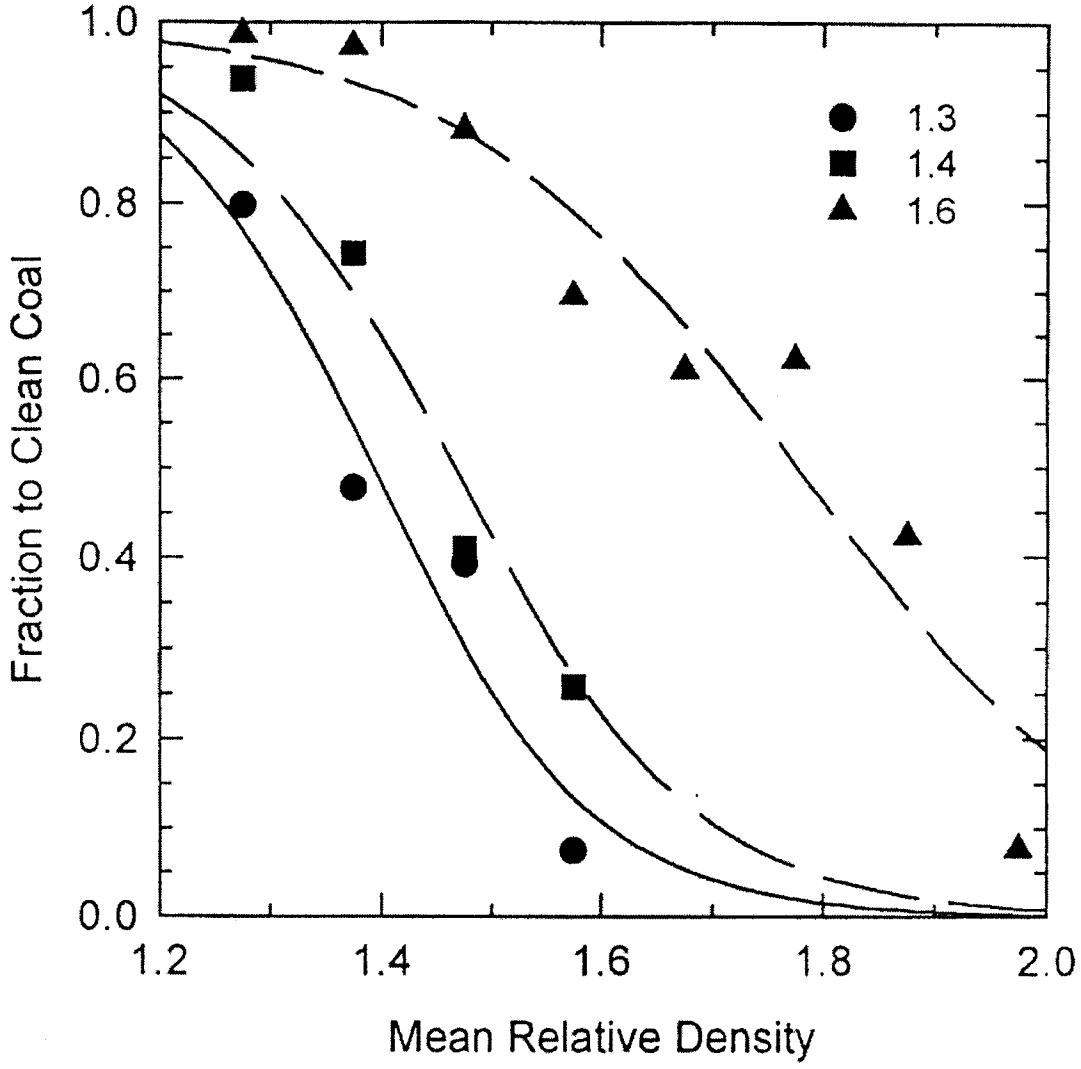

Figure 2.2.16 **PARTITION CURVES FOR THE MAGNETIC FLUID SEPARATOR AS A FUNCTION OF MEDIUM RELATIVE DENSITY AT A FLOW RATE OF 1.7 L/min FOR THE 28x32 MESH UPPER FREEPORT SEAM COAL**

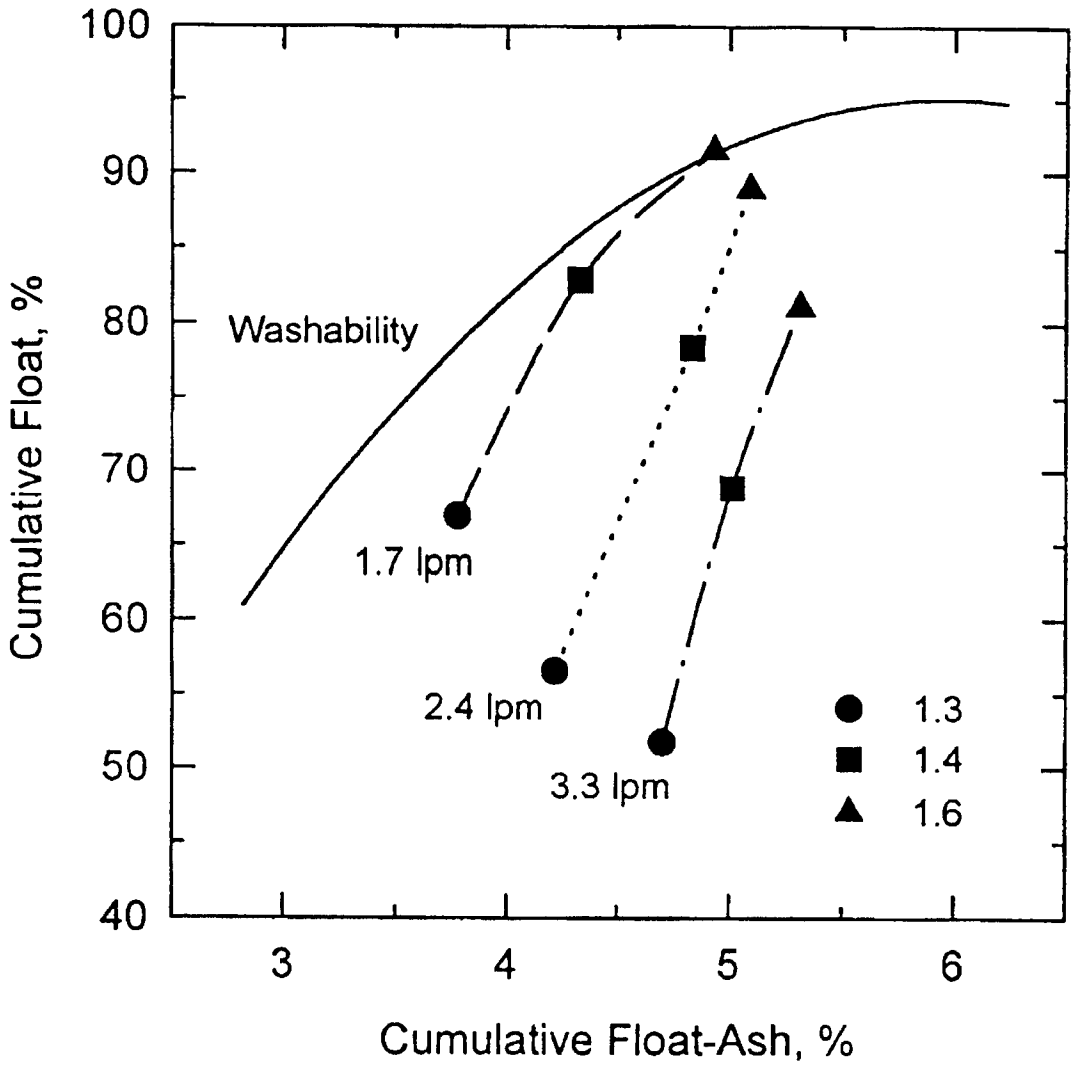

Figure 2.2.17 EFFECT OF FLOW RATE AND MEDIUM DENSITY ON THE GRADE-YIELD VALUES FOR THE 28x32 MESH UPPER FREEPORT SEAM COAL

for each flow rate and medium density to the washability curve for the 28x32 mesh coal. As can be seen, magnetic fluid separation approached the theoretical curve at the lower flow rates (longer retention times) and for the higher densities of separation.

Baseline testing of a centrifugal magnetic fluid separator was also performed. In this case, a Dynawhirlpool-type separator, which was designed to fit between the pole pieces of the Frantz electromagnet, was constructed out of Plexiglas. A schematic of the flow circuit is shown in Figure 2.2.18. This device was selected over a hydrocyclone for several reasons. Because a Dynawhirlpool consists only of a cylindrical portion, the unit could fit between the existing magnet poles. Also, the design lends itself to staging whereby the clean coal leaving the first device could be injected directly into a second separator. The second unit would be operated at a lower density by using a weaker magnetic field. Thus a two-stage separation, producing a high quality clean coal, a lower quality middling, and a refuse fraction, could be obtained using the same fluid. This approach is similar to the Tri-Flo separator, which uses a magnetite or ferrosilicon-based system as opposed to a magnetic fluid.

Unlike a hydrocyclone, two feed ports are used in a Dynawhirlpool separator. The feed coal enters at the top of the device, along with a portion of the medium (Figure 2.2.18). The remaining medium enters the separator tangentially, near the bottom of the device. This imparts the desired flow pattern in the separator to produce the necessary centrifugal force for separation. The refuse is driven outward and is carried up the separator wall where it exits tangentially near the top of the device. The clean coal is driven inward and exits at the bottom of the device.

For the test circuit, the coal was fed to the unit from a vibrating feeder. The magnetic fluid was pumped from a sump and was split prior to entering the separator. Approximately 15% of the fluid was combined with the feed coal, with the remaining fluid entering the medium inlet. The concentration of the feed coal was around 2% solids by weight. The product streams were directed into filter bags where the coal was collected. The filtrate was recovered and recirculated through the circuit, providing a continuous operation.

Initially, a 1.30 relative density zinc bromide solution was used as the separating medium to validate the operation of the device. Upper Freeport seam coal (28x32 mesh)

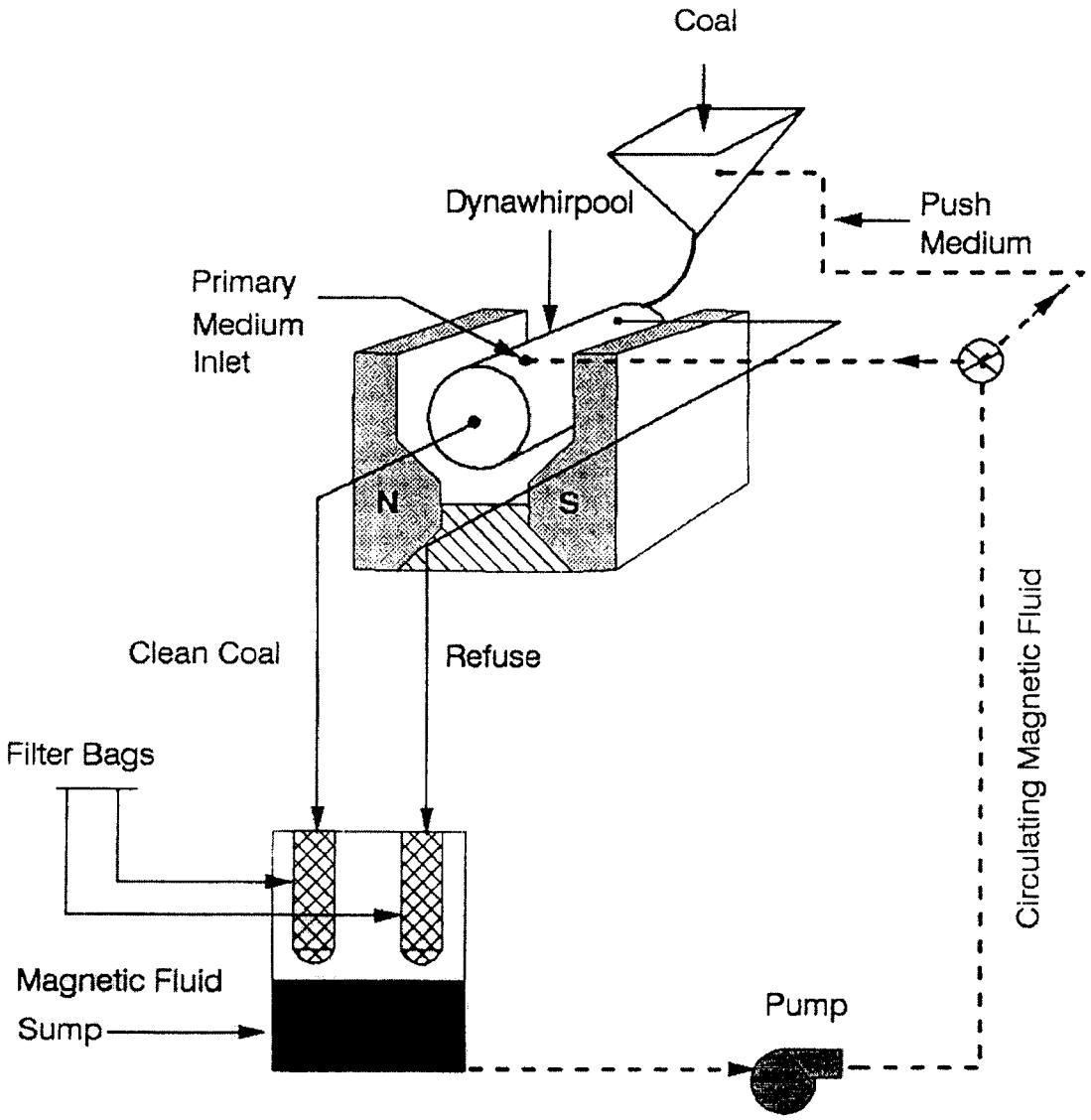

Figure 2.2.18 DYNAWHIRLPOOL MAGNETIC FLUID SEPARATOR TEST CIRCUIT

was passed through the device and the products were collected. Approximately 60% of the coal reported to the overflow (clean coal) stream. In comparison, no coal reported to the overflow stream when only water was used as the separating medium, as was expected.

Tests were then conducted using the magnetic fluid as the separating medium, along with the 28x32 mesh Upper Freeport seam coal. In all cases, no separation

occurred and all the coal reported to the refuse stream as when only water was used. The same results were obtained even when the concentrated magnetic fluid was used at maximum field strength. The addition of the centrifugal acceleration negated the buoyancy effect created by the magnetic fluid. To counteract this effect, a stronger magnetic field would be needed, which could not be obtained with the existing Frantz electromagnet (Fofana 1997).

2.2.4 Centrifugal/Flotation Separations

Dense-medium processes are capable of separating coal over a wide range of relative densities. Because the separations can be controlled with great precision (e.g., within $\pm$0.005 relative density units), dense-medium separation is the choice for processing difficult-to-clean coals such as those containing large amounts of near-density material. Moreover, it is the only technique capable of making separations at low relative densities (e.g., <1.4). Such separations are often required to produce low-ash, low-sulfur (e.g., compliance) coal.

Dense-medium separation is used extensively for cleaning coarse coal (e.g., +9.5 mm) and intermediate coal down to ~0.6 mm (28 mesh). In some cases, the bottom size has been extended to about 100 mesh (Kempnich et al., 1993). The processing of finer size fractions of coal has not always been successful because of poor cyclone performance and inefficient dense-medium recovery circuits. This has generally led to higher than expected processing costs.

Testing of a micronized-magnetite cycloning process to treat sizes as fine as ~0.038 mm (400 mesh) was carried out by the U.S. Department of Energy (Klima et al., 1990) and Custom Coals International (Kindig 1992). In these cases, the separations were made using micronized (e.g., -10 μm) magnetite as opposed to the more typical coarser grades of magnetite (e.g., -50 μm). The fineness of the magnetite allows higher operating pressures and in turn greater separating forces (i.e., increased g's) to be employed, which are required to process ultrafine coal particles. However, the use of micronized magnetite adds additional problems in regards to dense-medium recovery, including the need to remove the non-magnetic material from the medium prior to reuse in the system.

Currently, froth flotation is the only technique that has found widespread commercial use for treating coal finer than about 100 mesh. This process is very effective in rejecting ash-forming mineral matter, but it often lacks the selectivity in rejecting pyritic sulfur, an important consideration when attempting to produce low-sulfur coal.

One method of overcoming the limitations of dense-medium cycloning and froth flotation is through the use of an integrated circuit. Miller (1989) proposed a combined dense-medium/flotation process for beneficiating coal while increasing magnetite recovery. His process takes advantage of the natural hydrophobicity of coal compared to the hydrophilic magnetite. Because flotation is generally more effective than dense-medium processes for cleaning fine coal size fractions, it can be used to recover fine coal that is misplaced to the medium, reducing the load on the dense-medium recovery circuit. In one study using several grades of commercial magnetite, it was found that increased coal cleaning occurred in addition to magnetite recovery (Polat et al., 1993).

Subsequent work was carried out using this integrated approach to fine coal cleaning but using ultrafine magnetite as part of the dense medium (Polat et al., 1995). Samples were taken from the overflow and underflow streams of a 25 mm diameter cyclone processing -100 mesh Upper Freeport seam coal. The samples were analyzed for ash and total sulfur content. Flotation separations were then carried out on a separate sample of each cyclone product. For comparison, additional tests were carried out using froth flotation to clean the -100 mesh Upper Freeport seam coal directly, i.e., no dense-medium separation.

Figure 2.2.19 shows the yield and ash contents when separating the -100 mesh Upper Freeport seam coal using cycloning only, flotation only, and the combined cycloning-flotation process. The washability curve, which gives the theoretical best separation, is also included. It can be seen that dense-medium cycloning is more effective than froth flotation alone for producing a specified ash content at a given clean coal yield. However, the cyclone results were still lower than the washability results obtained by float-sink testing. The results from the integrated process were much better than cycloning alone, with ash contents similar to those obtained for the float-sink tests. The improved performance of the intergrated circuit can be attributed to the rejection by

flotation of the very fine mineral matter particles, which invariably report to the clean coal stream of the cyclone.

Figure 2.2.20 shows the yield and corresponding sulfur contents for the same separations. This figure demonstrates the sulfur reduction capability of the cyclone compared to froth flotation. In fact, the cyclone results are comparable to the washability curve. Integration does not provide any additional benefit in terms of sulfur rejection.

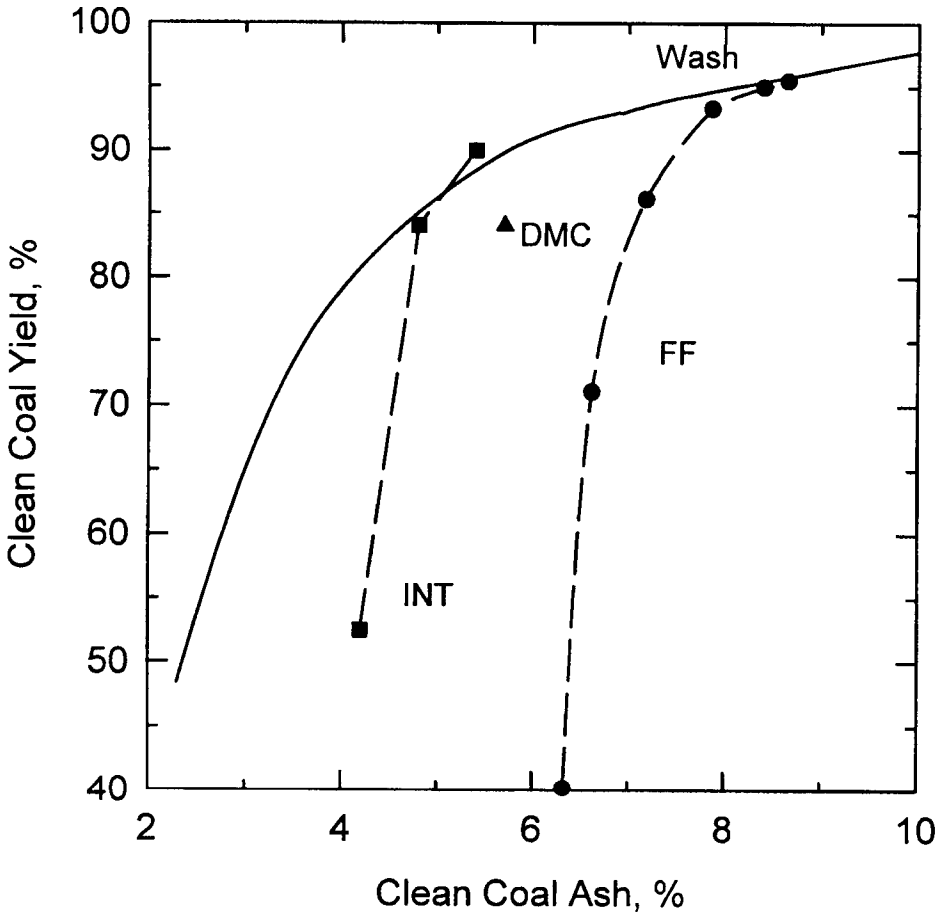

Figure 2.2.19 CLEAN COAL YIELD - ASH CURVES WHEN SEPARATING –100 MESH UPPER FREEPORT SEAM COAL USING DENSE-MEDIUM CYCLONING (DMC), FROTH FLOTATION (FF), AND THE INTEGRATED PROCESS (INT)
The washability curve is also included (Wash).

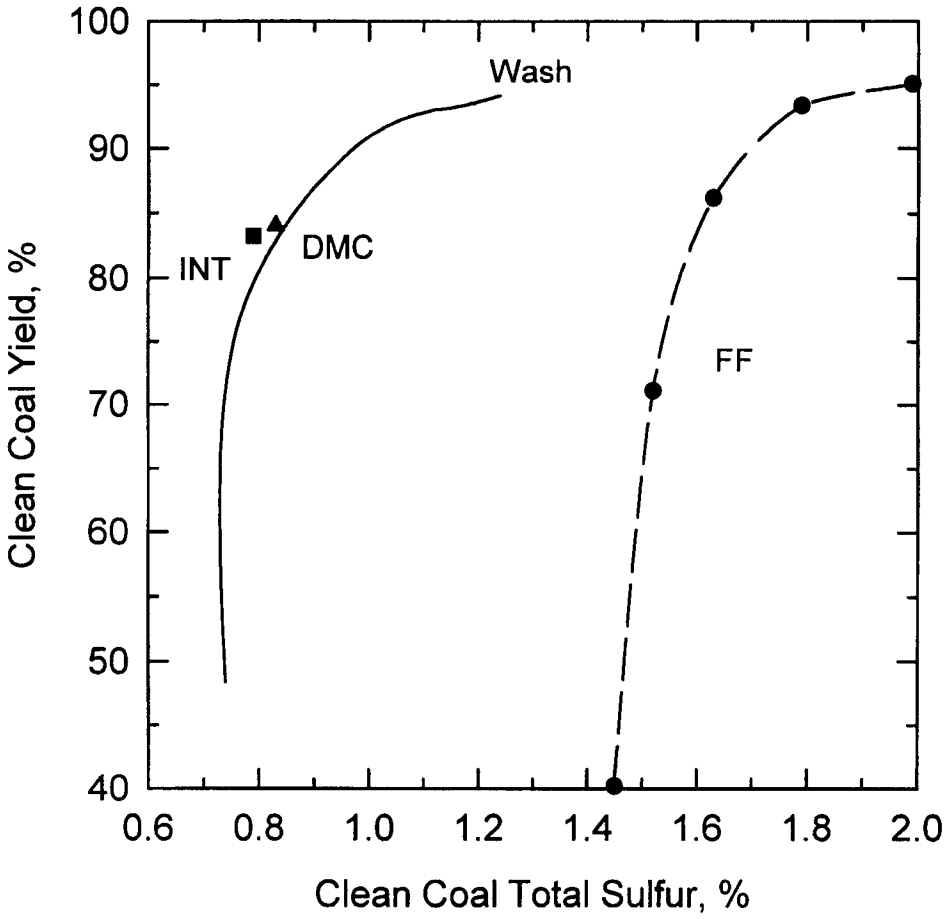

Figure 2.2.20 CLEAN COAL YIELD - SULFUR CURVES WHEN SEPARATING –100 MESH UPPER FREEPORT SEAM COAL USING DENSE-MEDIUM CYCLONING (DMC), FROTH FLOTATION (FF), AND THE INTEGRATED PROCESS (INT) (The washability curve is also included (Wash))

2.3 Surface Based Separation Processes

2.3.1 Continuous Froth Flotation

The continuous flotation tests were conducted on a pilot-plant scale froth flotation circuit. The continuous circuit has a capacity of about 8 gallons/min. The flotation circuit was designed for cleaning coal in two stages. The coal to be fed to the flotation circuit was ground in a stirred ball mill. The ball mill had a total capacity of 30 gallons and a working capacity of about 20 gallons. The operating conditions were selected so as to produce a size distribution of about 100% passing 28 mesh as shown in Figure 2.3.1.

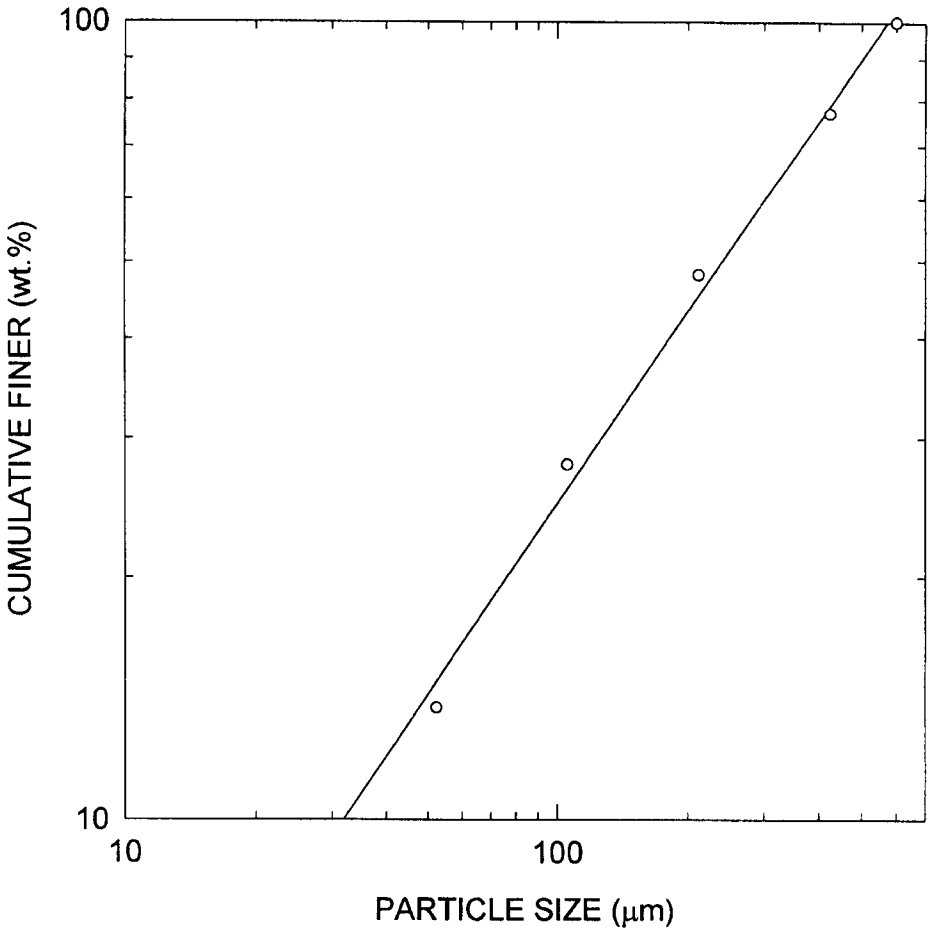

Figure 2.3.1 SIZE DISTRIBUTION OF THE FEED

During grinding, the slurry contained about 20-35% solids and the product was transferred to the 500 gallon capacity head tank as shown in Figure 2.3.2. The slurry from the head tank was pumped by a Moyno pump at a flow rate that was set depending on the circuit requirements and the percent solids in the feed slurry. A flow meter was connected after the pump to monitor the slurry flow rate from the head tank.

The rougher circuit consisted of:

1. 20 gallon feed tank with mixer
2. Four, WEMCO cells of 1.4 cubic feet capacity each
3. 5 gallon frother tank

4. 1 gallon collector tank with mixer
5. Quinn froth pump, with a flow meter
6. Sampling system

The coal-water slurry at 20-35% solids from the head tank was fed into the feed tank where it was diluted with water to make slurry containing about 5% solids. The amount of water added to the feed tank depended on the solids content of the feed slurry from the head tank. A rotameter was used in series with the water line to measure the flow rate. The water flow rate was adjusted so as to obtain the desired total flow rate.

The MIBC frother, and the dodecane collector were each mixed with water in a ratio of 1 to 400, in the frother and collector tanks, respectively. The frother and the collector were pumped into the feed tank where the feed was diluted as required. During some tests the collector was fed to cells 3 and 4 only, to avoid overloading the froth in cells 1 and 2, and to increase recovery in cells 3 and 4.

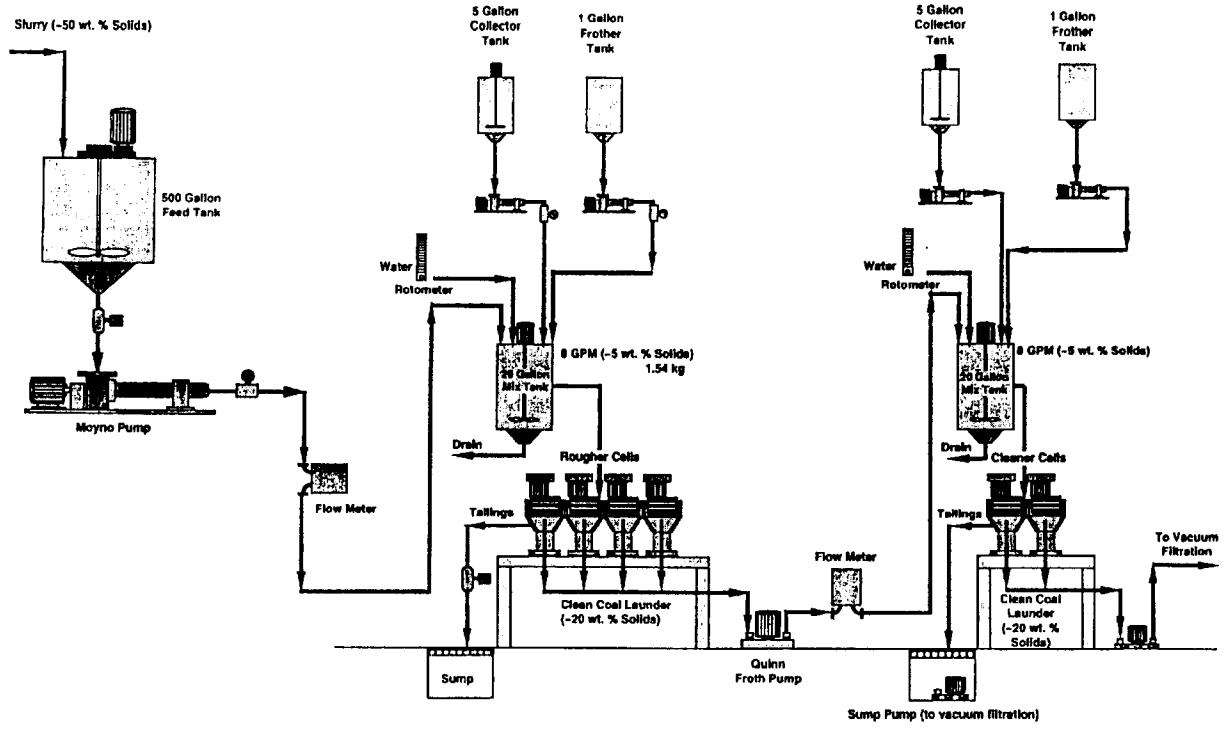

Figure 2.3.2 ROUGHER-CLEANER FLOTATION CIRCUIT USED IN CONTINUOUS FLOTATION TESTS

The coal-water slurry containing 5% solids, the frother and collector were fed to the series of four cells. The impellers in the cells were rotated at a fixed speed of about 1,000 rpm, and the aeration was set to the maximum value. The froth containing clean coal flowed above the weir of the cells and was removed into the launders on each side of the cells by rotating paddles. The wash water washed down the froth in the launders. The wash water flow rate was about 1 gpm, and was monitored by a rotameter.

The froth product from the circuit was collected in plastic storage drums, which was subsequently taken for filtration. If an additional cleaner circuit was used, the froth was allowed to flow down into a froth sump, from where it was pumped to the cleaner circuit. The tailings from the last cell in the rougher circuit were sent to a sump.

The cleaner circuit consisted of:

1. 20 gallon feed tank with mixer
2. Two flotation cells of 1.4 cubic feet capacity each
3. 5 gallon frother tank
4. 1 gallon collector tank with mixer

The froth product from the rougher circuit was pumped to the cleaner circuit feed tank where it was diluted to about 5% solids with water. The water flow rate into the feed tank was adjusted to get the desired total flow rate, and was monitored using a rotameter. The frother and collector could be fed into the feed tank as desired. The froth product from the cleaner cells was collected in drums, and the tailings from the last cell flowed down into a sump. If required, the cleaner tailings could be recycled to the rougher cells.

The product from the cleaner circuit was filtered on a vacuum filter. The tailings in the trench sump, now containing very low percent solids, were pumped using the trench pump to an overhead tank, where it was mixed with a solution of dissolved calcium chloride, and the solids were allowed to flocculate and settle overnight. The clear water on the top was decanted, and the slurry with settled solids was pumped to the vacuum filtration system.

For the Lower Kittanning seam coal tested in this part of the investigation, the ash analysis of samples taken from the rougher and cleaner circuits during preliminary tests, showed that the froth product from the rougher circuit satisfied the ash content

requirement for subsequent combustion tests. Therefore most of the tests with this coal sample were performed using only the rougher circuit consisting of the bank of four cells.

To evaluate the performance of the circuit, slurry samples were taken from the froth product from all four cells, the feed and the tailings streams. To maximize the probability of representative sampling, whole streams were diverted into sampling containers and samples were taken simultaneously from every stream. The samples collected were subsequently filtered, dried, weighed and analyzed for ash content. Two sets of samples were collected for each test to determine whether the circuit was operating at steady state, as assumed. The samples collected from one test were sieved using 28, 48, 100, 200, and 400 mesh sieves to obtain the size distribution of each stream. From the weight and ash analysis of various samples, the flotation response of the different size fractions could be determined.

2.3.1.1 Results and Discussion

Lag Time

During laboratory tests, it is often observed that the froth flows over the weir of the cell only after a finite time has elapsed after the air is turned on. This time lapse is called 'lag time'. The time when the froth starts flowing over the weir is often set as flotation time 'zero'. The mean residence time of the slurry in a cell or a bank of cells is calculated by the relation

$$\tau = \frac{V}{Q} \tag{2.3.1}$$

where V is the effective volume and Q is the flowrate of the slurry. Here, it is assumed that that the slurry acts as a liquid, and the liquid mean residence time would represent that of the whole slurry. Assuming that about 15% of the cell volume is occupied by air, the mean residence time for a 1.4 ft^3 cell at a flow rate of 6 gpm, is calculated to be 1.485 minutes.

The cumulative weight percent of material remaining in the each cell is plotted in Figure 2.3.3. It is assumed that the mean residence time is the same for each cell, and the total residence time of the material in any cell is the cell number multiplied by the mean residence time for one cell. The curves joining the recovery points at different conditions

do not merge to 100 percent at time 0 or cell 0. The lag time is different, ranging from 0.2 cell to 0.5 cell, under different operating conditions. Agar et al. (1980) proposed a flotation rate model that takes the induction time into account. To calculate the lag time a modified form of the classical first order was used.

$$R = R_{\infty}(1 - e^{-k(t + t_L)}) \tag{2.3.2}$$

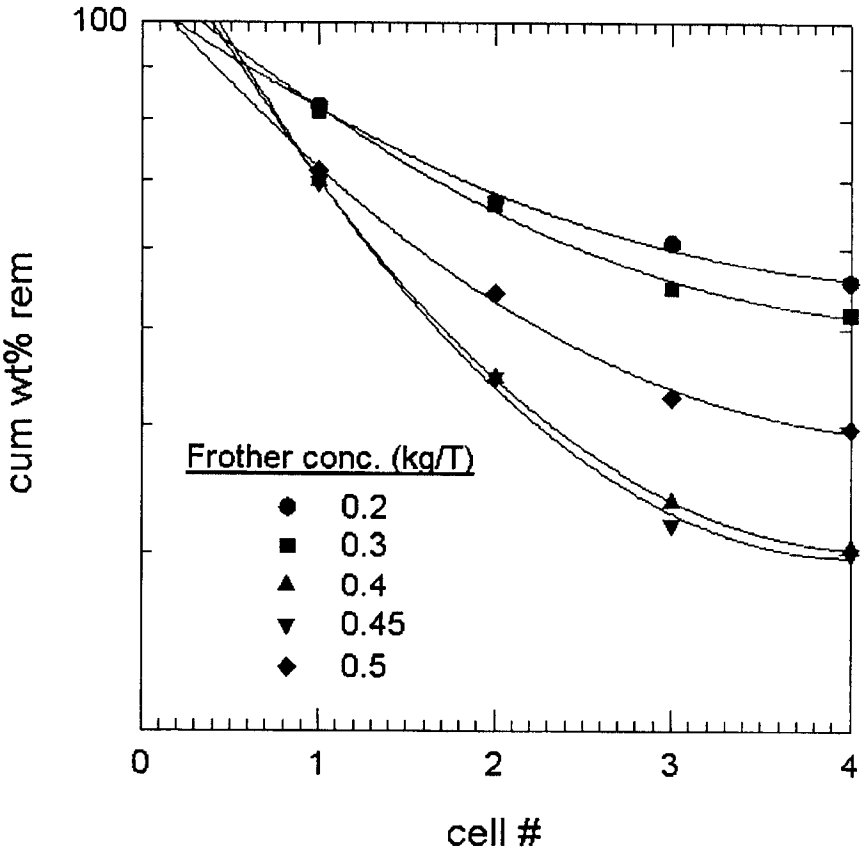

Figure 2.3.3 ESTIMATION OF INDUCTION TIME

where t_L is the lag time. The induction time for the rougher circuit was estimated to be 0.4 times the mean residence time of a cell, which is 0.594 minutes.

Effect of Frother Concentration

Figures 2.3.4 and 2.3.5 show the effect of frother concentration on the recovery from each cell in the bank of flotation cells. Figure 2.3.4 shows the cumulative recovery at each cell. As expected, the cumulative recovery curves shifted to higher values as the cell number increased. In each curve the cumulative recovery attains a maximum in the frother concentration range of 0.4 kg/T to 0.45 kg/T. Figure 2.3.5 shows the fractional recovery from each cell as a function of frother concentration. In the first two cells the recovery increased with increase in frother concentration in the range 0.2 kg/T to 0.4 kg/T. The recovery remained fairly constant in the range 0.4 to 0.45 kg/T, and then decreased as the frother concentration was increased further. In cell # 3, the recovery increased when the frother concentration was increased from 0.2 kg/T to 0.3 kg/T, and then remained relatively constant. In cell # 4, the fractional recovery decreased slightly when the frother concentration was increased at low concentrations. The recovery remained relatively constant at higher frother concentrations.

The flotation recovery from each cell is the maximum at a frother concentration in the range 0.4 kg/T to 0.45 kg/T. It is concluded that, under the used operating parameters this frother concentration range is optimum for the flotation of Lower Kittanning seam coal in the pilot plant flotation circuit.

Kinetics

The flotation results are plotted in Figure 2.3.6 after incorporating the lag time. Since the data fit the first order model only in the initial stages, the data up to cell 3 were used to estimate the rate constants from Figure 2.3.7. The flotation rate increased with frother concentration in the range 0.2 kg/T to 0.4 kg/T. The rate remained constant in range 0.4 kg/T to 0.45 kg/T. The flotation rate decreased with further increase in frother concentration. The flotation rate constants are given in Table 2.3.1.

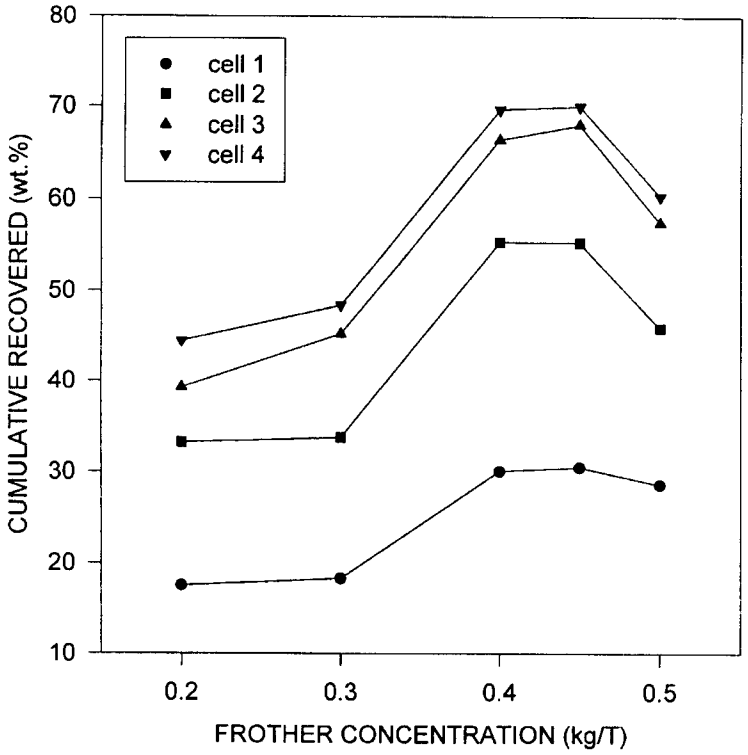

Figure 2.3.4 CUMULATIVE RECOVERY FROM EACH CELL AT DIFFERENT FROTHER CONCENTRATIONS

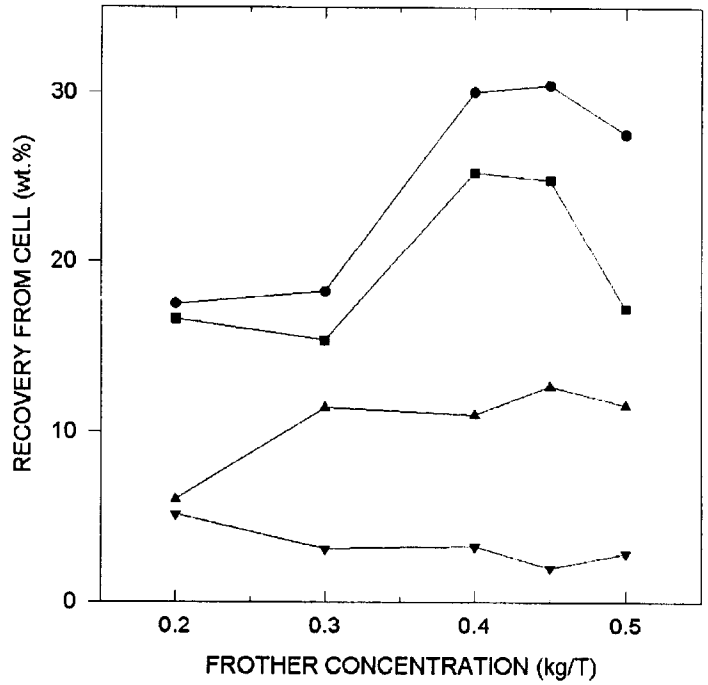

Figure 2.3.5 FRACTIONAL RECOVERY FROM EACH CELL AT DIFFERENT FROTHER CONCENTRATIONS

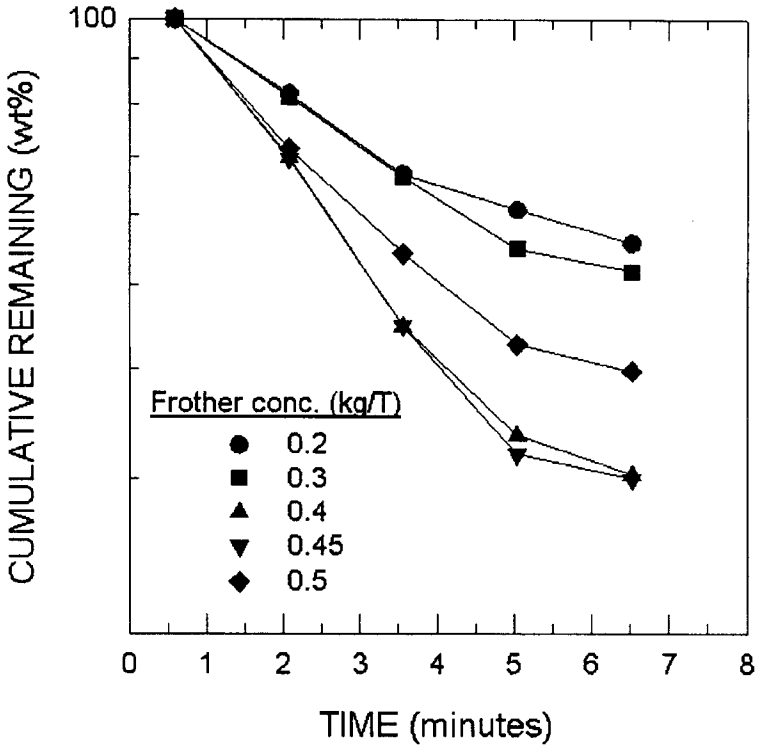

Figure 2.3.6 KINETICS PLOTS AT DIFFERENT FROTHER CONCENTRATIONS

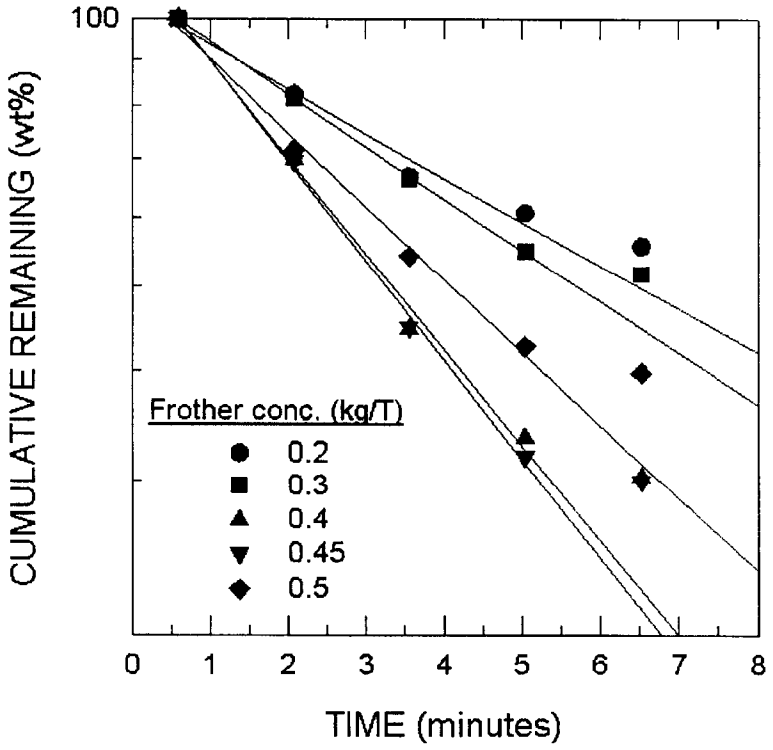

Figure 2.3.7 ESTIMATION OF FLOTATION RATE CONSTANTS

Table 2.3.1 Flotation Rate Constants at Different Frother Concentrations

Frother concentration (kg/T of coal)	Flotation rate constant (per min)
0.20	0.1148
0.30	0.1355
0.40	0.2503
0.45	0.2599
0.50	0.1910

Effect of Collector Concentration

The kinetics plots for tests performed with a fixed frother concentration of 0.3 kg/T and varying the collector concentration from 0 to 0.1 kg/T are shown in Figure 2.3.8. Most of the coal that floated was recovered in the first two cells. Though the flotation rate increased with the addition of collector, the froth in cells 3 and 4 became very stable resulting in a stagnant froth. As a result, the particles in the froth fell back into the cell, and the recovery decreased.

Independent control of the pulp level in each cell and a mechanism to selectively add frother and collector to cells 3 and 4 could improve recovery. The flotation rate constants for different collector concentrations are shown in Table 2.3.2.

Flotation Rates of Various Size Fractions

To determine the behavior of coal in various size fractions, a series of tests was conducted. The samples obtained from the test conducted with a frother concentration of 0.5 kg/T were sieved to obtain the size distribution in each stream. Each size fraction was treated independently and compared with respect to flotation response. The kinetics plots for the different size fractions are shown in Figure 2.3.9. The flotation rate and final recovery increased as the particle size decreased from 600 μm to 37 μm. The flotation rate and recovery were lower for the -400 mesh size fraction while the 200 x 400 mesh fraction had the highest flotation rate and final recovery.

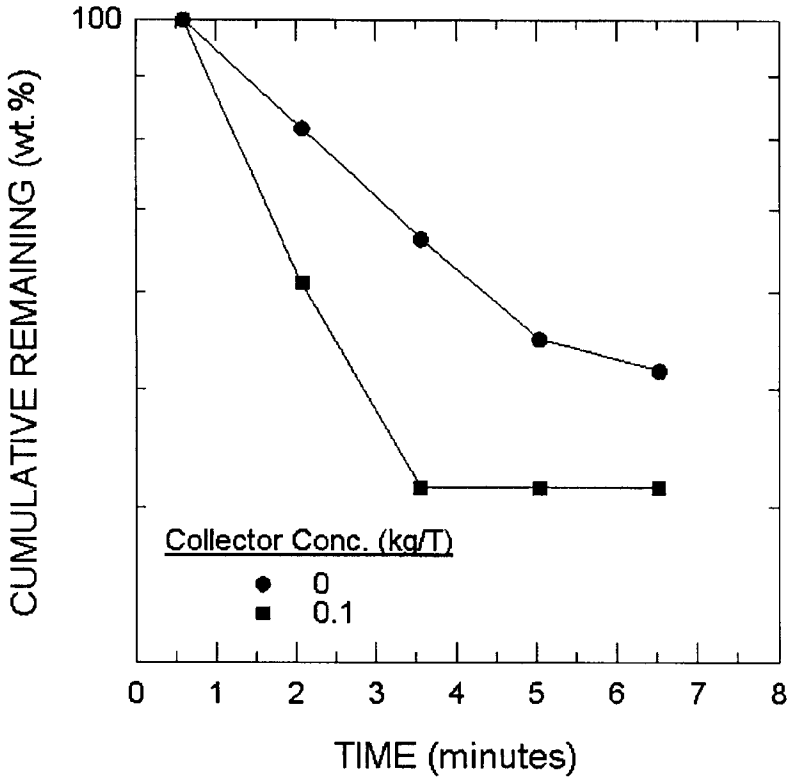

Figure 2.3.8 KINETICS PLOTS AT DIFFERENT COLLECTOR CONCENTRATIONS (frother conc.=0.3 kg/T)

Table 2.3.2. Flotation Rate Constants at Different Collector Concentrations

Collector concentration (kg/T) (frother : 0.3 kg/T)	Flotation rate constant (min^{-1})
0	0.1152
0.1	0.2520

The flotation rate regression lines are plotted in Figure 2.3.10. The flotation rate was calculated from the slope for each size fraction. The flotation rate constants for different size fractions are given in Table 2.3.3.

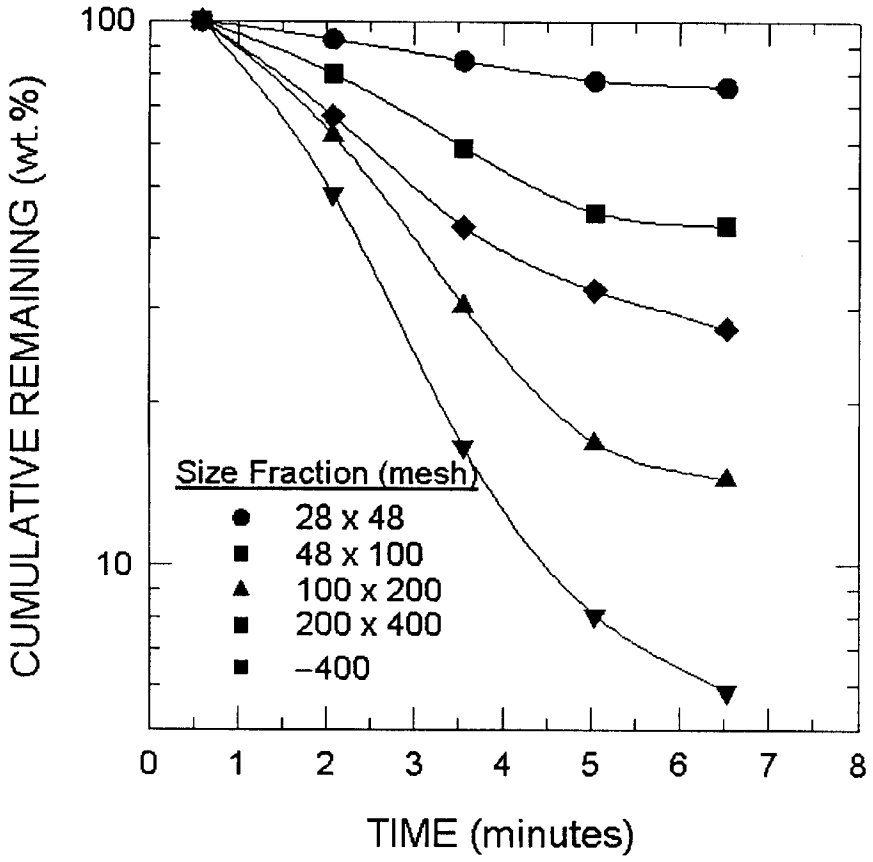

Figure 2.3.9 KINETICS PLOTS FOR DIFFERENT SIZE FRACTIONS FOR TESTS CONDUCTED AT A FROTHER CONCENTRATION OF 0.3 kg/T

The flotation rate constants for different size fractions, plotted in Figure 2.3.11, show that the flotation rate of coal particles increases as the size decreases to about 400 mesh, and decreases with further decrease in size.

The cumulative recovery of each size fraction from the four cells is shown in Figure 2.3.12. Maximum recovery was obtained for the 200 x 400 mesh fraction. The expected increase in the coarser material in cells 3 and 4 was not observed, probably because the level in these cells could not be controlled independent of cells 1 and 2. The froth mobility in cells 1 and 2 was very different from that in cells 3 and 4. It might be possible to increase recovery in cells 3 and 4 by using a frother which is more effective for coarse particles.

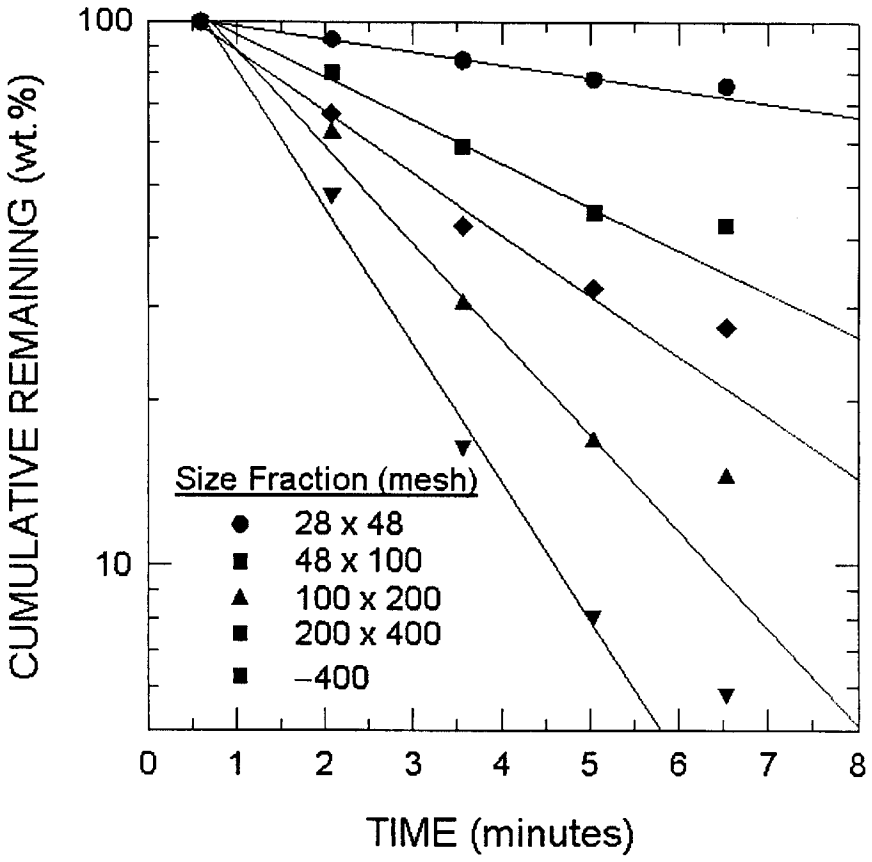

Figure 2.3.10 ESTIMATION OF KINETICS RATE CONSTANTS FOR EACH SIZE FRACTION

Table 2.3.3 Flotation Rate Constants for Different Size Fractions

Size fraction (mesh)	Flotation rate constant (min^{-1})
28 x 48	0.0557
48 x 100	0.1829
100 x 200	0.4079
200 x 400	0.5801
-400	0.2595

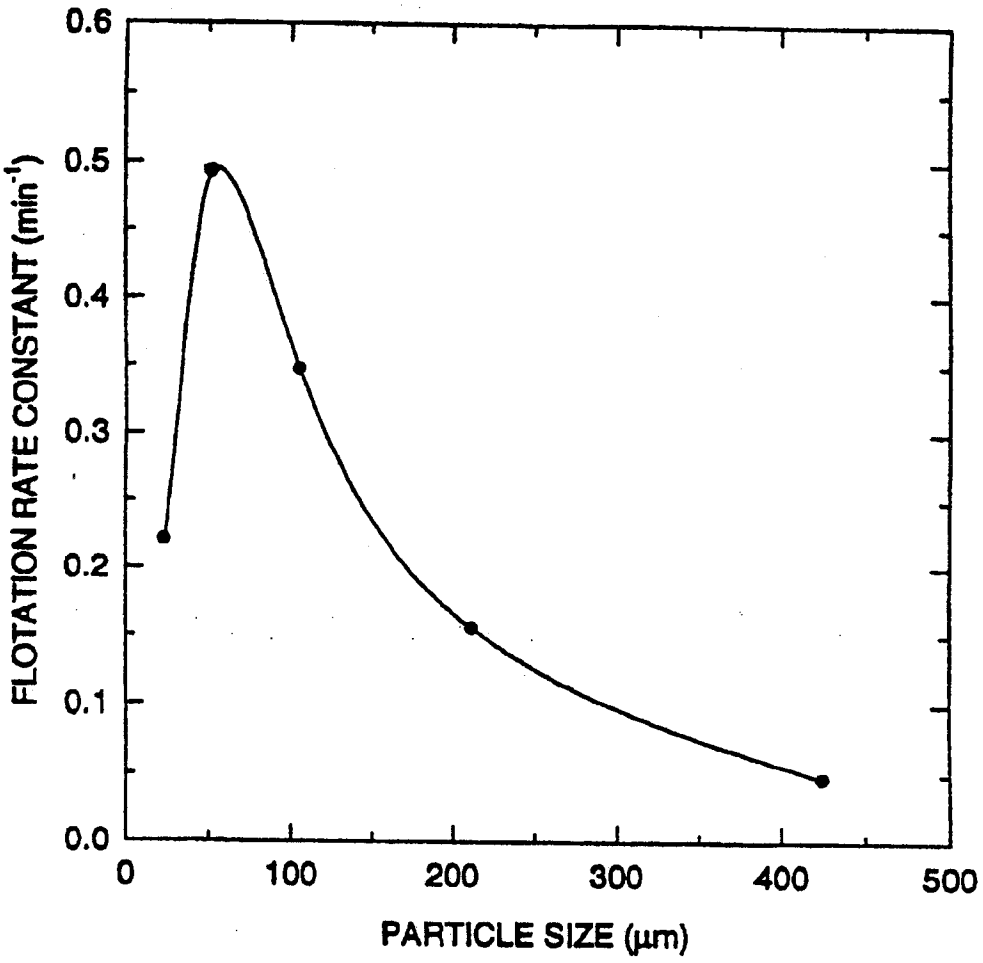

Figure 2.3.11 VARIATION OF FLOTATION RATE CONSTANT WITH PARTICLE SIZE

Evaluation of Flotation System Performance

The rate constants for the batch, batch with no paddling (batch*), and pilot-plant tests are given in Table 2.3.4 for different frother concentrations. In these tests the batch data refer to a typical kinetics test in which froth is removed continuously by manual paddling. A comparison of the rate constants for the three cases is given in Figure 2.3.13, in which the data are plotted as a function of frother concentration. The plant data refer to the flotation kinetics tests obtained in the pilot plant circuit consisting of four cells. The data marked as batch* refer to the tests in which no paddling was employed and the froth was allowed to flow on its own accord. The results confirm that froth mobility plays a very significant role in determining the overall kinetics in a continuous operation.

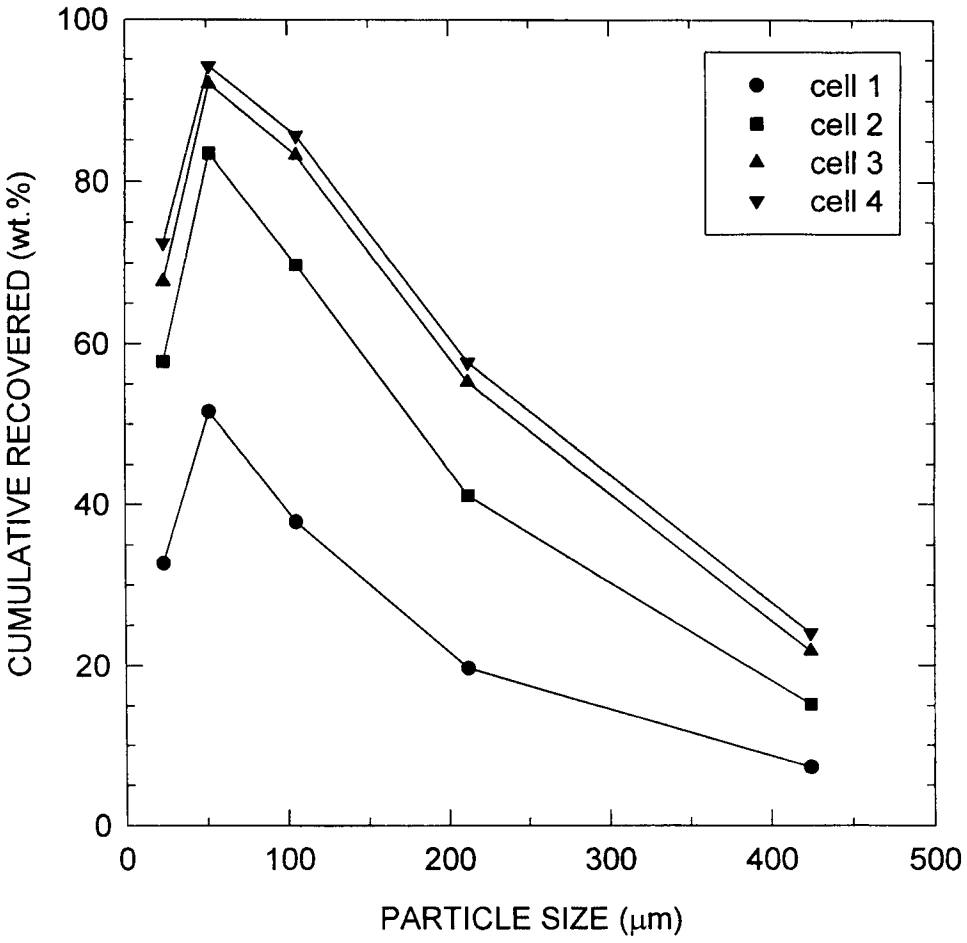

Figure 2.3.12 CUMULATIVE RECOVERY OF EACH SIZE FRACTION FROM EACH CELL

Table 2.3.4 Flotation Rate Constants and Froth Factors for the Batch, Batch with no Paddling (Batch*), and Pilot Plant Tests

Frother conc. (kg/T)	Rate constants (min^{-1})			Froth Factor (k_{lab}/k_{plant})	
	Batch	**Batch***	**Plant**	**Batch***	**Plant**
0.2	1.7517	0.5995	0.1149	2.92	15.25
0.3	1.9205	0.7198	0.1356	2.67	14.61
0.4	2.1737	0.9704	0.2505	2.24	8.68
0.45	2.0228	0.9068	0.2601	2.23	7.78
0.5	2.0528	0.8636	0.1912	2.38	10.74

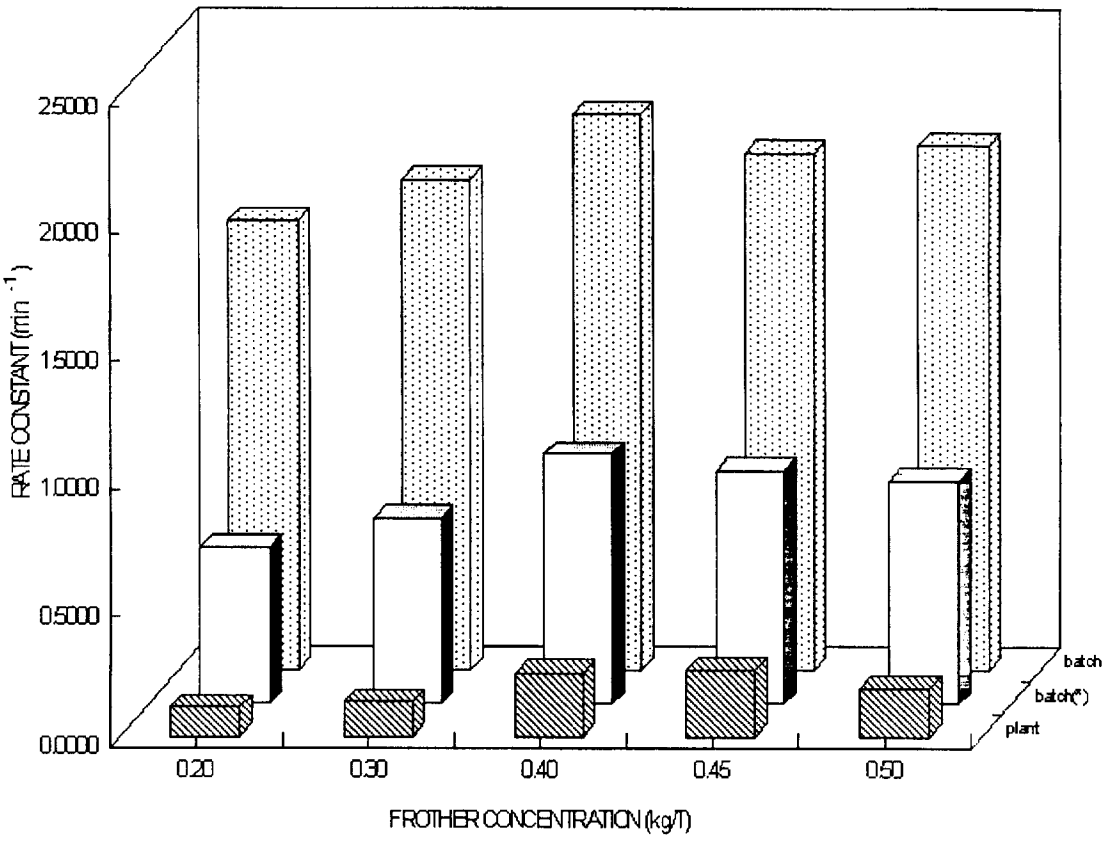

Figure 2.3.13 COMPARISON OF FLOTATION RATE CONSTANTS FOR THE BATCH, BATCH WITH NO PADDLING (BATCH*), AND PILOT PLANT TESTS AT DIFFERENT FROTHER CONCENTRATIONS

This effect is commonly ignored in laboratory testing. At the beginning of this project, motorized paddles were placed on top of the laboratory cell but were found to be unsatisfactory. A large number of particles was sticking to the paddles. The froth factor, defined as the ratio of the rate constant for the laboratory test to the pilot plant test or the batch flotation rate without paddling, is a function of the frother concentration. In the presence of an oily collector, such as dodecane, the froth factor was smaller as can be seen from the results in Table 2.3.5 and Figure 2.3.14. These results are not surprising since the collector is likely to increase froth stability.

Table 2.3.5 Change in Flotation Rate Constants and Froth Factors Due to the Addition of Collector for the Batch, Batch with no Paddling (Batch*), and Pilot-Plant Tests

Collector conc. (kg/T)	Rate constants (min^{-1})			Froth Factor (k_{lab}/k_{plant})	
	Batch	Batch*	Plant	Batch*	Plant
0	1.9205	0.7198	0.1356	2.67	14.16
0.1	2.5493	0.9068	0.2964	2.81	8.60

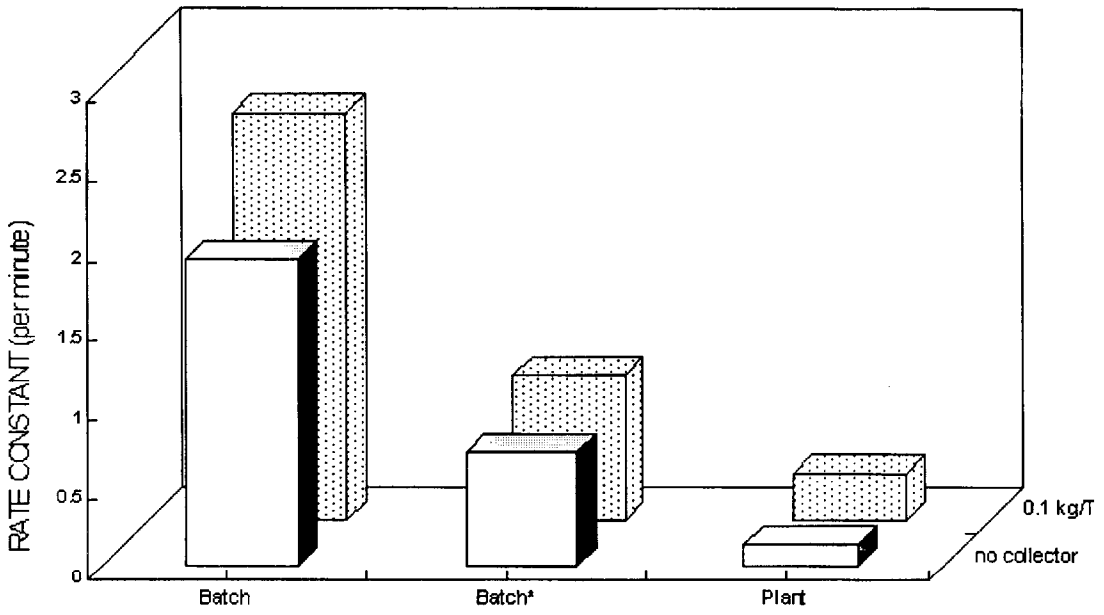

Figure 2.3.14 EFFECT OF COLLECTOR ADDITION ON FLOTATION RATE CONSTANT FOR THE BATCH, BATCH WITH NO PADDLING (BATCH*), AND PILOT PLANT TESTS

From these studies, it can be concluded that the lower than expected recovery in the pilot plant flotation circuit was due to low mobility and less stability of the froth. It should be possible to improve the performance with the help of a frother, which is likely to give a more mobile froth. The use of an appropriate frother will also improve the recovery of coarse particles in the pilot plant or plant operation.

2.3.1.2 Conclusions

- The flotation rate and recovery increased as the frother concentration was increased, and reached a maximum at a concentration of 0.4 kg/T to 0.45 kg/T, and then decreased.
- The froth was stagnant in cells 3 and 4 when collector was added. Most of the material that floated was recovered in the first two cells.
- The flotation rate and recovery increased as the particle size decreased. More than 95% of the 200 x 400 mesh size fraction was recovered, while about 75% of the 28 x 48 mesh fraction was lost on the tails. This shows that MIBC is not especially suited for coarse particle flotation. The recovery of this fraction could have been greater if an alternate frother such as Dowfroth was used.

2.3.2 Column Flotation

Continuous flotation experiments were carried out in a 0.076 m x 3.55 m pilot flotation column. The flotation column was fitted with six high-accuracy pressure sensors (Cole Palmer, H-68971 series) at varying axial locations. The outputs from these sensors were fed to a 386 SX Everex computer at a frequency of 0.2 Hz. The desired hydrostatic head in the column (the liquid level) was set using the pressure sensor located at the bottom of the column. By regulating the tailings pump using an icon-based control program (COLUMNCT.VI), the hydrostatic head was maintained at the set value. The column program was developed using Labview Student Edition, provided by National Instruments. A detailed description of the column with other ancillary instrumentation has been provided in a previous report (Miller et al., 1993). Figure 2.3.15 shows a schematic diagram of the experimental set-up.

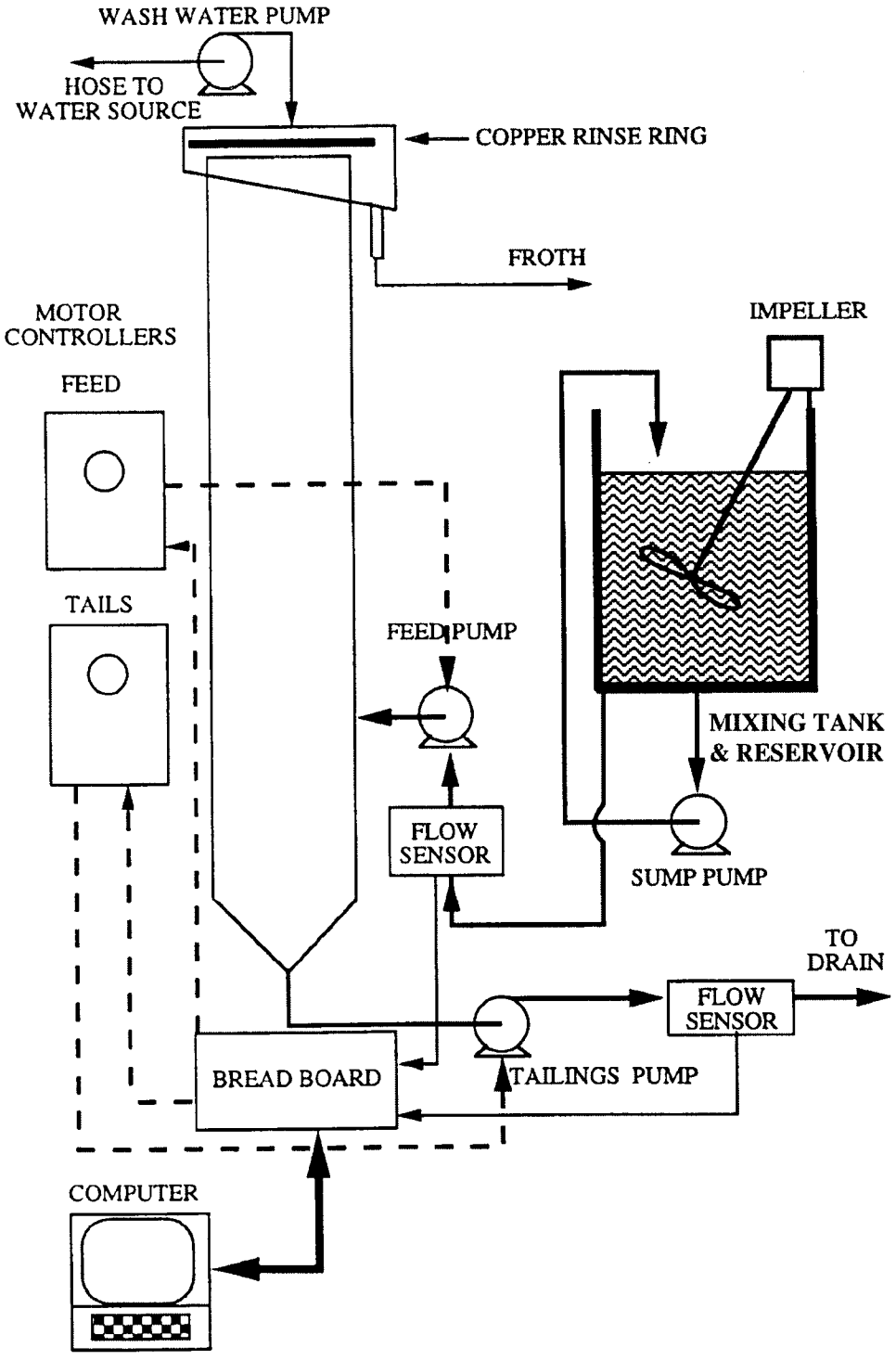

Figure 2.3.15 A SCHEMATIC REPRESENTATION OF THE EXPERIMENTAL SET-UP

The flotation experiments were carried out using - 100 mesh Lower Kittanning seam coal with feed ash and sulfur contents of 9.4% and 0.78%, respectively. For each experiment, approximately 100 liters of a 5 wt. % coal slurry was prepared. The required amount of frother was added directly to the slurry in the reservoir. Except where indicated, the frother used was methyl-iso-butyl-carbinol, MIBC.

The feed was introduced into the column at the desired flow rate with the air turned off. When the desired hydrostatic head in the column was attained, aeration was turned on. Collection of timed froth and tailings samples was initiated the moment the froth overflowed the cell lip. For the froth samples, collection was over 30 sec and 1 minute intervals for the first minute and remainder of the experimental run, respectively, while for the tailings stream, sampling was over 10 s, 15 s, 20 s, 30 s or 40 s intervals. In preliminary experiments, it was observed that froth removal would present a significant bottleneck in the accurate determination of the concentrate flow rate. This problem was overcome with the installation of a water ring spray on the outer periphery of the cell lip. For all the experiments reported here, the wash-water addition rate was fixed at 1.2 liters per minute. Figure 2.3.16 shows the variation of concentrate flow rate, percent solids in the tailings stream, and concentrate and tailings grades with flotation time. The results show that steady state conditions were achieved in about 2 to 4 minutes. Subsequently, this mode of column operation was adopted for all of the experimental runs.

The initial studies were carried out with the column equipped with a Mott porous gas sparger having an average pore size of 2 μm. In these experiments, the slurry feed was introduced into the column at varying inlet positions, which ranged from 0.43 m to 2.37 m from the gas distributor. With these experiments, the effect of recovery zone height on yield (and concentrate production rate) was determined. Additional experiments were also carried out at varying slurry concentrations of 2.5% to 10% (by weight), air flow rates of 1.5 to 6 L/min, and hydrostatic pressure settings of 1.5 m to 2.0 m.

In order to evaluate the effectiveness of a novel bubble generator that is under development at Penn State, flotation experiments were also carried out on the column equipped with the Vortactor turbulent contactor. A schematic diagram of the

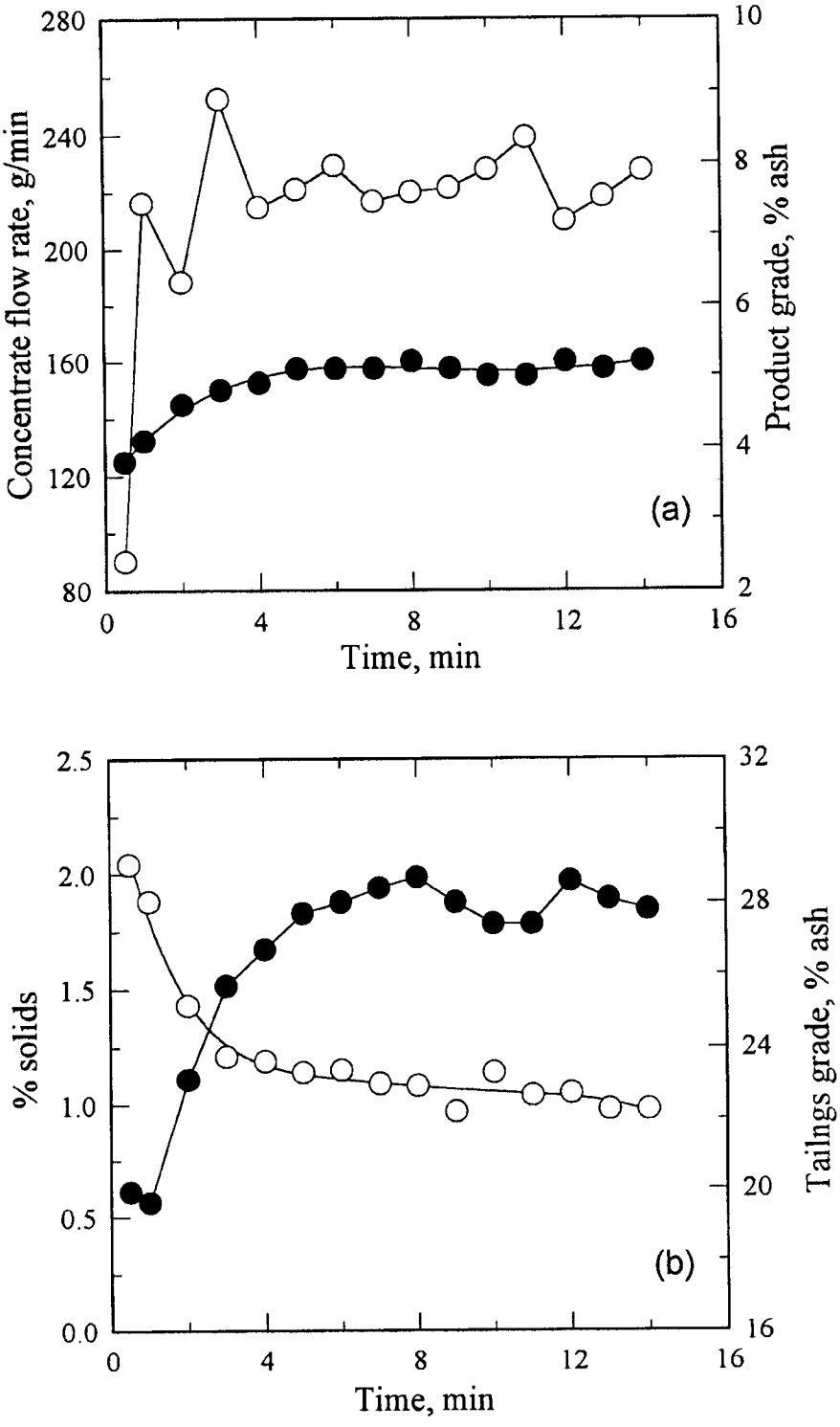

Figure 2.3.16 **EXPERIMENTAL VERIFICATION OF THE ATTAINMENT OF STEADY STATE: (a) CONCENTRATE; (b) TAILINGS MATERIAL (Filled symbols represent the concentrate and tailings grade)**

Vortactor turbulent contactor is shown in Figure 2.3.17. In these experiments, the slurry feed and air were brought into intimate contact in the vortactor chamber where the pressure was set at 138 kPa. A detailed description of the vortactor turbulent contactor and its operation can be found elsewhere (Ityokumbul et al., 1996). The slurry-air mixture was also introduced into the column at two axial locations to provide a preliminary evaluation of the effect of recovery zone height.

The froth and tailings samples were filtered, dried and weighed. For the tailings samples, the amount of water was also measured in order to determine the tailings flow rate at any given time interval, and the per cent solids in the tailings stream. All of these values were used to determine the attainment of steady state in the experiments (see Figure 2.3.16).

The particle size distributions of the feed and tailings samples were determined. Approximately 50 g of the coal was placed in a beaker containing tap water. A small amount of Calgon and a few drops of Coal Master dispersant were added. The beaker was placed in a sonicating bath for 2 to 3 minutes to break the agglomerates. The sonicated coal slurry was then wet sieved through a 400-mesh screen, and the two fractions obtained were dried and weighed. The +400 mesh sample was dry screened. Approximately 1 g of the –400 mesh sample was dispersed in 100 ml of distilled water. After the addition of 0.1% Calgon solution and Coal Master, the particle size distribution was determined using a Leeds and Northrop SPA Microtrac. This procedure was repeated for the feed and tailings samples. The ash contents of the different fractions were determined in a Thermogravimetric Determinator (LECO TGA 501). From the weights of recovered coal and the ash contents, the yield, grade and ash rejections were calculated.

The static pressure measurements along the column height were used to compute the average gas hold-up in the recovery zone. Using the drift flux approach, the average bubble size in the recovery zone was estimated (Ityokumbul et al. 1995). From the particle size distribution analysis and the average bubble size, the ratio of projected particle surface area per unit bubble surface area was calculated for the different experimental runs.

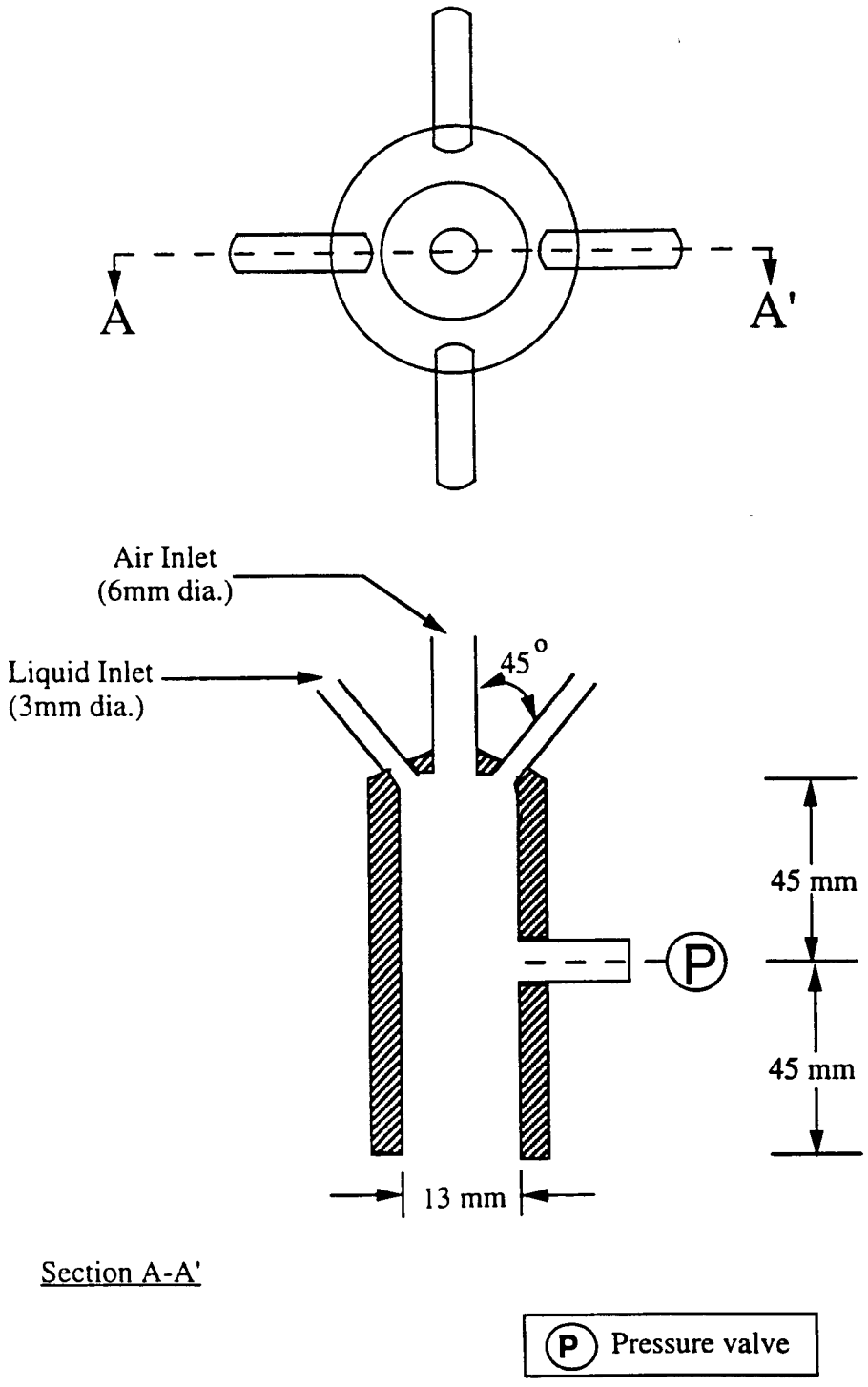

Figure 2.3.17 DETAILED DRAWING OF THE VORTACTOR TURBULENT CONTACT CHAMBER

2.3.2.1 Effect of Hydrostatic Pressure Setting

The variations of concentrate flow rate, grade, and froth phase gas hold-up with hydrostatic pressure setting are shown in Table 2.3.6. In these tests, the air flow rate was fixed at 6 L/min. The froth phase gas hold-up was estimated from the pressure sensor located 0.46 m from the cell lip. At hydrostatic pressure settings of 1.75 m and 2.0 m, the concentrate flow rate and product grade remained constant. By contrast, lowering the hydrostatic pressure setting to 1.5 m resulted in a sharp decline in the concentrate flow rate and ash content. The results obtained clearly show the importance of maintaining tight control of column operational parameters. For example, an increase of the froth phase gas hold-up from 59% to 69% reduced the concentrate flow rate by almost 50%. The reductions in the product ash content and concentrate flow rate are attributed to better drainage of the froth. In the case of the former, better drainage will mean recovery of less hydrophilic ash particles, while in the latter, better drainage will reduce the froth mobilities.

Table 2.3.6 Effect of Hydrostatic Pressure Setting on Froth Phase Gas Hold-up, Concentrate Flow Rate and Grade

Hydrostatic pressure setting, m	Average froth-phase gas hold-up, %	Concentrate flow rate, g/min	Product Ash (wt. %)
1.50	69	123	3.71
1.75	59	225	5.06
2.0	54	222	5.18

2.3.2.2 Effect of Recovery Zone Height

Figure 2.3.18 shows the effect of recovery zone height on yield and product ash content. These tests were carried out at a superficial gas velocity of 0.022 m/s (air flow rate of 6 liters per minute). The results show that the concentrate flow rate was largely independent of recovery zone height (236 ± 14 g/min). Several authors (e.g. see Bensley et al. (1985); Ounpuu and Tremblay, (1991); Ityokumbul, (1993)) have reported that the recovery zone height had negligible effect on the product yield. It is apparent from the foregoing that tall columns may not be required for the flotation of the Lower Kittanning

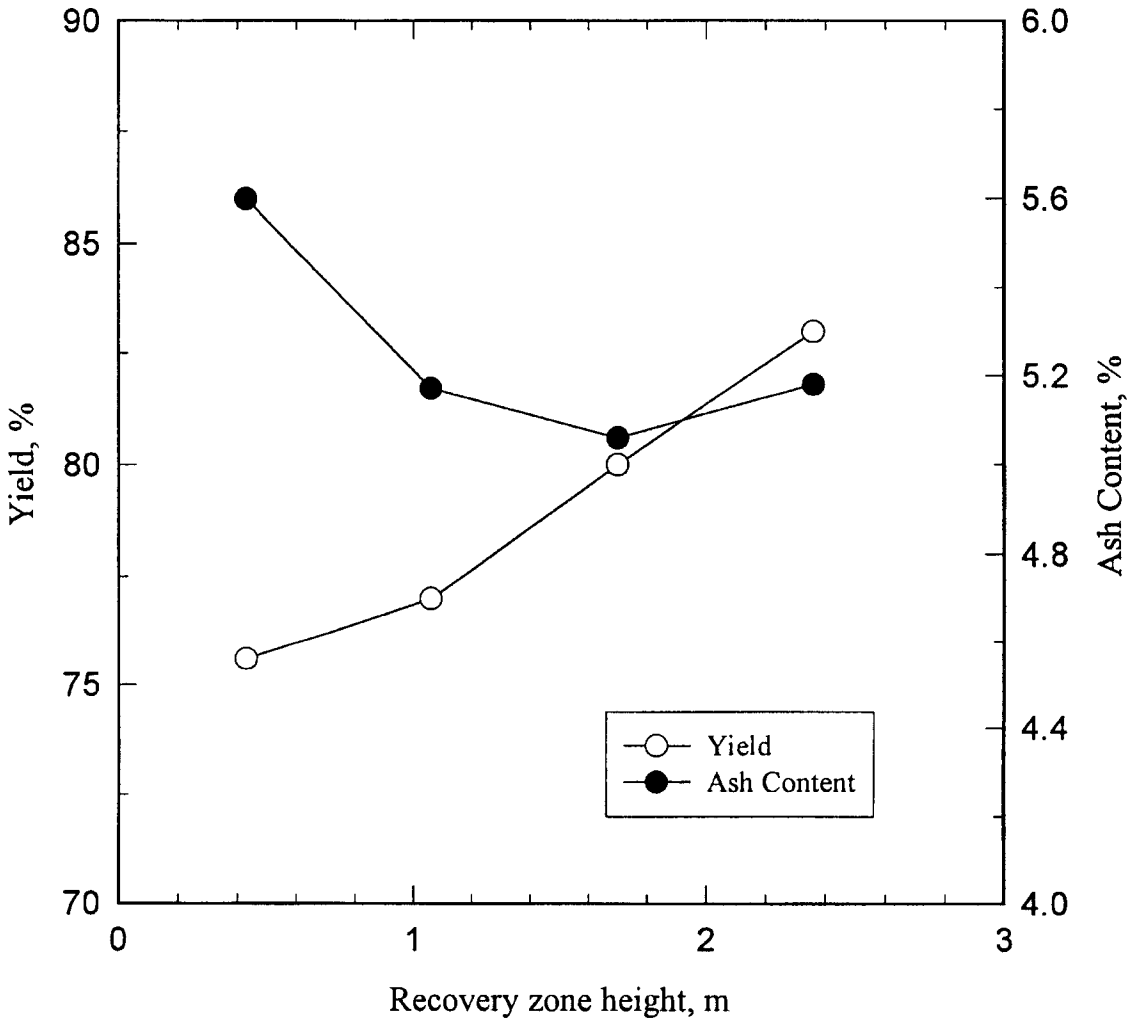

Figure 2.3.18 VARIATION OF CLEAN COAL YIELD AND GRADE WITH RECOVERY ZONE HEIGHT (Air Flow Rate=6 LPM)

seam coal used in the present study. This observation (i.e. negligible effect of recovery zone height on concentrate flow rate) is noteworthy as it illustrates the limitation of using statistical design in flotation column studies. For example, if the recovery zone height is one of the variables in a factorial design of column flotation experiments, the results show that no significant effect should be expected for recovery zone heights above 0.43 m.

The results show that with the exception of the lowest feed location, the product ash was fairly constant and was in the range expected for the observed yields. By contrast, Bensley et al. (1985) reported that the product ash increased as the feed location was raised. While the reasons for this are not entirely clear, it is noted that wash water was only employed in this study. With wash water addition, entrainment of fine refuse is suppressed.

2.3.2.3 Effect of Feed Solids Concentration

The effect of solids concentration on the yield, concentrate flowrate, and product ash was determined at an air flow rate of 3 L/min. In these experiments, the feed solid flow rate varied from 139 g/min (2.5% slurry) to 585 g/min (10% slurry) and the results are shown in Figure 2.3.19. The results show that the yield and product ash content decreased with increasing feed solid concentration, with the effect being more pronounced at solids concentration above 2.5%. Concurrently, a stable froth layer was observed in the collected tailing samples. Thus, the reduction in the concentrate flow rate is attributed, in part, to the loss of overloaded bubbles that lack the buoyancy to reach the froth phase (King et al., 1974; Szatkowski and Freyberger, 1984).

The results obtained at the high solids feed rates simulate column applications in cleaning duty. Typically, the separation in cleaner operations involves material that is hydrophobic. Because the transfer of particles to the bubble surface will not be rate limiting, the bubble loading process will be relatively fast. Thus, the use of tall columns will result in highly overloaded bubbles, which may lack the buoyancy to reach the froth zone. Thus, for cleaner operations, the use of short columns is strongly recommended. This may be the reason that Mines Gaspé currently operates a 3.66-m tall column in their copper cleaning circuit (Comeau 1995).

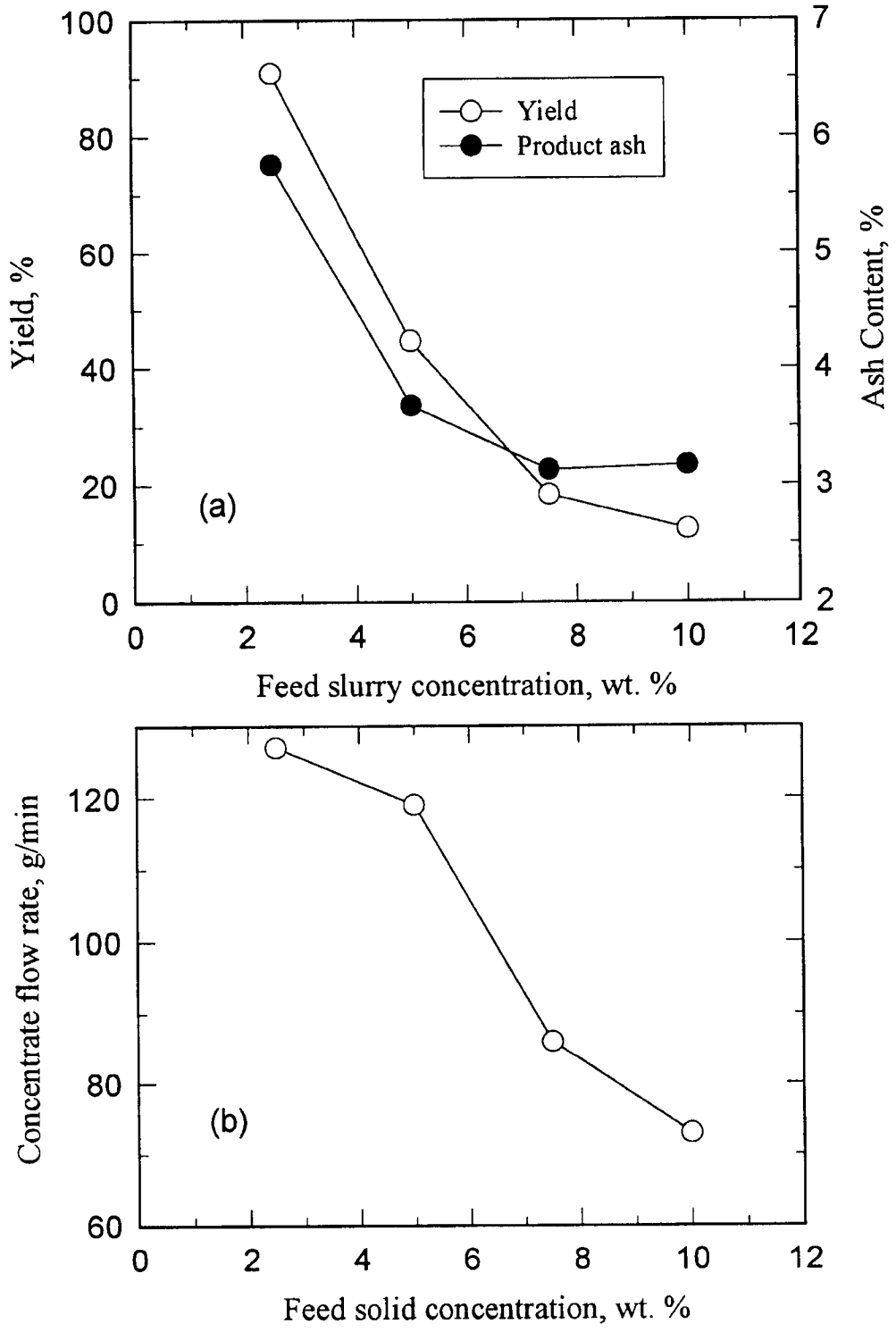

Figure 2.3.19 **EFFECT OF FEED SOLIDS CONCENTRATION ON FLOTATION RESPONSE (a) CLEAN COAL YIELD AND GRADE (b) CONCENTRATE FLOW RATE (Air Flow Rate=3 LPM**

The results of the study show that the clean coal ash content decreased with increasing feed solids concentration. At feed solids concentration greater than 5%, the bubble surface availability appears to be rate limiting. Under bubble surface limiting conditions, the competition for the available surface clearly favors the more hydrophobic material (cleanest product). By contrast, at a feed solids concentration of 2.5%, the availability of bubble surface was not rate limiting. Under these conditions (free flotation), less hydrophobic material is not rejected from the froth zone. Furthermore, analysis of the froth did not show any significant differences in the product fineness. Thus, the drop in product ash content from 5.76 % to less than 3.2% as the feed solids concentration was increased from 2.5% can only be explained on the basis of limiting bubble surface area availability. Since the project objective called for a 5% ash product, operation of the column under surface limiting conditions is not recommended.

2.3.2.4 Effect of Air Flow Rate

The variation of clean coal yield and product grade with air flow rate is shown in Figure 2.3.20. These tests were carried out using a 5 wt. % feed slurry. The results show that the yield, concentrate flow rate and product ash content increased with air flow rate. This trend is expected since the available bubble surface area increases with air flow rate. Bensley et al. (1985) have reported similar results. For a solids feed rate in the range 240-320 g/min, it appears that conditions of free flotation are encountered at air flow rates above 3 L/min. This is consistent with earlier observations on the presence of air bubbles in the tailing samples collected at low air flowrates. Since the project objective called for the production of clean coal with an ash content of 5%, a single column flotation stage is sufficient with a yield of 66-80%.

2.3.2.5 Evaluation of Vortactor Turbulent Contactor

The Mott porous sparger used in the studies reported above was replaced with the Vortactor. Table 2.3.7 shows the preliminary results obtained with the Vortactor bubble generator. The results show that flotation performance (yield, product ash and concentrate flow rate) was independent of feed location. This observation is consistent

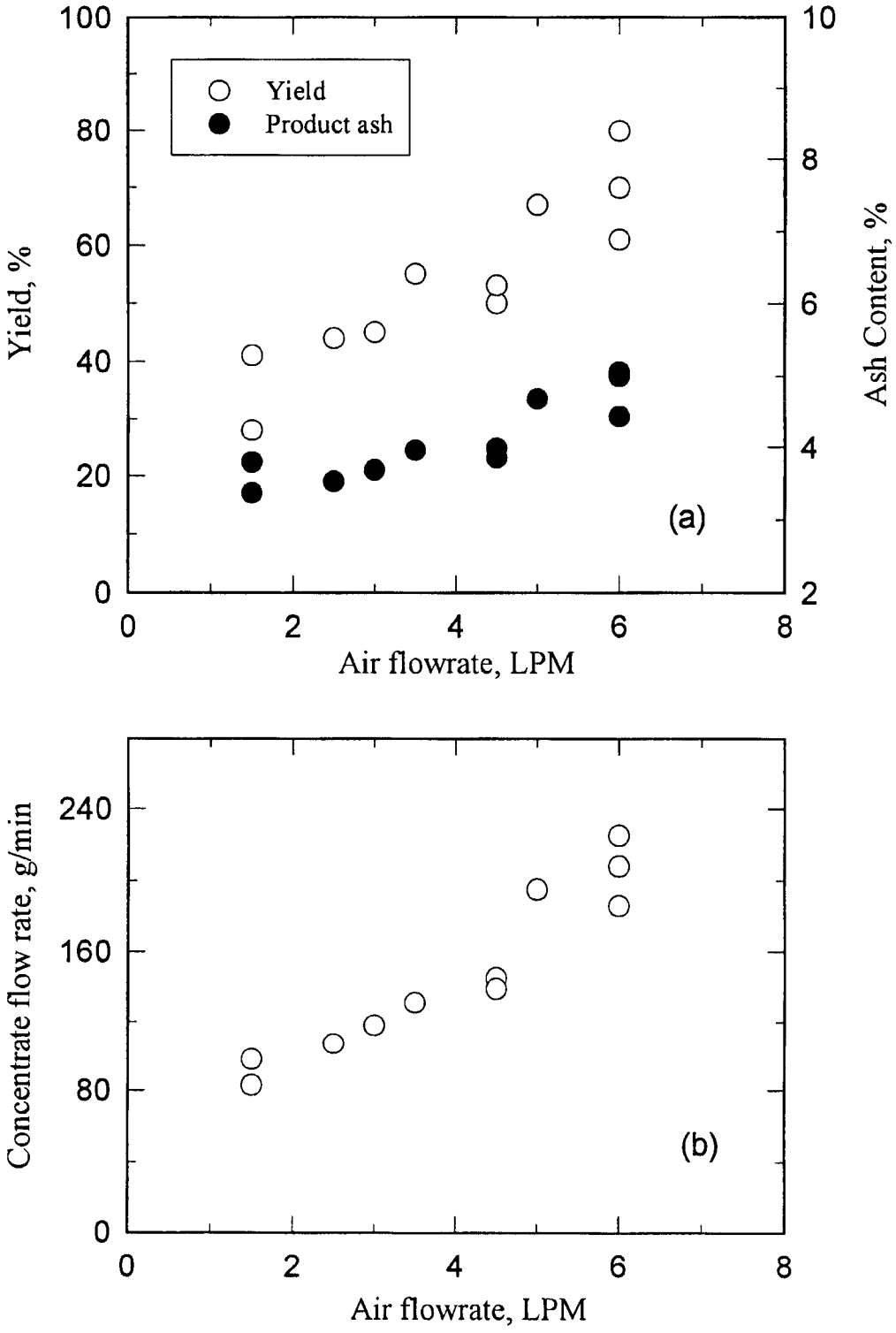

Figure 2.3.20 EFFECT OF AIR FLOW RATE ON (a) CLEAN COAL YIELD AND GRADE (b) CONCENTRATE FLOW RATE (Feed Solids Concentration = 5%)

with the results obtained with the Mott sparger. However, since there is no bulk transport of feed material above the inlet point, the results suggest that particle-bubble attachment is rather fast and takes place in the contact chamber and/or feed line.

Table 2.3.7 Preliminary Evaluation of Vortactor Bubble Generation in Fine Coal Cleaning

Air flowrate (liters/min)	Feed inlet[1] (m)	Yield (%)	Product Ash (wt. %)	Concentrate flowrate (g/min)
2	0.43	46.6	3.77	110
2	1.70	42.1	3.62	110
6[2]	1.70	70.1	5.40	181

[1] Distance from the bottom of the column
[2] The pulverizer used for coal preparation broke down and we had to change our coal preparation procedure.

Increasing the air flow rate from 2 L/min to 6 L/min increased the yield and concentrate flowrate to the levels obtained with the Mott porous sparger; however, the product ash was considerably higher. The reasons for the higher ash content observed with the Vortactor bubble generator at an air flow rate of 6 L/min are not entirely clear. However, the gas hold-up data suggest that the column operating conditions did not favor adequate drainage of the froth (Leffler 1997). This observation is partially supported by the recovery of coarse size fractions (i.e., +140 mesh and -140+200 mesh fractions) with unusually high ash content. The results obtained with an air flow rate of 2 L/min clearly show that increasing the recovery zone height (i.e., lowering the feed inlet point) did not have any effect on the yield and concentrate flow rate. As indicated with the Mott porous

sparger, this observation would suggest that tall columns are not required for fine coal flotation.

2.3.2.6 Correlation for Column Carrying Capacity and Yield

In flotation column separation, it is important to predict the yield and carrying capacity. These quantities are dependent on the column operational parameters. In the present case, the drift flux approach was used to estimate the average bubble size. From the measured particle size distribution, air flow rate and average bubble size, the projected particle to bubble surface area was determined. The clean coal yield was similarly determined from the measured rates of tailing and concentrate flows. From dimensional analysis, it can be shown that the column carrying capacity is related to the column operational parameters by the expression (Ityokumbul and Trubelja, 1998):

$$C_a = K\left(\frac{360\,U_g}{d_b\,S_p}\right) \tag{2.3.3}$$

where:

K is a constant (projected particle surface area per unit bubble surface).

U_g is the superficial gas velocity (cm/s),

d_b is the bubble diameter (cm), and

S_p is the projected particle surface area (cm^2/g).

The experimentally determined carrying capacities were plotted according to Equation 2.3.3 (see Figure 2.3.21). It can be seen that the data are well described by the relationship:

$$C_a = 0.5\left(\frac{360\,U_g}{d_b\,S_p}\right) \tag{2.3.4}$$

A comparison of Equations 2.3.3 and 2.3.4 reveal that K is equal to 0.5. This value is significant – it suggests that, in column flotation, the maximum carrying capacity will be obtained when 50% of the bubble surface in the recovery zone is covered by particles. While higher bubble loading is possible, the coalescence phenomena that occur in the froth zone would result in some of the collected particles being returned to the recovery zone. A comparison of the results of the present study with correlations currently

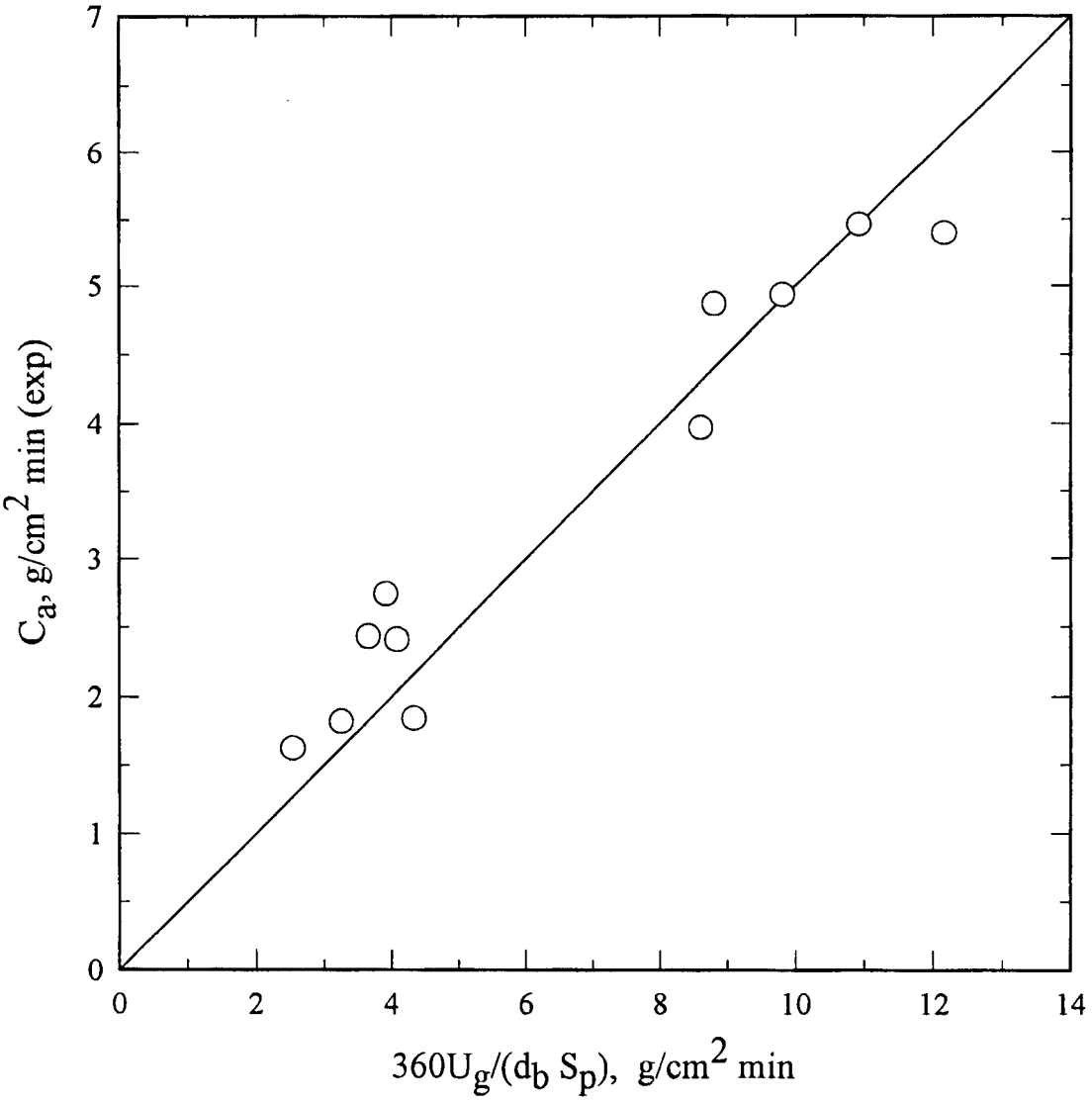

Figure 2.3.21 VARIATION OF CARRYING CAPACITY WITH COLUMN OPERATIONAL PARAMETERS

available in the literature gave good agreement only under free flotation conditions (Ityokumbul and Trubleja, 1998).

It is generally accepted that flotation is an interfacial phenomenon. However, availability of bubble surface is hardly considered in flotation analysis. For an interfacial phenomenon, the yield should decrease as the ratio of projected particle area to bubble surface increases. This hypothesis was tested by plotting clean coal yield as a function of

particle projected area per unit bubble surface (see Figure 2.3.22). Regression analysis of the data gave the relationship:

$$Yield = 0.445 \left(\frac{A_p}{A_b} \right)^{-1.05} \qquad (2.3.5)$$

where

A_p is the total projected particle surface area flux in the feed, and

A_b is the bubble surface area flux.

The regression coefficient for Equation 1.3.5 was 0.83. As expected, the yield decreases with increasing ratio of projected particle to bubble surface area. A similar trend was reported by Bradshaw and O'Connor (1996) with pyrite flotation, even though their tests were conducted in a semi-batch manner. This observation clearly supports the well-established practice of feed desliming prior to flotation. It is noted that there is an almost linear relationship between the yield and the ratio of the surface areas, as predicted by theory.

2.3.3 Overall Evaluation

In order to determine the optimum conditions for the processing of the Lower Kittanning seam coal, the yield index is plotted as a function of the ash rejection for all the tests carried out in the present study (see Figure 2.3.23). The results show that the optimum conditions will give a yield index of about 45-48% at an ash rejection of 60%. These optimum conditions will give a clean coal yield of 75 - 80% with an ash content in the range 4.8 - 5.1 %.

The operational parameter that affects the product grade is the gas hold-up in the froth phase. For effective removal of fine refuse the use of wash water has proven successful. However, these results also show that a well-drained froth having gas hold-up of 55-70% was necessary for achieving target grades (see Figure 2.3.24). Since the objective of the current study is to produce a clean coal product with an ash content of less than 5%, the results show that this can be done in a single stage of column flotation. The processing conditions necessary for achieving these target objectives are:

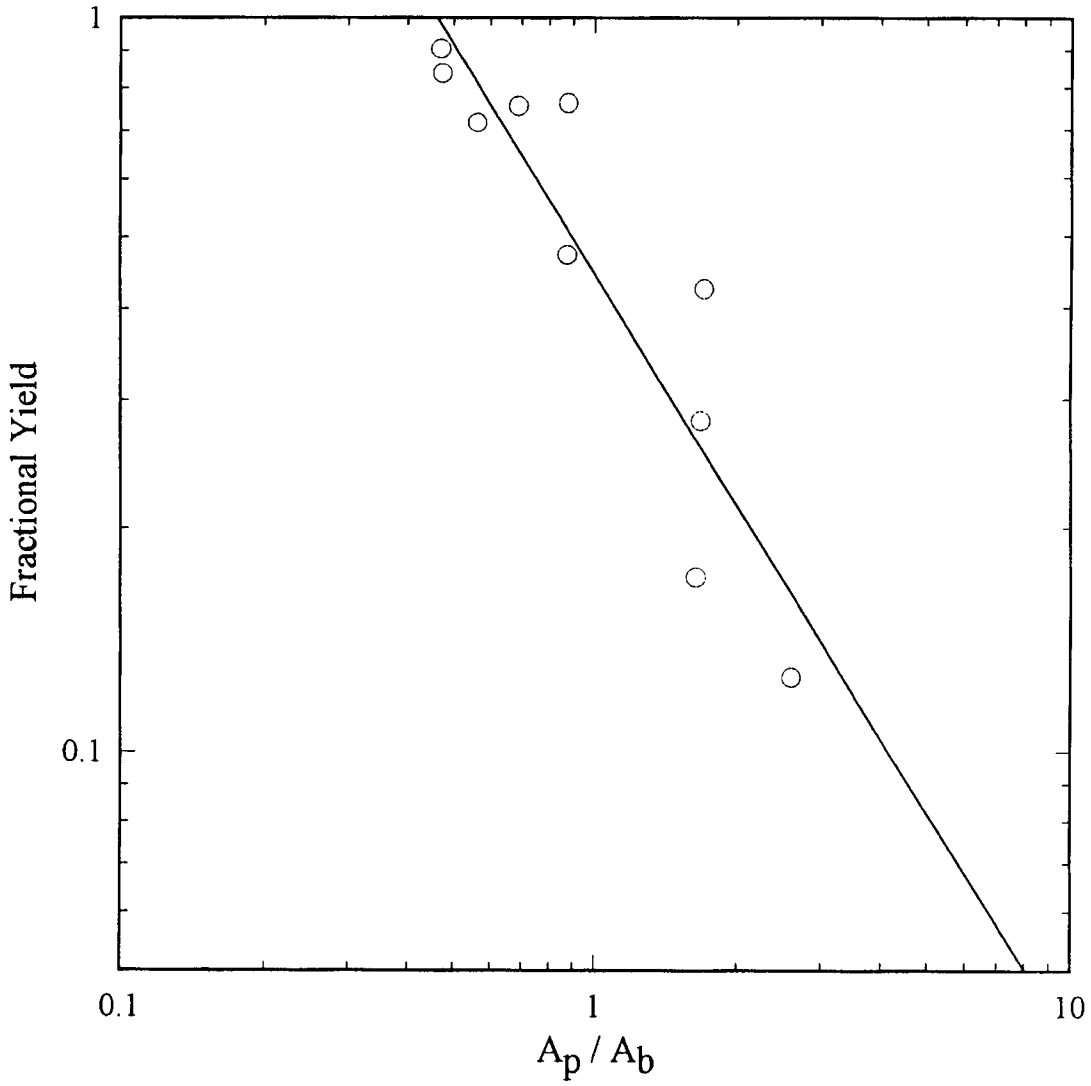

Figure 2.3.22 VARIATION OF FRACTIONAL YIELD WITH PARTICLE PROJECTED SURFACE AREA PER UNIT BUBBLE SURFACE AREA

- air flow rate of 6 liters per minute
- solid feed rate 240-280 g/min, and
- froth phase gas hold-up of at least 50%.

2.3.4 Conclusion

The results suggest that flotation columns may not be effective for cleaning duties (where bubble surface area is limiting), except where a high value product is to be

produced. Since the project objective called for a 5% ash product, operation of the column under bubble surface limiting conditions is not recommended. For optimum results in fine coal cleaning, the feed solid concentration should not exceed 5 wt. %. This observation is consistent with the results of Bahr et al. (1987).

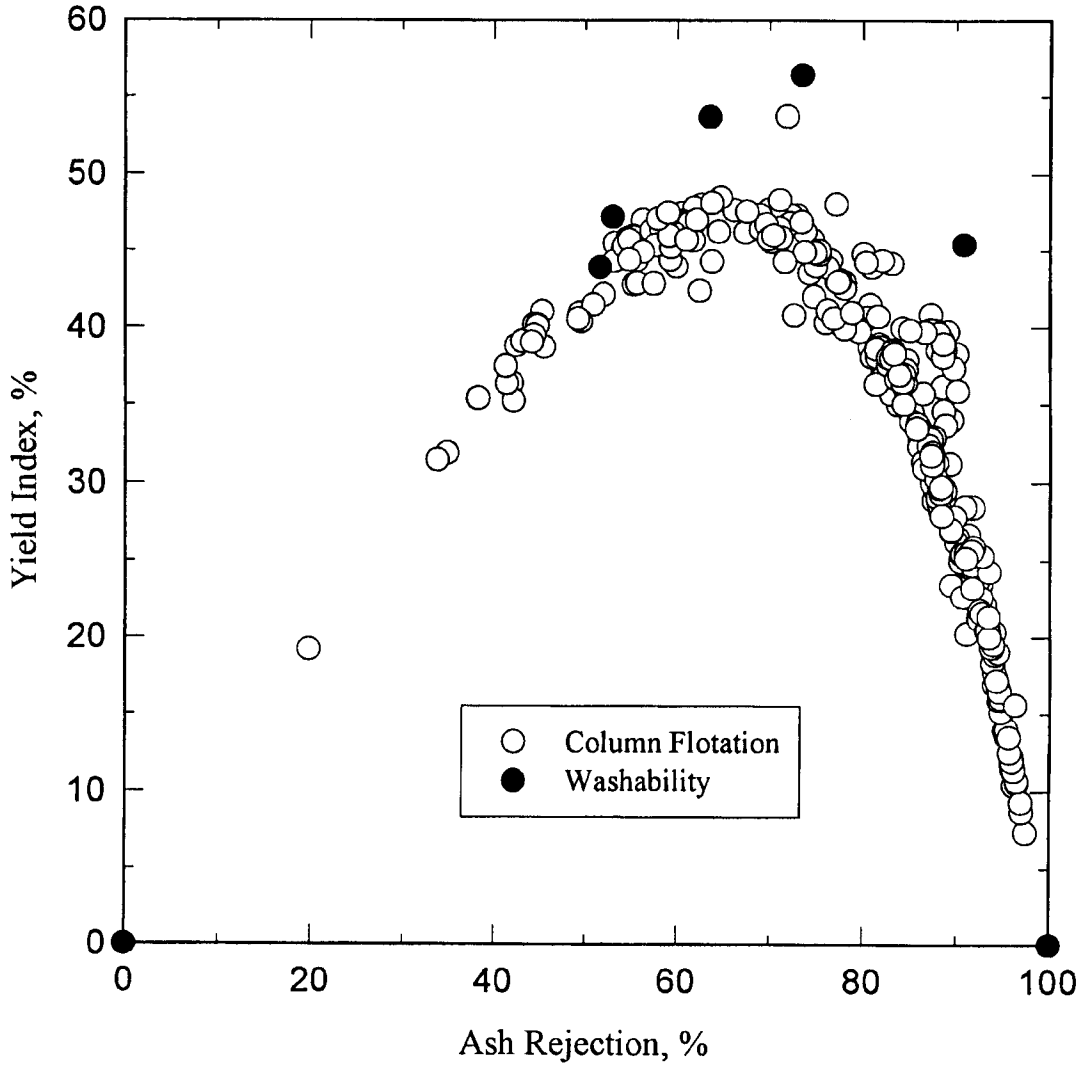

Figure 2.3.23 COMPARISON OF COLUMN FLOTATION AND WASHABILITY RESULTS

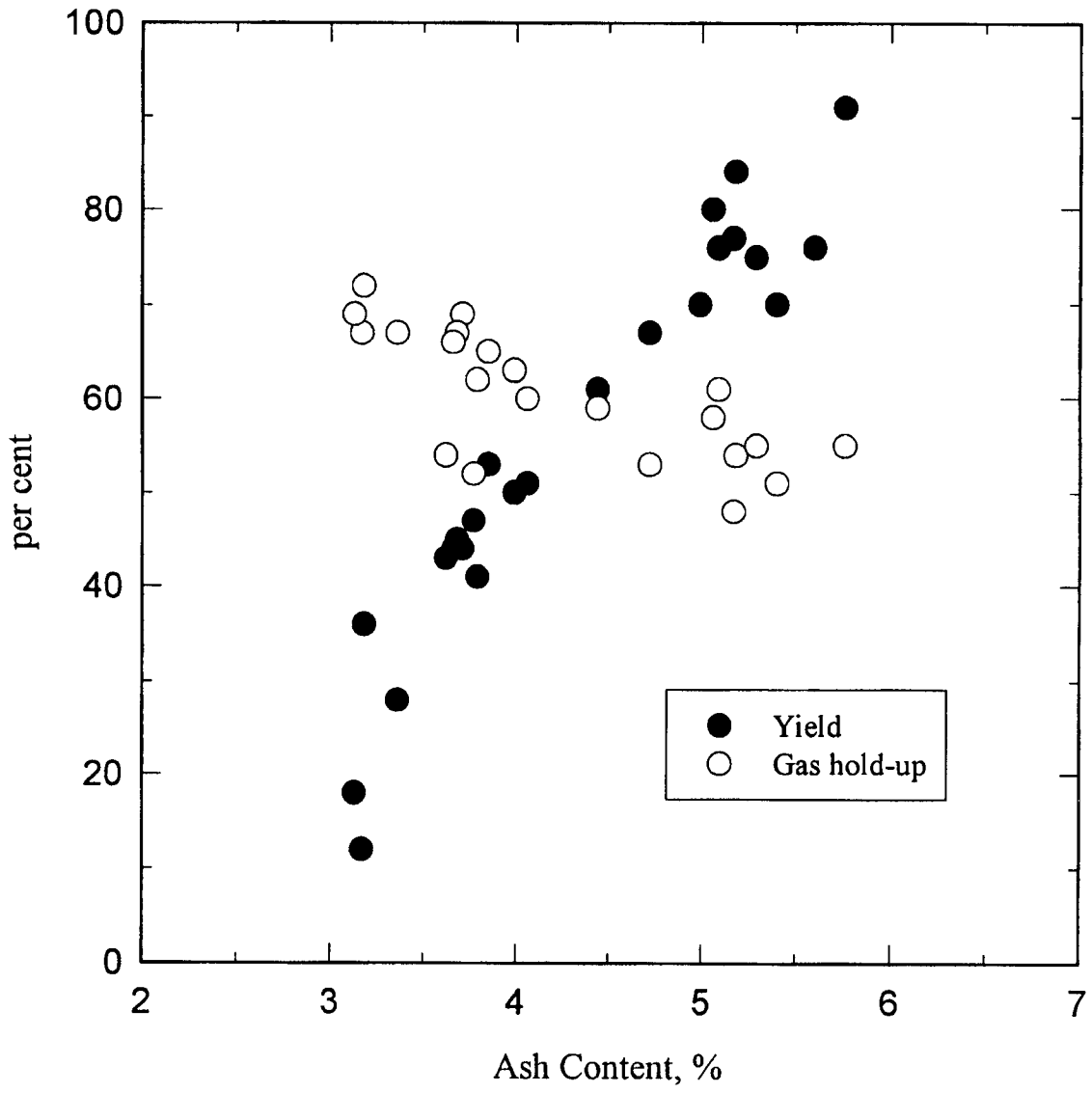

Figure 2.3.24 VARIATION OF CLEAN COAL YIELD AND GRADE WITH FROTH PHASE GAS HOLD-UP

2.4 Dry Processing

Dry separations of fine coal were carried out using triboelectrostatic separation. As part of this study, a laboratory electrostatic separator was constructed and tested to demonstrate the ability to clean fine dry coal on a continuous basis. The separations were evaluated in terms of clean coal yield and ash content. One of the potential problems of dry, fine coal separations is the tendency for particles to agglomerate. As such,

deagglomeration testing was also conducted. Finally, tests were conducted to verify the application of an integrated grinding/cleaning circuit.

2.4.1 Continuous TriboElectrostatic Separation

A continuous, laboratory triboelectrostatic separator was fabricated for use in this study. The test unit consisted of two, 600 mm diameter, rotating copper plates, which were spaced 100 mm apart (Figure 2.4.1). The plates were enclosed within a 810 mm high by 725 mm deep by 115 mm wide box constructed of 6.35 mm thick Plexiglas. The entire unit was mounted on a table. The diameter of the plates was based on the results from the batch testing, which showed that the bulk of the particles separated within a distance of 600 mm from the feed end (Weiland 1996).

The voltage was applied to each plate by attaching the positive or negative electrode from each power supply to a metal washer that "rides" on a rotating copper shaft, which was attached directly to the plate. The drive pulleys were insulated from the copper shafts. The plates were belt driven using a variable-speed motor.

The coal was fed with a vibrating feeder into a venturi feeder where it was entrained in a nitrogen stream. The solids were passed through an in-line copper static mixer to charge the particles. The solids were then discharged downward into the separator where they were collected electrostatically on the rotating plates. The separated material was scraped off at the bottom of the plates and allowed to fall into collection ports. A rotational speed of approximately 5 rpm was sufficient to facilitate product removal. After removal, the products were withdrawn under vacuum into separate Plexiglas cyclones where the solids were separated from the gas stream. The vacuum was provided by separate sweepers. The sweepers were also used to draw sweep air through the flow straighteners at the top of the separator.

Initial tests were carried out using -100 mesh Upper Freeport seam coal to establish an operating procedure and to determine limiting conditions for the separator. It was found that during operation of the separator, arcing occurred between the drive pulleys and the rotating plates at above approximately $\pm$15 kV, thus limiting the maximum operating voltage.

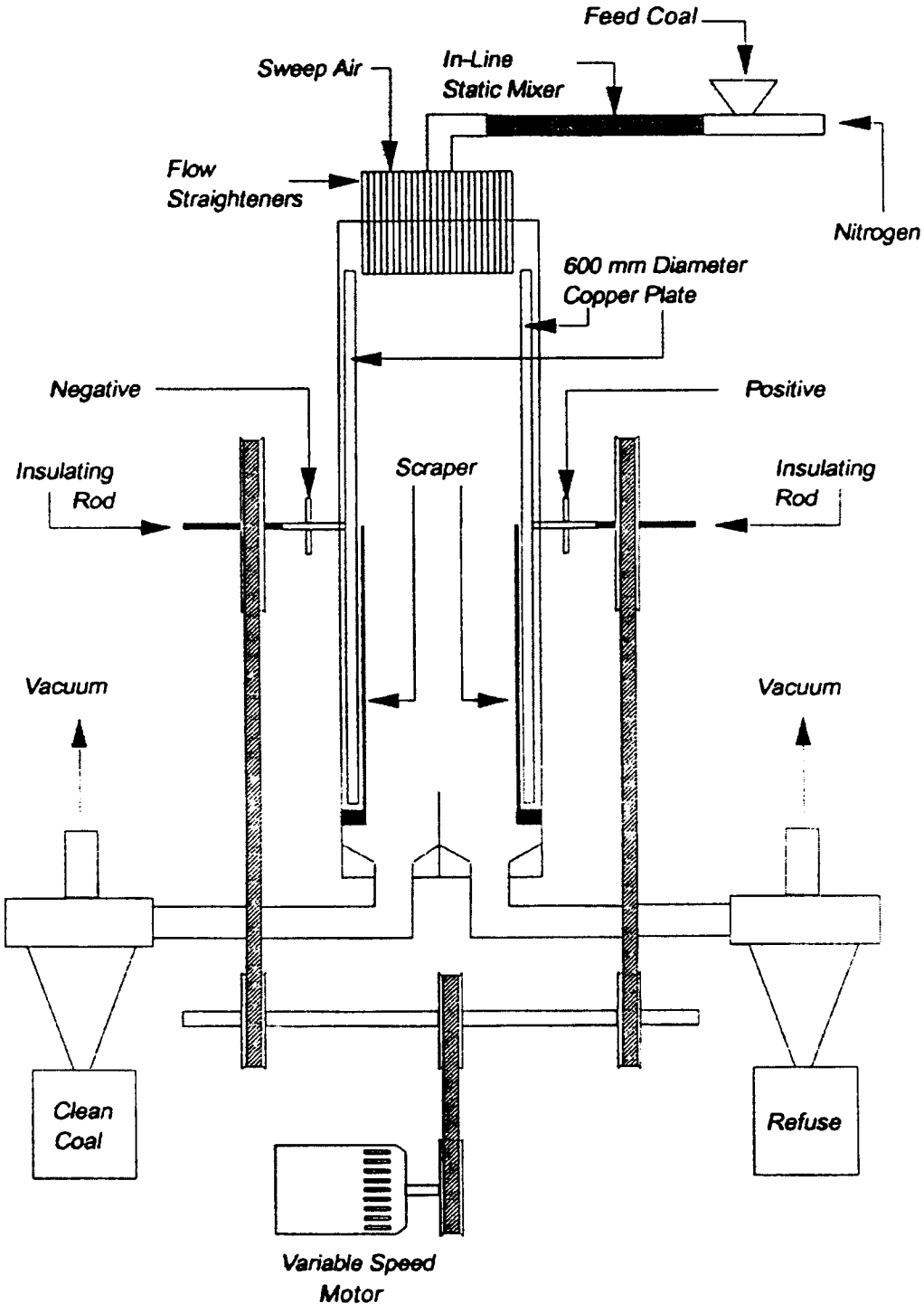

Figure 2.4.1 SCHEMATIC OF THE CONTINUOUS TRIBOELECTROSTATIC SEPARATOR

Ideally, after tribocharging, the coal and refuse would be collected onto the rotating plates and then removed as the material passed by the scraper. This material would fall into the collection trough where it would be drawn through the cyclones and then collected. However, several problems occurred during operation of the separator.

As the material was scraped from the plates, cross contamination occurred between the clean coal and refuse as the products fell toward their respective collecting troughs. The center splitter was extended to minimize this effect. Also, part of the recovered material was not carried into the cyclone collectors but remained in the collecting troughs. Although higher sweep air velocities would alleviate this problem, they could not be obtained with the circuit as tested.

Tests were carried out using Indiana, Pittsburgh, and Upper Freeport seam coals. The feed size for all coals was a nominal -100 mesh, which was obtained by stage crushing in disk and Holmes pulverizers. The Holmes pulverizer was the same as that used to integrate the grinding and batch electrostatic separation process, as discussed in a later section. However, for these tests, the -100 mesh coal was prepared separately and stored under argon in aluminum laminated bags until it was needed.

The coal was dried at approximately 100°C for two hours prior to separation. This material was then fed by a vibrating feeder into a venturi feeder and then passed through the in-line copper mixer (tribocharger) prior to electrostatic separation. Compressed nitrogen was used as the transport medium. Several hundred grams of coal were passed through the separator for a given test. Upon completion of the test, the coal and refuse were recovered from the plates, collecting troughs, and cyclones. The samples were weighed and analyzed for ash content.

Table 2.4.1 gives the weight distribution and ash values for the material collected from various parts of the separator and collection system. As can be seen, the results indicate that the device was able to separate the coal selectively. However, the overall separation was not as efficient as the batch separation because of the limitations discussed previously. Ideally, the bulk of the solids would be carried into the cyclone for collection in the cyclone underflow stream. As noted previously, some material will remain on the plates. For this unit, it was not possible or necessary to scrape all the material from the rotating plates after each revolution, and generally a thin layer of solids

remained on each plate. This buildup had a minimal effect on the collecting ability of the plates. Furthermore, the material remaining on the plates could benefit the process by reducing the wear on the plates, because the scraper would not contact the plates directly.

Table 2.4.1 Continuous Triboelectrostatic Separator Results when Processing -100 Mesh Indiana Seam coal (feed ash = 9.1%), -100 Mesh Pittsburgh Seam Coal (feed ash = 6.8%), and -100 Mesh Upper Freeport Seam Coal (feed ash = 11.2%)

	Clean Coal		Refuse	
Product	Weight, %	Ash, %	Weight, %	Ash, %
Indiana Seam				
Electrode (Plate)	20.4	3.1	11.2	22.4
Collecting Trough	12.3	5.4	6.7	16.9
Cyclone	26.3	6.2	23.2	10.8
Total	59.0	5.0	41.0	15.0
Pittsburgh Seam				
Electrode (Plate)	35.2	2.0	18.2	13.9
Collecting Trough	12.1	5.3	12.9	12.9
Cyclone	21.2	5.6	0.4	9.1
Total	68.5	3.7	31.5	13.4
Upper Freeport Seam				
Electrode (Plate)	37.7	3.5	19.8	21.1
Collecting Trough	11.0	9.4	14.4	22.3
Cyclone	15.6	8.0	1.5	17.7
Total	64.3	5.6	35.7	21.4

In addition to the solids on the plates, some material settled in the airways leading to the collection cyclones. However, because any material in the airways was in the proper product stream, it could be collected and included with the appropriate product. For a long time run in a continuous operation, it is likely that a steady state would be

reached such that a constant amount of material would build up on the plates and throughout the collection system, allowing a steady amount of product to be collected.

As seen in Table 2.4.1 for the Indiana seam coal, the ash content was reduced from 9.1% in the feed to 5.0% in the clean coal at a yield of 59%. The corresponding ash content of the refuse was 15.0%. In the case of the Pittsburgh seam coal, clean coal with an ash content of 3.7% was obtained at a yield of 68.5%, with a refuse ash content of 13.4%. For the Upper Freeport seam coal, the ash content was reduced from 11.2% to 5.6% at a yield of 64.3%. The corresponding ash content of the refuse material was 21.4%. In all cases, middling streams could be obtained from the system. These streams would be candidates for regrinding followed by reprocessing to recover additional coal.

In all cases, the lowest ash material was found on the negative (clean coal) collecting plate and represented over 50% of the total clean coal in some cases. Similarly, the highest ash content material was typically found on the positive (refuse) collecting plate and also represented a significant portion of the respective product. Even though the splits among the plate, collecting trough, and cyclone would change depending on the total quantity of coal being fed to the unit, the overall yield and product quality should remain constant.

Some of the material for each product passed through the cyclone overflow and into the sweeper and could not be recovered. This represented between 10 and 20% of the total amount of coal that was fed to the separator. However, based of the comparison of the calculated and measured ash contents of the feed coals, it was likely that the losses were distributed in the same proportions as the product yields. Hence, the overall results would not be affected.

2.4.2 Charging/Deagglomeration Testing

Charging/deagglomeration testing was carried out using the batch triboelectrostatic separator. A fluidized-bed unit was used for deagglomerating and charging the coal simultaneously. The fluidized-bed unit was constructed out of a 1-5/8 inch diameter steel pipe, which was 8 inches long. The unit was sealed at both ends using threaded steel caps. The fluidized bed consisted of a layer (~3/4 inch thick) of either steel or copper beads, which were supported on a screen located in the middle of

the tube. A second screen was located one inch above the lower screen. The nitrogen-entrained coal particles were injected into the fluidized bed from below through a pipe in the side of the steel tube. Contact with the fluidized bed was used to promote deagglomeration and particle charging simultaneously. After passing through the fluidized bed, the coal particles were carried out through a tube, which extended from above fluidized bed down through the bottom cap. The particles discharged into either the copper in-line mixer or a copper transfer pipe prior to injection into the separator. For this testing, -6 mm Upper Freeport seam coal was pulverized to nominal -100 mesh using disk and Holmes pulverizers. The size reduction was done immediately before the testing. After size reduction, the coal was dried for two hours at 100°C. The dried coal was then fed into a venturi feeder, which was connected to the fluidized bed unit. Nitrogen was used as the transport gas. In the first test, the coal was passed through the fluidized bed (containing the copper beads) and then through the in-line mixer before being injected into the batch electrostatic separator. The batch separator consisted of two 48 inch long by 12 inch wide parallel copper plates, which were spaced 4 inches apart (Figure 2.4.2). This unit was the same as that used in previous testing (Weiland, 1996). A voltage of approximately $\pm$20 kV was used for the current tests. Approximately 100 g of coal were used for each test.

Upon completion of the test, the material was recovered from sections spaced along the length of the separator plates. The samples were weighed and the clean coal and refuse yields were calculated. Ash analyses were then performed on all samples. Additional tests were conducted using the following conditions: fluidized bed with steel beads and in-line mixer; fluidized bed with copper beads and transfer pipe; and, in-line mixer only.

Figure 2.4.3 shows the variation of clean coal and refuse yields as a function of distance along the plate for all conditions. As seen, the bulk of the clean coal and refuse material was collected along the first 40 cm of the separator plates. Up until this distance, the highest clean coal yield was obtained using only the in-line mixer, while the lowest yield was for the copper beads/transfer pipe combination. However, over the entire length of the separator, the yields were comparable.

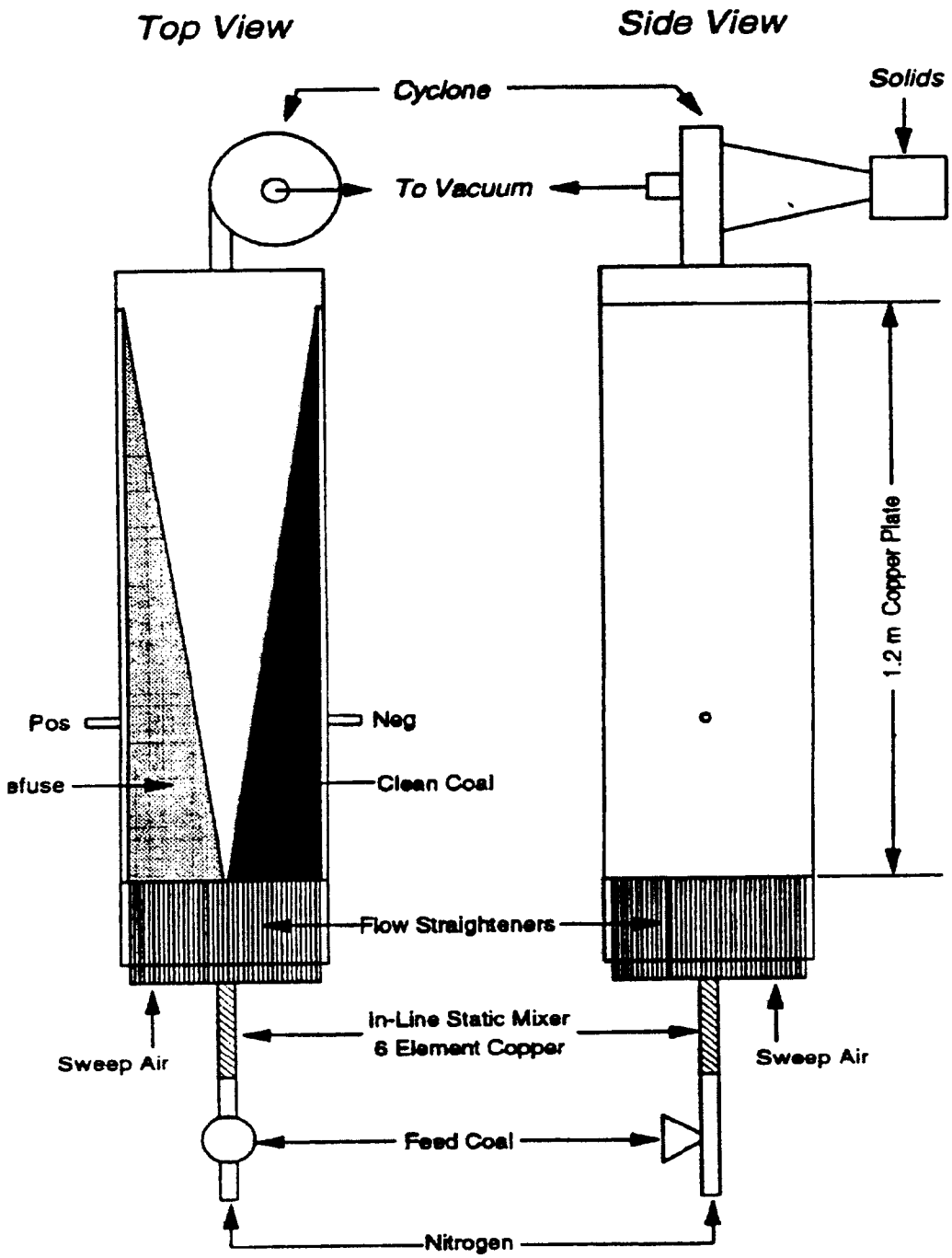

Figure 2.4.2 SCHEMATIC OF THE BATCH TRIBOELECTROSTATIC SEPARATOR

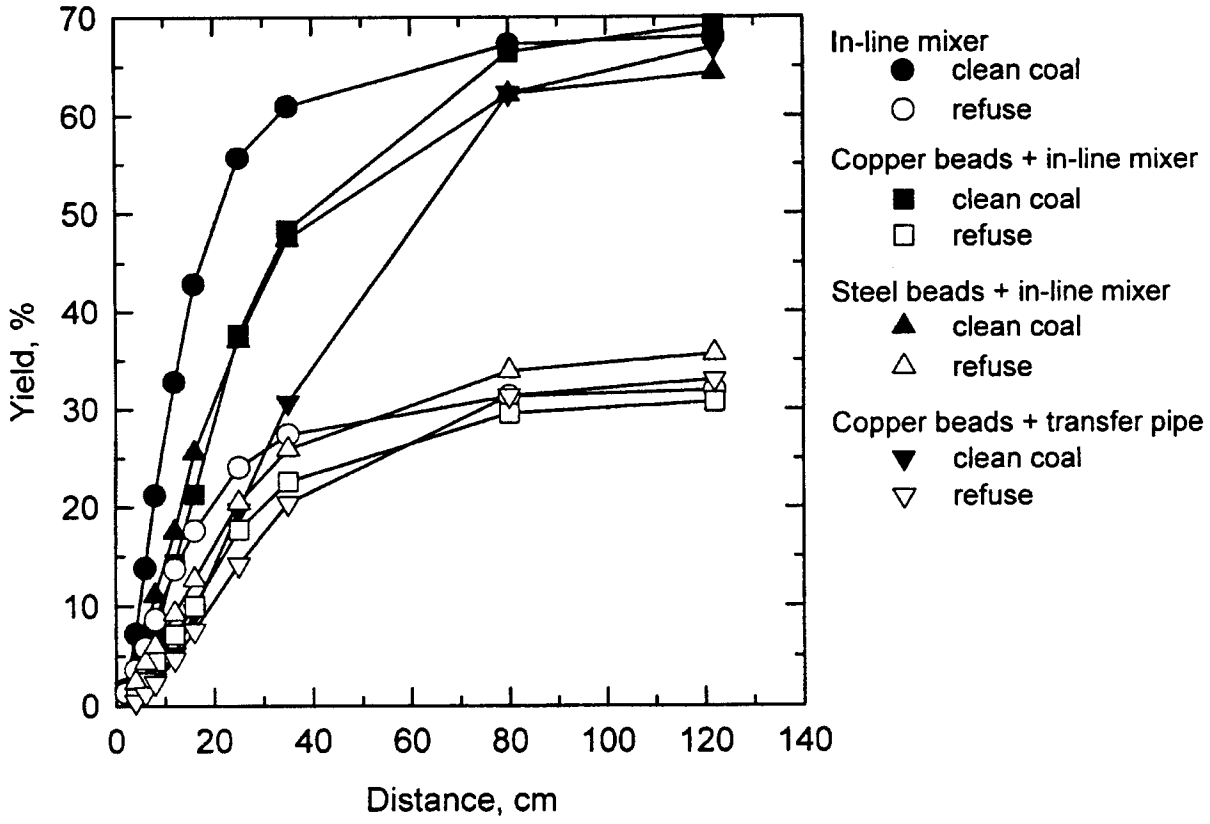

Figure 2.4.3 CLEAN COAL AND REFUSE YIELDS AS A FUNCTION OF DISTANCE ALONG THE BATCH SEPARATOR FOR DIFFERENT CHARGING / DEAGGLOMERATION TECHNIQUES WHEN PROCESSING –100 MESH UPPER FREEPORT SEAM COAL

Figure 2.4.4 shows the variation in the cumulative ash as a function of distance for the same tests. The ash content of the clean coal was very similar in all cases. However, the ash contents of the refuse streams were different, especially for the copper beads/transfer pipe combination. The grade-yield curves for these tests are shown in Figure 2.4.5. As can be seen, for a given yield, the lowest ash content was obtained for the copper beads/in-line mixer combination, followed by the steel beads/in-line mixer combination. This indicates that the fluidized-bed unit may be helping to deagglomerate the particles prior to charging. Furthermore, it also demonstrates that contact with the beads without the in-line mixer may not be sufficient to charge the particles adequately.

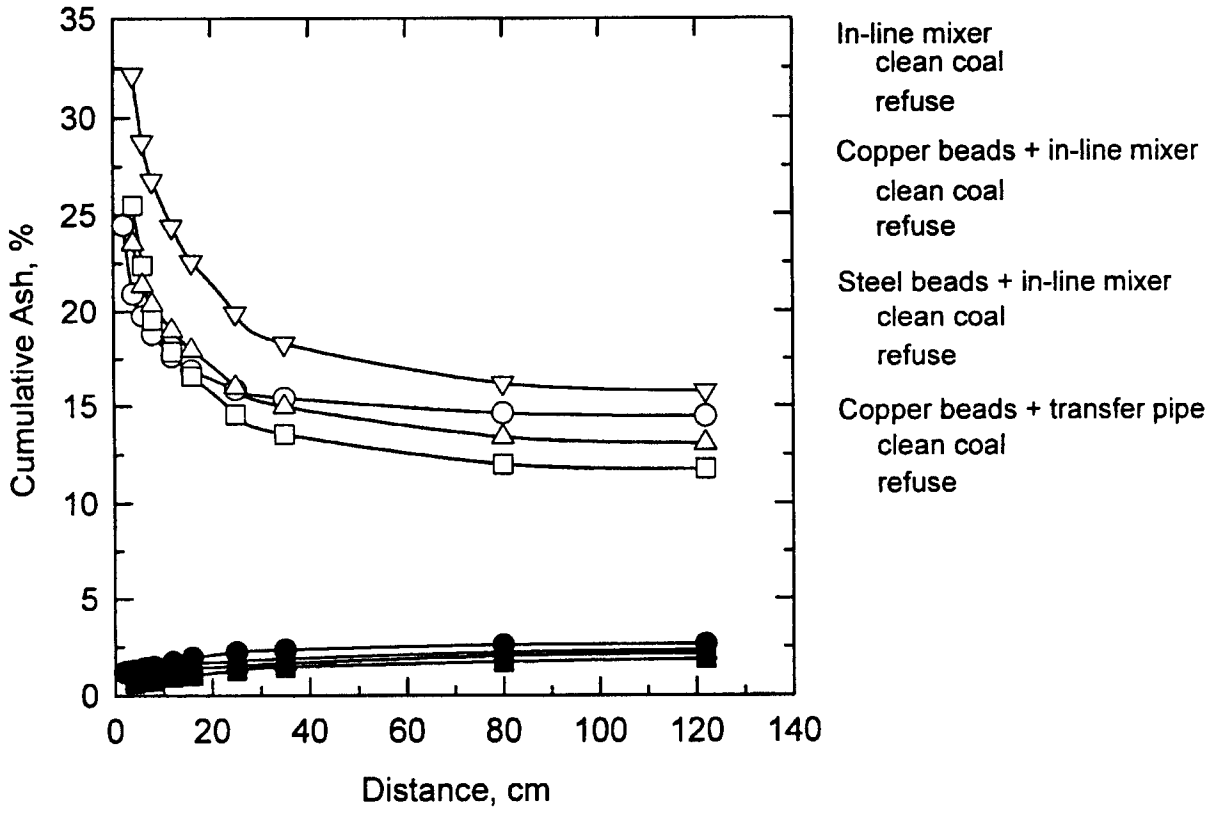

Figure 2.4.4 CUMULATIVE ASH CONTENT FOR THE CLEAN COAL AND REFUSE STREAMS AS A FUNCTION OF DISTANCE ALONG THE BATCH SEPARATOR FOR DIFFERENT CHARGING / DEAGGLOMERATION TECHNIQUES WHEN PROCESSING –100 MESH UPPER FREEPORT SEAM COAL

2.4.3 Integrated Grinding/Separation

Integrating a grinding device prior to triboelectrostatic separation was also investigated. In such cases, the goal would be to achieve sufficient liberation of the coal from the mineral matter with minimal grinding, while adequately charging the particles prior to separation. A Holmes high-speed pulverizer was used for size reduction in combination with the batch triboelectrostatic separator. As noted previously, this pulverizer was also used to prepare the -100 mesh coal that was used in the previous triboelectrostatic separation tests. However, in those cases, the pulverized coal was

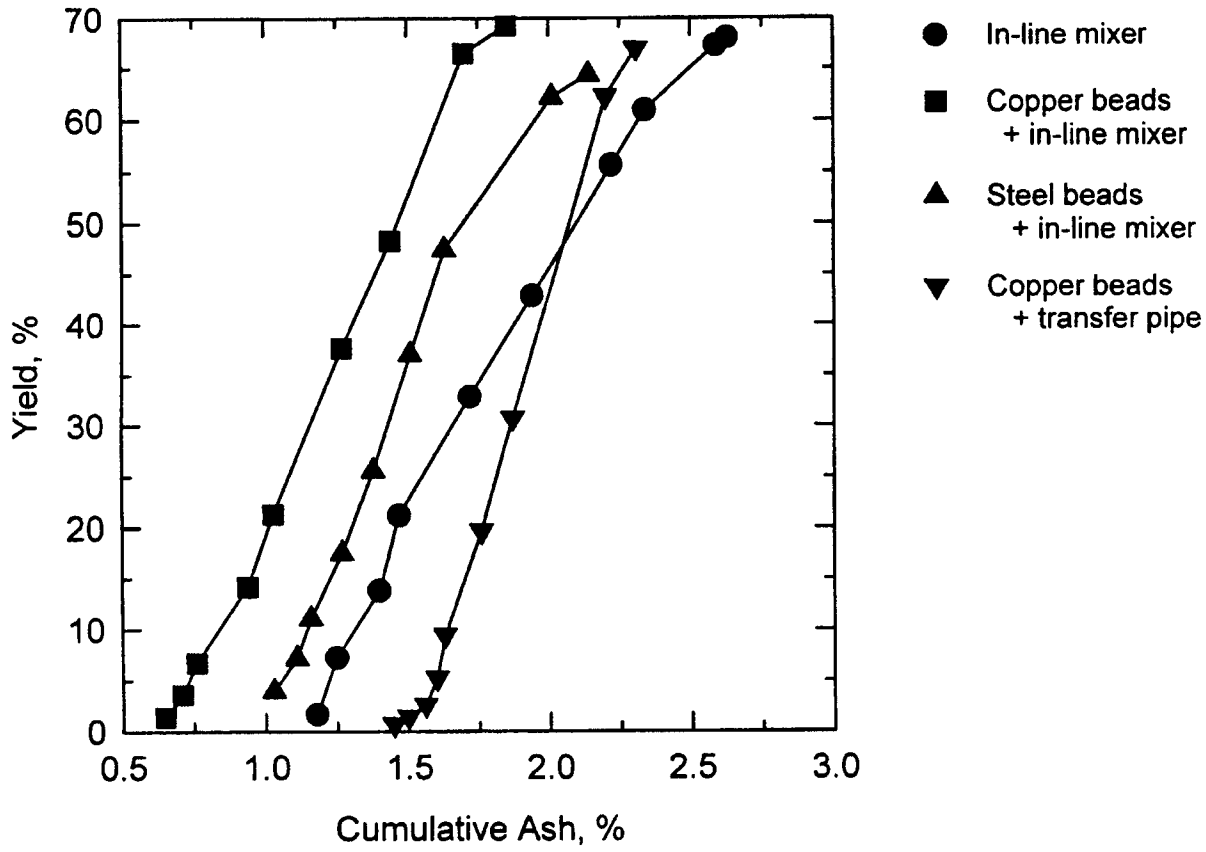

Figure 2.4.5 CLEAN COAL ASH-YIELD CURVES FOR DIFFERENT CHARGING / DEAGGLOMERATION TECHNIQUES WHEN PROCESSING –100 MESH UPPER FREEPORT SEAM COAL IN THE BATCH SEPARATOR

stored under argon for up to several weeks prior to tribocharging and separation. In this case, the coal was used directly after size reduction.

Nominal -28 mesh Upper Freeport seam coal was fed to the pulverizer. As the coal passed through the device, it was pulverized by rotating steel hammers. A stainless steel screen, having nominal 0.2 mm openings, was used to produce a product of approximately -100 mesh. Contact with the hammers and screen provided the opportunity for tribocharging the coal.

In order to provide a direct feed to the separator, the collection bin was removed and a funnel was attached to the pulverizer discharge. The funnel discharge was placed over the venturi feeder of the batch electrostatic separator, which had the in-line tribocharger removed. Nitrogen was used as the transport medium. As in the previous tests, the solids were separated and collected along the copper plates. Upon completion of the test, the material was removed in increments along each plate. Each sample was weighed to determine the incremental yield. Ash and total sulfur analyses were performed on each sample. These results are plotted in Figure 2.4.6.

As can be seen, the overall clean coal yield was about 55% with an ash content of about 4%. The clean coal sulfur content was about 1%. As was found in the previous tests, the lowest and highest ash fractions were obtained near the feed end of the separator. Based on these results, separation immediately after grinding should be possible.

2.5 References

Agar, G.E., Stratton-Crawley, and Bruce, T.J., 1980, "Optimizing the Design of Flotation Circuits," CIM Bulletin, Vol. 73, No. 824, 173.

Austin, L.G., Klimpel, R.R., and Luckie, P.T., 1984, Process Engineering of Size Reduction: Ball Milling, AIME, New York.

Bahr, A., Legner, K., Ludke, H. and Mehrhoff, F.W., 1987, "5 years of Operational Experience with Pneumatic Flotation in Coal Preparation," Aufbereitungs Technik, 28, pp. 1-9.

Becker, M., Kwade, A. and Schwedes, J., 1997, "Influence of the Stress Intensity on the Comminution of Ceramics in Stirred Ball Mills," in Fine Powder Processing, Eds., R. Hogg, R.G. Cornwall, and C.C. Huang, Penn State University. pp. 51-58.

Bensley, C.N., Roberts, T. and Nicol, S.K. 1985, "Column Flotation for the Treatment of Fine Coal," Proceedings of the 3rd Australian Coal Preparation Conference, Woollongong, Australia, pp. 87-103.

Blecher, L. and Schwedes, J., 1996, "Energy Distribution and Particle Trajectories in a Grinding Chamber of a Stirred Ball Mill," Int. J. Miner. Process, 44-45, pp. 617-627.

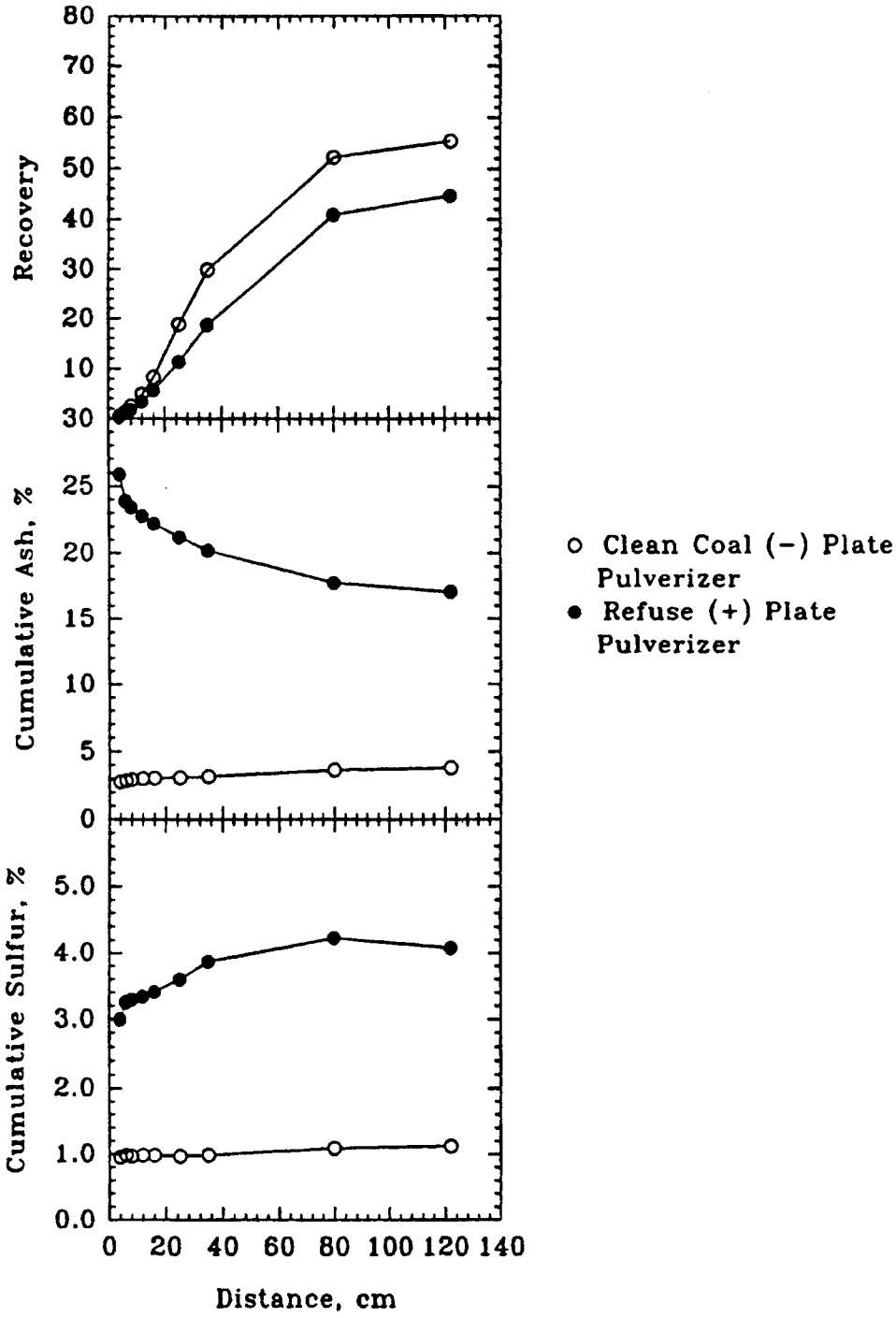

Figure 2.4.6 RESULTS FOR THE INTEGRATED PULVERIZER / ELECTROSTATIC SEPARATOR CIRCUIT WHEN PROCESSING UPPER FREEPORT SEAM COAL

Bradshaw, D.J. and O'Connor, C.T. 1996, "Measurement of the Sub-processes of Bubble Loading During Flotation," Minerals Engineering, 2, pp. 443-448.

Cho, H. and Hogg, R, 1995, "Breakage Parameters for Ultrafine Grinding in Stirred-Media Mills," Proceedings, XIX International Mineral Processing Congress, San Francisco, Aa, 2 pp. 53-57.

Cho, H., Waters, M.A. and Hogg, R, 1996, "Investigation of the Grind Limit in Stirred-Media Milling," Int. J. Miner. Process, Vol. 44-45, pp. 607-615.

Comeau, G., 1995, Personal Communication.

Davis, E.W., 1919, "Fine Crushing in ball Mills," Trans. AIME, Vol. 61, pp. 250-296.

Fofana, M., 1997, "Evaluation and Design of Magnetic Fluid Separators for Density Separations", Ph.D. Thesis, The Pennsylvania State University.

Gao, M.W. and Forssberg, E., 1992, "Increasing the Specific Surface Area of Dolomite by Stirred Ball Milling," in Comminution-Theory and Practice Symposium, S. K. Kawatra (ed.), SME/AIME, Littleton, CO.

Gao, M. W. and Forssberg, E., 1993, "A Study on the Effect of Parameters in Stirred Ball Milling," Int. J. Miner. Process., 3, pp. 45-59

Gao, M. W. and Forssberg, E., 1995, "Prediction of Product Size Distributions for a Stirred Ball Mill", Powder Technol., 84, pp. 101-106.

Gao, M. W., Forssberg, E. and Weller, K. R, 1996, "Power Prediction for a Pilot Scale Stirred Ball Mill," Int. J. Miner. Process., 44-45, pp. 641-652.

Herbst, J. A. and Sepulveda, J. L., 1978, "Fundamentals of Fine and Ultrafine Grinding," Proceedings, The International Powder and Bulk Solids Handling and Processing Conference, Chicago, IL, pp. 452-470.

Ityokumbul, M.T., 1993, "Selection of Recovery Zone Height in Flotation Column Design," Chem. Eng. Process., 32, pp. 77-82,.

Ityokumbul, M.T., Mahajan, D. and Trubelja, M.P., 1996, "Evaluation of a Vortactor (Turbulent Contact) Gas Sparging System', Proceedings of the International Symposium on Column Flotation, C.O. Gomez and J.A. Finch (eds.), CIM, Montreal, Canada, pp. 25-36.

Ityokumbul, M.T., Salama, A.I.A. and Al Taweel, A.M., 1995, "Estimation of Bubble Size in Flotation Columns," Minerals Engineering, 8, pp. 77-89.

Ityokumbul, M.T. and Trubelja, M.P., 1998, "Carrying Capacity in a Pilot Flotation Column," Minerals Engineering, 15, pp.41-46.

Kempnich, R.J., van Barneveld, S., and Lusan, A., 1993, "Dense-Medium Cyclones on Fine Coal - The Australian Experiece," 6th International Coal Preparation Conference, Mackay, pp. 272-288.

Kindig, J.K., 1992, "Self-Scrubbing Coal - An Integrated Approach to Clean Air," Coal Prep '92 Conference, pp. 110-123.

King, R.P., Hatton, T.A. and Hulbert, D.G., 1974, "Bubble Loading During Flotation," Trans. Inst. Min. Metal., Sect. C: Mineral Process. Extr. Metall., 83, pp. C112-C115.

Klima, M.S., Killmeyer, R.P., and Hucko, R.E., 1990, "Development of a Micronized-Magnetite Cycloning Process," 11th International Coal Preparation Congress, Tokyo, pp. 145-149.

Klimpel, R.R., 1980, "Estimation of Weight Ratios Given Component Make-up Analyses of Streams," Trans., SME-AIME, 266, pp. 1882-1886.

Kwade, A., Blecher, L. and Schwedes, J., 1996, "Motion and Stress Intensity of Grinding Beads in a Stirred Media Mill. Part 2: Stress Intensity and its Effects on Comminution," Powder Technol., 86, pp. 69-76.

Kwade, A., 1998, "Wet Comminution in Stirred-Media Mills – Research and its Practical Application," Preprints, 9th European Symposium on Comminution, Albi, France, pp. 23-32.

Leffler, M.P., 1997, "A Comparative Study of Batch and Continuous Column Flotation of Fine Coal," Ph.D. Thesis, The Pennsylvania State University, University Park, PA, 210 p.

Mankosa, M. J., Adel, G. T., and Yoon, R. H., 1986, "Effect of Media Size in Stirred Ball Mill Grinding of Coal," Powder Technol., 49, pp. 75-82.

Mankosa, M. J., Adel, G. T., and Yoon, R. H., 1989, "Effect of Operating Parameters in Stirred Ball Mill Grinding of Coal," Powder Technol., 59, pp. 255-260.

Miller, F.G., 1989, "Method for Recovering Fine Coal," U.S. Patent No. 4,802,976.

Miller, B.G., J.L. Morrison, R. Sharifi, J.F. Shepard, A.W. Scaroni, R. Hogg, S. Chander, M.T. Ityokumbul, M.S. Klima, P.T. Luckie, A. Rose, S. Addy, T.J. Considine, R.L. Gordon, K. McClain, A.M. Schaal, P.M. Walsh, J. Xie, P.C. Painter, B. Veytsman, M. J. Rini, M. Jha, D. Morrison, T. Melick, and T.M. Sommer, "The Development of Coal-Based Technologies for Department of Defense Facilities, Semiannual Technical Progress Report for the Period 03/28/1993 to 09/27/1993," Prepared for the U.S.

Department of Energy Pittsburgh Energy Technology Center, Pittsburgh, Pennsylvania, December 17, 1993, DE-FC22-92PC92162.

Miller, B.G., A.L. Boehman, P. Hatcher, H. Knicker, A. Kirshnan, J. McConnie, S. Falcone Miller, B. Moulton, S.V. Pisupati, J. F. Shepard, M. Vittal, R.T. Wincek, A.W. Scaroni, R. Hogg, S. Chander, H. Cho, M.T. Ityokumbul, M. S. Klima, P.T. Luckie, A. Rose, S. Addy, D.R. Crombie, R.L. Grodon, K. Harley, G. Jung, J. Lazo, P.C. Li, K. McClain, A.M. Schaal, J. Smead, K. Strellac, A. Manousr, W. Humphrey, and N. Chigier, "The Development of Coal-Based Technologies for Department of Defense Facilities Phase II Final Report, Prepared for the U.S. Department of Energy Federal Energy Technology Laboratory, Pittsburgh, Pennsylvania, July 31, 2001, DE-FC22-92PC92162, 784 pages.

Ounpuu, M. and Tremblay, R., 1991, "Investigation into the Effect of Column Height on the 1200 mm Diameter Column at Matagami," Proceedings of the International Conference on Column Flotation, Sudbury, Ontario, Canada, pp. 303-316.

Polat, M., Klima, M.S., Chander, S., and Ahuja, G., 1995, "The Use of Flotation to Separate Fine Coal and Ultrafine Magnetite from Dense-Medium Cyclone Products," High Efficiency Coal Preparation: An International Symposium, S.K. Kawatra, ed., SME, Littleton, CO, pp. 187-195.

Polat, M., Miller, F.G., and Chander, S., 1993, "An Integrated Heavy Media Cyclone-Flotation System for Fine Coal Cleaning," Minerals and Metallurgical Processing, 10, November, pp. 206-212.

Rajamani, R. K. and Bourgeois, F., 1990, "Energy Efficiency of Silicon Carbide Grinding in a Stirred Ball Milling, " Preprints, World Congress Particle Technology, Kyoto, Japan, pp. 369-375.

Rushton, J.H., Costich, E.W. and Everett, H.J., 1950, "Power Characteristics of Mixing Impellers, Parts I and II," Chem. Eng. Progr., 46, pp. 395-404; pp. 467-476.

Stehr, N. and Schwedes, J., 1983, "Investigation of the Grinding Behavior of a Stirred Ball Mill," Ger. Chem. Eng., 6, pp. 337-343.

Stehr, N., Mehta, R. K., and Herbst, J. A., 1987, "Comparison of Energy Requirements for Conventional and Stirred Ball Milling of Coal-Water Slurries," Coal Preparation, 4. pp. 209-226.

Strazisar, J. and Runovc, F., 1996, "Kinetics of Comminution in Micro and Sub-micrometer Ranges," Int. J. Miner. Process., 44-45, pp. 673-682.

Szatkowski, M. and Freyberger, W.L., 1985, "Kinetics of Flotation with Fine Bubbles," Trans. Inst. Min. Metal., Sect. C: Mineral Process. Extr. Metall., 94, pp. C61-C69.

Tangsripongkul, S., 1993, "Breakage mechanisms in Autogenous Grinding," PhD Thesis, The Pennsylvania State University.

Weiland, R.H., 1996, Triboelectrostatic Separation of Fine Coal, M.S. Thesis, The Pennsylvania State University.

Yildrim, K., 1987, "On the Mathematical Modeling and Optimization of Grinding Circuits," M.S. Thesis, The Pennsylvania State University.

Zheng, J, Harris, C. C. and Somasundaran. P., 1995, "A Study on Grinding and Energy Input in Stirred Media Mills," SME Annual Meeting, Denver, CO.